6-10-2015 12:00 AM

Nicotinamide Riboside Delivery Generates NAD+ Reserves to Protect Vascular Cells Against Oxidative Damage

Krista M. Hawrylyshyn
The University of Western Ontario

Supervisor
Dr. J.G. Pickering
The University of Western Ontario

Graduate Program in Biochemistry
A thesis submitted in partial fulfillment of the requirements for the degree in Master of Science

NICOTINAMIDE RIBOSIDE DELIVERY GENERATES NAD^+ RESERVES TO PROTECT VASCULAR CELLS AGAINST OXIDATIVE DAMAGE.

Thesis format: Monograph

by

Krista Hawrylyshyn

Graduate Program in Biochemistry

A thesis submitted in partial fulfillment
of the requirements for the degree of
Masters of Science

The School of Graduate and Postdoctoral Studies
The University of Western Ontario
London, Ontario, Canada

ABSTRACT

The ability of vascular cells to withstand oxidative insults is critical to vascular health. NAD^+, which drives poly (ADP-ribose) polymerase (PARP) and sirtuin (SIRT) reactions, can be compromised and strategies for overcoming this limitation in the vasculature do not exist. This study determines if nicotinamide riboside (NR) delivery can augment NAD^+ stores and fuel resistance to oxidative stress. I established that oxidative-stress insult on vascular cells decreased NAD^+ levels, accompanied by a striking increase in nuclear PAR-chain accumulation. PARP inhibition abolished PAR-chain formation and preserved NAD^+ levels, establishing PARP in NAD^+ consumption in this model. NR delivery protected against cell-shrinkage and cell death and promoted DNA repair efficiency. PARP inhibition mimicked NR's beneficial effects on cell-shrinkage and viability but at the cost of DNA repair efficiency. Interestingly, the beneficial effects of NR on viability and DNA repair were abrogated upon SIRT1 knock-down (KD). SIRT6 KD was similarly implicated in NR-mediated DNA repair. Furthermore, NR delivery protected against oxidative-stress-induced senescence. This protection was partially lost by SIRT1 KD. NR delivery protects vascular cells from H_2O_2–induced cell death, cytoskeletal collapse and senescence and promotes DNA repair efficiency. This NAD^+ fueling strategy may offer new opportunities for resisting oxidative-stress insults in the aging vasculature.

KEYWORDS:

NAD+, nicotinamide riboside, oxidative stress, hydrogen peroxide, PARP, sirtuin, SIRT1, SIRT6

ACKNOWLEDGMENTS

First and foremost, I would like to express my gratitude to Dr. Geoffrey Pickering who has patiently provided direction and guidance. Dr. Pickering's extensive background as a both a scientist and cardiologist grounded interpretation of data and inspired insight for implications of this vascular aging project. Further, as a wizard with words, he has assisted in magically transforming scholarship applications, abstract submissions and thesis drafts. Additionally, I would like to thank the rest of my committee, including Dr. Huff and Dr. Shilton, for their help at all levels of this research project.

Without the collaborative support of the Pickering Lab members, this thesis would not have been possible. Firstly, Dr. Hao Yin has been a constant superhero within the lab to develop protocols and offer his perspective, established by experience and far-reaching pools of knowledge. Caroline O'Neil and Alanna Watson have offered technical support to develop experimental skills and protocols. Last but not least, invaluable peer support networks were built. A big thank you to many for watching seminar rehearsals, editing thesis drafts and uniquely adding to a fulfilling research experience.

I would like to recognize sources of funding, without which this project would not have been possible. I acknowledge CIHR and the Department of Biochemistry at Western University for their support.

Finally, my family and friends are the foundation for all my wildest adventures. Thank you for hiking alongside me on this particular journey.

CONTRIBUTIONS

- Alanna Watson shared her breadth of knowledge related to NAD^+ metabolism, supporting experimental design considerations. In addition, she generated the global *NAMPT* KO mice described in Section 2.2 and she supplied *NAMPT* KO tissues used for experiments reported in Figure 3.1.
- Caroline O'Neil contributed technical support through protocols and assistance with cell culture of both vascular cell lines.
- Kevin Leung, PhD candidate in the Shilton Lab, synthesized the NR for preliminary experiments, as described in section 3.3.
- Zengxuan Nong contributed his immunostaining expertise to produce the HSMC 8-oxoguanine staining images reported in Figure 3.3B.
- Dr. Hao Yin has been engaged in every level of this project from assistance with experimental design, data interpretation, statistical analysis and technical skills.

TABLE OF CONTENTS

ABSTRACT II
ACKNOWLEDGMENTS III
CONTRIBUTIONS IV
TABLE OF CONTENTS V
LIST OF FIGURES VIII
LIST OF ABBREVIATIONS X
LIST OF APPENDICES XI
1 – INTRODUCTION 1
1.1 Vascular Aging: Contributing Cellular Changes 1
1.1.1 Endothelial Dysfunction 2
1.1.2 Senescence 4
1.1.3 Loss in Number and Function of Vascular Progenitor Cells 7
1.2 Aging as a Gradual Accumulation of Damage 9
1.2.1 Oxidative and Metabolic Stress 9
1.2.2 Inducing Oxidative Stress (H_2O_2) 11
1.2.3 Oxidative Stress in Pathological Conditions 15
1.2.4 Effects of ANG II on the Vasculature 17
1.3 Managing Oxidative Stress Insults 18
1.3.1 Cellular Anti-Oxidant Machinery 18
1.3.2 DNA Repair Pathways 19
1.3.3 Role of Poly (ADPribose) Polymerase Mediated DNA Repair 20
1.3.4 Caloric Restriction 24
1.3.5 The Sirtuin Family of Proteins 24
1.3.6 Cell Death: Modes and Stimuli 29
1.3.7 The Central Role of NAD^+ in Managing Oxidative Stress 32
1.4 Therapeutic Potential of Exogenous NAD^+ Precursors 32
1.4.1 Aging as an NAD^+-Deficient System 33
1.4.2 Uptake Transporter 33
1.4.3 Key Enzymes Involved in NAD^+ Salvage Pathway 34

1.4.4 Nicotinamide Riboside Supplementation 39
1.5 Aims and Hypothesis 42
2 – MATERIALS AND METHODS 43
2.1 Reagents 43
2.2 Global *Nampt* knockout mice 43
2.3 mRNA Extraction From Tissue and Cells 44
2.4 High Capacity cDNA Reverse Transcription 44
2.5 Qualitative PCR DNA Amplification 45
2.5.1 Gel Electropheresis 45
2.6 Quantitative Real Time-PCR Analysis (TaqMan) 45
2.7 Cell Culture 46
2.8 Western Blot of Nrk1 46
2.9 Determination of Commercial NR structure by NMR 47
2.10 NAD^+ Quantification 47
2.10.1 Experimental Set-Up 47
2.10.2 NAD/NADH isolation from Cells 48
2.10.3 NAD/NADH Quantification 48
2.11 Immunostaining 49
2.11.1 8-oxoguanine 49
2.11.2 PAR chains 49
2.12 Cell Shrinkage and Viability 50
2.13 Actin Cytoskeleton Staining 50
2.14 Alkaline Comet Assay 51
2.14.1 Experimental Set-Up 51
2.14.2 Single Cell Gel Electrophoresis Assay 51
2.14.3 CometAssay Analysis 52
2.15 Quantitative Real Time-PCR Analysis (SYBR Green) 52
2.16 siRNA Transfection to knockdown SIRT1-7 53
2.17 Senescence Associated β-Gal 53
2.18 Statistical Analyses 53
3 - RESULTS 55

3.1 NAD^+ Deficient Environment Upregulates Nrk1 mRNA Abundance 55
3.2 NR Delivery Increases NAD^+ Content in a Dose-Dependent Manner 59
3.3 Source for NR Supplementation 60
3.4 Acute Oxidative Stress Induces PARP-Dependent NAD^+ Depletion 64
3.5 NR buffers NAD^+ content, preserves morphology integrity and increases cell survival after oxidative stress insult 68
3.6 NR Preserves Morphology by Maintaining Cytoskeletal Integrity 74
3.7 NR delivery promotes DNA repair efficiency. 77
3.8 NAD^+ precursors NA, Nam and NMN similarly protect against H_2O_2-induced cell shrinkage and death. 84
3.9 PARP inhibition maintains NAD^+ levels to promote morphology and viability, but impairs DNA repair responses. 87
3.10 Role of the sirtuin family of enzymes in oxidative stress responses. 91
3.11 NR delivery protects vascular cells from chronic H_2O_2-induced senescence, in a partially SIRT1 and SIRT6 dependant manner. 98
4 – DISCUSSION 102
4.1 Potential of NR Delivery in Vascular Aging 102
4.2 Intracellular NAD^+ Pools Fuel Oxidative Stress Response 103
4.3 Limitations to PARP Inhibition 106
4.4 NR as a Superior NAD^+ Precursor 106
4.5 NR-mediated SIRT Activation in DNA Damage and Repair 107
4.6 SIRT Involvement in Enhanced Viability 110
4.7 Role of SIRTs in Maintaining Cytoskeleton Integrity 110
4.8 Implications of SIRTs in Vascular Aging 111
4.9 Limitations 111
4.10 Future Directions 113
4.11 Conclusion 114
5 –REFERENCES 116
APPENDICES 133
CURRICULUM VITAE 134

LIST OF FIGURES

Figure 1.1 Aging on a cellular level centres on oxidative stress.. 8

Figure 1.2 Common ROS-induced oxidative lesion resulting in DNA mutation. 13

Figure 1.3 Chemical sites where ROS can directly attack sugar-phosphate backbone and/or DNA bases. 14

Figure 1.4 The balance between repair and death hinges on PARP activity. 22

Figure 1.5 Determination of cell death subroutines following oxidative stress. 31

Figure 1.6 Pathways for NAD^+ regeneration. 35

Figure 1.7 A closer look at NAD^+ salvage pathway. 37

Figure 3.1 Expression profile of enzymes within the NAD^+ regeneration pathway and sirtuin family of enzymes in *Nampt* knockout mouse tissues and wild-type littermates. 57

Figure 3.2 Model for NR delivery in vascular cells..... 62

Figure 3.3 H_2O_2-induced oxidized DNA lesions, PAR-chain accumulation and NAD^+ depletion in vascular cells. 66

Figure 3.4 NR buffers H_2O_2-induced consumption of intracellular NAD^+ levels. 70

Figure 3.5 H_2O_2-induced cell shrinkage and cell death is attenuated by NR delivery in vascular cells.. 72

Figure 3.6 NR delivery results in actin re-organization and protects from H_2O_2-induced cytoskeletal collapse in vascular cells..... 75

Figure 3.7 NR promotes DNA repair. 80

Figure 3.8 Anti-oxidant gene expression remains unchanged following NR delivery.. 82

Figure 3.9 NAD^+-precursors similarly protect vascular cells from H_2O_2-induced cell shrinkage. 85

Figure 3.10 PARP inhibition mimics beneficial effects of NR, but at the cost of DNA repair efficiency..... 89

Figure 3.11 Role of Sirtuin family of enzymes in DNA damage response.. 94

Figure 3.12 Sirtuins mediate NR's protection against H_2O_2-induced cell shrinkage and cell death in vascular cells.. 96

Figure 3.13 DPQ and knockdown of SIRT1 or SIRT6 partially abolish NR's protection against H_2O_2-induced senescence. 100

Figure 4.1 NR fuels PARP function to support DNA repair during oxidative insults..... 105

Figure 4.2 Increased SIRT1 & SIRT6 activity may enhance NRs protection through improved defence systems and repair responses. 109

LIST OF ABBREVIATIONS

Abbreviation	Meaning
ANGII-	angiotensin II
BER-	base excision repair
cADPR-	cyclic ADP ribose
H_2O_2-	hydrogen peroxide
HAEC-	human aortic endothelial cells
HIF-1α-	hypoxia-inducible factor 1-alpha
HSMC-	human smooth muscle cells
KD-	knockdown
KO-	knockout
NA-	nicotinic acid
NAD(P)H-	nicotinamide adenine dinucleotide phosphate oxidase
Nam-	nicotinamide
NAMPT-	nicotinamide phosphoribosyltransferase
NER-	nucleotide excision repair
NFAT-	nuclear factor of activated T-cells
NMN-	nicotinamide mononucleotide
NMNAT-	nicotinamide mononucleotide adenylyltransferase
NO-	nitric oxide
NOS-	nitric oxide synthase
NR-	nicotinamide riboside
PARP-	poly (ADP-ribose) polymerase
RT PCR-	reverse transcription-quantitative polymerase chain reaction
ROS-	reactive oxygen species
SIRT-	sirtuin
SMC-	smooth muscle cells
SOD-	superoxide dismutase
STAT3-	signal transducer and activator of transcription 3
Tna-1-	high-affinity nicotinic acid transporter

LIST OF APPENDICES

Appendix A – List of Primer Probes used in this Thesis.....133

1 – INTRODUCTION

This introduction will begin with a review of factors that contribute to cellular aging, highlighting the central role oxidative stress plays in these pathways. In the next section, oxidative stress will then be discussed in more detail, including its involvement in disease progression. In the third section, cellular response pathways to oxidative stress will be introduced, and critically, the central role of NAD^+ in regulating these pathways is highlighted. The final introductory section will focus on NAD^+ and the potential benefits of delivery of the NAD^+ precursor nicotinamide riboside (NR).

1.1 Vascular Aging: Contributing Cellular Changes

Age is a major risk factor of cardiovascular disease. Even in elderly individuals without cardiovascular disease, characteristic arterial wall changes occur including dilation, stiffening and intimal thickening (1). How these changes contribute to cardiovascular disease progression is not completely understood, but aging of vascular cells themselves is considered to be a critical factor (1). Endothelial cells and vascular smooth muscle cells (SMCs) are key components of the artery wall. Most vessel formation will begin with an endothelial tube surrounded by pericytes. Subsequently, all vessels larger than capillaries will acquire a concentric SMC coat through a process known as arteriogenesis (2). This enables regulation of vascular tone and blood flow through SMCs contractile properties. During times of stress or disease, vascular SMCs are also involved in functions independent of their contractile properties in processes such as replication, migration and altering extracellular matrix proteins (3). Accordingly, aging of vascular cells can contribute to changes in vessel structure or function that could have critical consequences for blood pressure, heart attacks, and strokes (1). Additionally, as we age the ability to repair and respond to stress declines through loss of angiogenic and replicative potential within

cardiovascular tissues. Critical to these changes are the loss in number and function of progenitor cells, which are undifferentiated cells with pre-determined target cell types.

1.1.1 Endothelial Dysfunction

Endothelial dysfunction and its interplay with vascular smooth muscle cells contribute to decreased vessel compliance as we age. This is mediated by decreased endothelial cell replacement and impaired signalling to vascular smooth muscle cells limiting vasodilation (1). One such vasodilator, nitric oxide (NO), is produced by nitric oxide synthase (NOS); more specific to endothelial cells, the enzyme isoform eNOS is present. This enzyme will use L-arginine, molecular oxygen and nicotinamide adenine dinucleotide phosphate (NADPH) as substrates, and in the presence of three cofactors, generates NO through a five electron oxidation step. An imbalance of cofactors can result in NOS producing superoxides instead of NO, which will alter regulation of NO levels but can also induce oxidative stress (4). Oxidative stress is the imbalance of reactive oxygen species (ROS) production and the ability of the cell to neutralize those species. Further regulation of NO production is enabled through binding sites for both heme and calmodulin, which are required for proper eNOS enzyme function (4). Expression of eNOS predominates in the endothelium of larger vessels and enzyme activity can be controlled at transcription, post-transcription and, considerably, post-translational levels (5). Basal expression levels are also subject to various extrinsic stimuli; specifically, eNOS can be up-regulated by stimuli including hydrogen peroxide, insulin and low levels of oxidized LDL (6-8).

Proper regulation of NO production enables endothelial cells to respond to external stimuli and communicate the appropriate response to blood vessels to maintain homeostasis. Endothelial cells will produce NO, which signal for SMCs to relax. When this physiological condition is disrupted, it will lead to pathological conditions through either endothelial or SMC dysfunction. This

balance is lost during the aging process because of either decreased eNOS expression or loss of proper enzyme activity with increasing age (9-13). Further reducing NO production is the bioavailability of precursor L-arginine, this is because arginase (the final enzyme in the urea cycle) is upregulated in aged vasculature (14). The consequence of lower NO levels can be observed through vasomotor dysfunction (15, 16).

In addition to contributing to endothelial dysfunction, low NO production results in microvasculature rarefaction, through increased endothelial cell death (12). NO inhibits inflammation, thus decreased NO production has been linked to age-associated chronic inflammation. Independent of NO, loss of cells occurs during aging as a result of up-regulation of tumor necrosis factor alpha (TNF-α) and increased mitochondrial oxidative stress (17, 18). This is further aggravated by impaired angiogenesis (19) and loss of function of progenitor cells, discussed later.

Another contributor to endothelial dysfunction is NAD(P)H oxidase. This plasma membrane protein will transfers electrons from NADPH to molecular oxygen to form extracellular superoxide anions, which will interfere with extracellular signalling (20-24). Coronary artery disease and stroke in elderly patients is linked to this aging-induced increase in oxidative stress, caused in part through increased NAD(P)H oxidase activity (22, 25). The superoxide anion, produced in high concentrations as a consequence of aging, also attenuates NO function by reacting with it to form peroxynitrite. This reaction reduces NO bioavailability and further, it mediates the adverse consequences of oxidative stress (26).

In summary, changes of the cellular level that alter vascular tone regulation include decreased production of vasodilators and instead predominance of vasoconstrictors, in parallel with vascular wall structural changes. Endothelial dysfunction can be broadly defined by these imbalances and

more specifically identified by a decline in NO. This pathological state of the endothelium is thought to be a major phenotype in development of cardiovascular disease. Accelerated vascular aging and shorter lifespan can be modelled by defects in genes associated with endothelial dysfunction, such as the *Klotho* gene in mice (27, 28). The *Klotho* gene codes for a membrane protein that is associated with β-glucosidase and defects have been linked to chronic renal failure as well as ageing. More recent evidence has supported *Klotho* gene's role in inhibiting ROS production and attenuating inflammation (29, 30). Thus, interventions to improve vascular function in aged organisms may hinge on managing cellular ROS production and/or the subsequent oxidative stress response.

1.1.2 Senescence

Senescence is a permanent exit from the cell cycle, where cells typically take on a flattened and enlarged morphology. The senescent phenotype is associated with an accumulation of negative cell cycle regulators including p53, p16 and p21. Additionally, using X-gal to stain for increased β-galactosidase activity at a pH of 6.0 is a recognized biomarker of senescent cells (31). Lysosomes and the associated β-galactosidase accumulate in senescent cells, although it is not required for the acquisition of the senescent phenotype. As discussed above, decreased production of vasodilators, such as NO, contributes to changes in tissue structure, thereby promoting cardiovascular disease. The decrease in NO production is also seen in senescent vascular cells, presenting a link between endothelial dysfunction, senescence and vascular aging. An increase in NO by eNOS activation, on the other hand, can delay endothelial senescence (32). In addition, senescent cells disrupt tissue structure through harmful secretions including degradative enzymes, inflammatory cytokines, and growth factors which act to stimulate aging, thus playing a more complex role in promoting vascular disease phenotypes (33, 34). This senescence associated secretory phenotype further aggravates the system by inducing low-grade chronic inflammation within vascular tissues (35). There are two types

of senescence- replicative senescence and stress-induced premature senescence. Both have been linked to aging.

Replicative Senescence

Replicative senescence arises as a result of telomere shortening. Telomeres are repeating units of deoxyribonucleic acid (DNA) present on the ends of chromosomes. They help overcome the end replication problem arising due to the semiconservative nature of DNA replication by providing a buffer of telomeric repeats. Telomerase will add repeating segments of bases determined by an RNA template, and within vascular cells telomerase activity is low (36). Telomeres will associate with protein to form complexes to support the stability of chromosomes and DNA replication. Thus, progressive shortening of telomeres each time the cell replicates its DNA and low telomerase activity eventually leads to chromosomes with hanging ends that resemble damaged DNA. Following accumulation of p53 in response to this "damaged DNA"; downstream pathways will push towards the senescent phenotype.

Within vascular endothelial cells, the lengths of telomeres were observed to be indirectly proportional to age (37, 38). With each cell division telomere length is expected to decrease, however there is also a decrease in expression of the catalytic component of telomerase with age, further contributing to progressive shortening of telomeres and loss of chromosomal integrity (39). Shortening of telomeres in vitro was observed to contribute to endothelial dysfunction through changes including decreased NO synthase activity, the effects of which were discussed above (9, 40). In addition, stress resulting from cardiovascular disease risk factors, or shear stress from a position at a more dynamic region of flow, forces endothelial cells to replace damaged cells more frequently, also accelerating telomere shortening (38). Thus, natural aging involving gradual telomere shortening

combined with changes in gene expression will contribute to replicative senescence. A cells ability to manage and repair stress is an indirect contributing factor to replicative senescence.

Stress-Induced Premature Senescence

This form of senescence results from activation of cellular stress pathways, causing the cell to enter a senescent phenotype before reaching its age-determined replicative limit. In the case of DNA damage, whether by intrinsic sources such as ROS or mechanical stress (41), or by extrinsic sources such as radiation can induce stress-induced premature senescence. Upon DNA damage, p53 will be phosphorylated causing dissociation from mdm2 (an E3 ubiquitin-protein ligase) and promoting downstream expression of p21 or p16 which act to pause the cell cycle (42, 43). This allows time for the cell to respond to damage. However, there is a carefully regulated balance. If damage is not repaired, accumulation of phosphorylated p53 will tip the cell to favour fates other than repair, such as pre-mature senescence or, if the damage is too detrimental, cell death (42). Therefore, managing cytotoxic stressors through carefully regulated repair pathways play a critical role in maintaining genome integrity, but also play a role in managing the aging process.

Oxidative stress is a major stimulus, activating downstream pathways to initiate senescent phenotypes. Endothelial cells exposed to oxidative stress were pushed towards a pre-mature senescent phenotype, and in another study the results were supported through a contrasting experiment where anti-oxidants were able to delay the onset of senescence if damage was still at a manageable level (44-46). TNF-α and angiotensin II (ANGII) have also been implicated in the induction of senescence, both of which are upregulated in aging (17, 18, 21, 47). This implicates prolonged cytotoxic stress as a major contributor to cardiovascular disease through stress-induced pre-mature senescence.

Likely, a combination of both telomere-dependent and -independent mechanisms contributes to aging on a cellular level. Extrinsic factors that induce cell stress will push pathways of stress-induced premature senescence, but also result in higher cell turnover thereby accelerating telomere shortening and acquisition of replicative senescent phenotype (48).

1.1.3 Loss in Number and Function of Vascular Progenitor Cells

Circulating within peripheral blood are angiogenic cells, some being derived from the bone-marrow, which have been hypothesized to play a role in vascular repair (49). The role these progenitor cells play is still controversial, however the decreased number and function of circulating cells has been correlated to vascular disease, cardiovascular risk factors and age (50). In addition to gradual loss of progenitor cell numbers, these cells are also subject to replicative and stress-induced pre-mature senescence further contributing to impaired repair response (48). Linking progenitor cell function to vascular aging, the number of senescent progenitor cells is correlated with human patient age and risk of cardiovascular disease (51, 52). Critical to the functioning of these cells is the level of telomerase activity to enable effective replenishment of endothelial cell pools with sufficient replicative life. Both increased oxidative stress and Ang II levels have been implicated in diminishing telomerase activity (53). Both of these stressors are also known to contribute to stress-induced pre-mature senescence in progenitor cells.

Changes in gene expression, gradual loss of cell function, telomere shortening and loss of progenitor cells throughout an organism's lifetime is expected and contributes progressively to the aging process. The gradual accumulation of damage, linked to oxidative stress, is the basis of these age-associated changes in vascular cells (Fig 1.1). *Strategies promoting more effective vascular cell stress response, allowing cells to resist aging, could be vital to optimizing healthspan.*

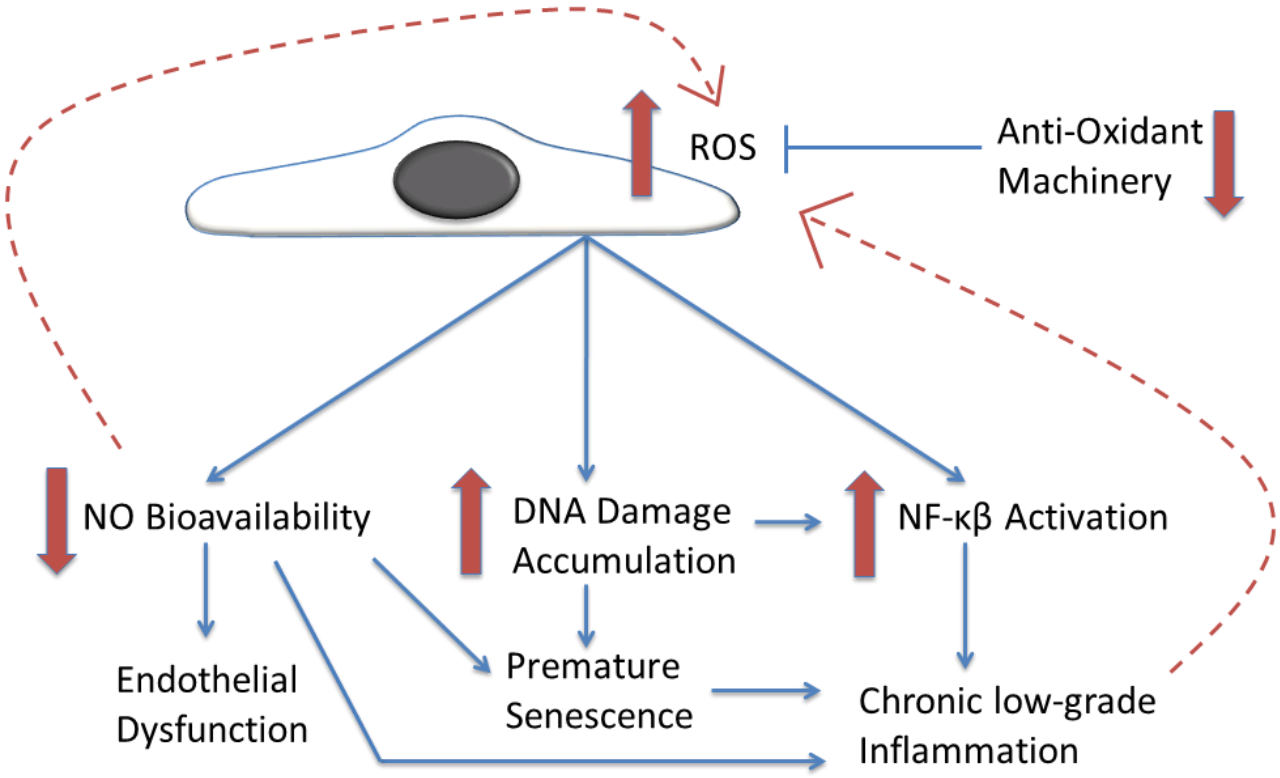

Figure 1.1 Aging on a cellular level centres on oxidative stress. NO will react with ROS, decreasing NO bioavailability. Decreased NO has implications on endothelial function, inflammation and senescence. ROS will react with DNA to form oxidative lesions that will activate PARP. The resulting PAR chain formation will activate NF-κβ. Accumulation of DNA damage can promote a senescent phenotype. Senescence-associated secretory phenotype and NF-κβ activation will promote inflammatory phenotype. Age-associated decrease in anti-oxidant machinery, discussed in section 1.3.1, will also increase ROS levels. Importantly, consequences of oxidative damage will feedback to further generate ROS.

1.2 Aging as a Gradual Accumulation of Damage

After acknowledging that aged arteries are more susceptible to cardiovascular disease, it is important to understand the involvement of senescence and vascular cell dysfunction in pathological progression. Further, gaining an understanding of pathways that accelerate these processes is essential. Oxidative stress was identified as a common contributor to cellular changes in the first section. This section will directly consider the influence of oxidative stress in development of cardiovascular disease. Importantly, in vivo and in vitro models to study oxidative stress will be reviewed.

1.2.1 Oxidative and Metabolic Stress

Some level of oxidative stress is natural and occurs as ROS (including superoxide anions, hydroxyl radicals and hydrogen peroxide) are produced as a by-product of metabolism and in the production of ATP. These ROS play a role in signalling pathways for normal cell functioning and growth, but are also recognized as the major contributor to aging through their ability to cause molecular damage (54).

ROS is generated throughout the cell for various purposes. Key contributing compartments include the plasma membrane, home to NAD(P)H Oxidases noted previously (55); the peroxisomes, which contain enzymes involved in lipid metabolism; and cytosolic enzymes, such as prostaglandin-endoperoxide synthase, which produce lipid-based signaling molecules. It is postulated that these compartments are the source of about 10% generated ROS, the remaining attributed to mitochondrial processes (56). ATP production utilizes oxidative phosphorylation to create an electric potential across the mitochondrial inner membrane, generating ROS as a by-product. The controlled oxidation of NADH and FADH pulls electrons into a cytochrome chain, along which there are opportunities for electrons to react with oxygen and electron acceptors to produce superoxide anions (56). These

mitochondrial redox events account for the majority of cellular oxidative stress, when ROS overwhelms anti-oxidant systems.

Free radicals, produced during ATP production, react rapidly or are dismutated to less damaging molecules by anti-oxidant machinery. On a molecular level, ROS pose a liability to cells through oxidized proteins altering catalytic activity through structural changes; oxidized lipids interfering with membrane fluidity and permeability; and oxidized DNA preventing transcription (57). Oxidized DNA poses a threat to genome integrity as a causative factor of DNA lesions in the form of single base modification, single strand breaks, double strand breaks or inter-strand crosslinks (58). The lesions can interfere with normal functioning, but if not repaired can also contribute to apoptosis, senescence or cancerous phenotypes.

Additionally, oxidative stress has been linked to changes in mitochondrial density, function, number and homeostasis (57). Underlying causes of these changes include decreased expression of key mitochondrial proteins (decreased mRNA levels and protein synthesis), lower mitochondrial DNA copy number, increased nucleic acid oxidative damage and oxidative-damage-induced dysfunctional proteins (57). Mitochondrial DNA and proteins are more susceptible to oxidative damage as a result of their proximity to the electron transport chain, generating ROS. In addition, mitochondrial DNA lacks the protection provided by nuclear histones. Damage induced by mitochondrial oxidative stress alters function of aged mitochondria, further producing more ROS and less ATP (56). Impaired mitochondrial biogenesis has been reported in arteries (59) and capillaries (60) of aged mammals; both reports implicated increased ROS in these changes. In humans, impaired mitochondrial biogenesis and function has been well documented in aging populations (57).

Thus, there exists an optimal balance to attenuate ROS-mediated oxidative stress and promote somatic maintenance, but at the cost of energy-demanding growth and reproductive functions. This

link has been recognized for some time and the impact of caloric restriction on life-span, through reduced metabolic stress, has been noted (61).

1.2.2 Inducing Oxidative Stress (H_2O_2)

A common ROS is hydrogen peroxide (H_2O_2), which acts as both an important cellular signal (62, 63) and initiator of adverse downstream consequences. Free radicals generated in the mitochondria and dismutated to H_2O_2 will passively transport through the mitochondrial membrane into the cytoplasm; higher cytoplasmic levels of H_2O_2 can push endothelial cells towards a proinflammatory phenotype through NF-κB activation (64). Further aggravating this process, an imbalance of ROS (generated by NAD(P)H oxidases) and cytoplasmic H_2O_2 activate poly(ADP-ribose) polymerase 1, also leading to NF-κB-dependent gene transcription. The ensuing inflammation itself adds to cellular oxidative stress by cytokine-mediated activation of NAD(P)H oxidases. The production of H_2O_2 occurs more frequently in aged cells, potentially advancing cardiovascular pathologies (65).

H_2O_2 is a powerful oxidizing agent and can alter the structure of DNA, protein and lipids. By definition, oxidation is the loss of electrons, reported as an increase in oxidation number of molecules, atoms or ions. A number of important biomarkers of DNA damage have become essential to the study of oxidative stress (66). One of the most common oxidative lesions is the oxidation of the double bond of guanine minor ring (Fig. 1.2). Although non-toxic, it can be highly mutagenic if not repaired through transversion reactions from G-T, as a result of binding to adenine (67, 68). Other direct oxidative stress-induced non-helix distorting lesions include thymine glycol, hydroxycytosine, formamidopyrimidines and hydroxymethylcytosine (69). In addition to damage directly to bases, ROS can directly cause base release or strand cleavage by attacking the glycosidic bond or nucleotide sugar ring, respectively (Fig. 1.3). More complex secondary reactions occur

following lipid peroxidation and subsequent reactions with DNA to produce helix-distorting or bulky lesions (66).

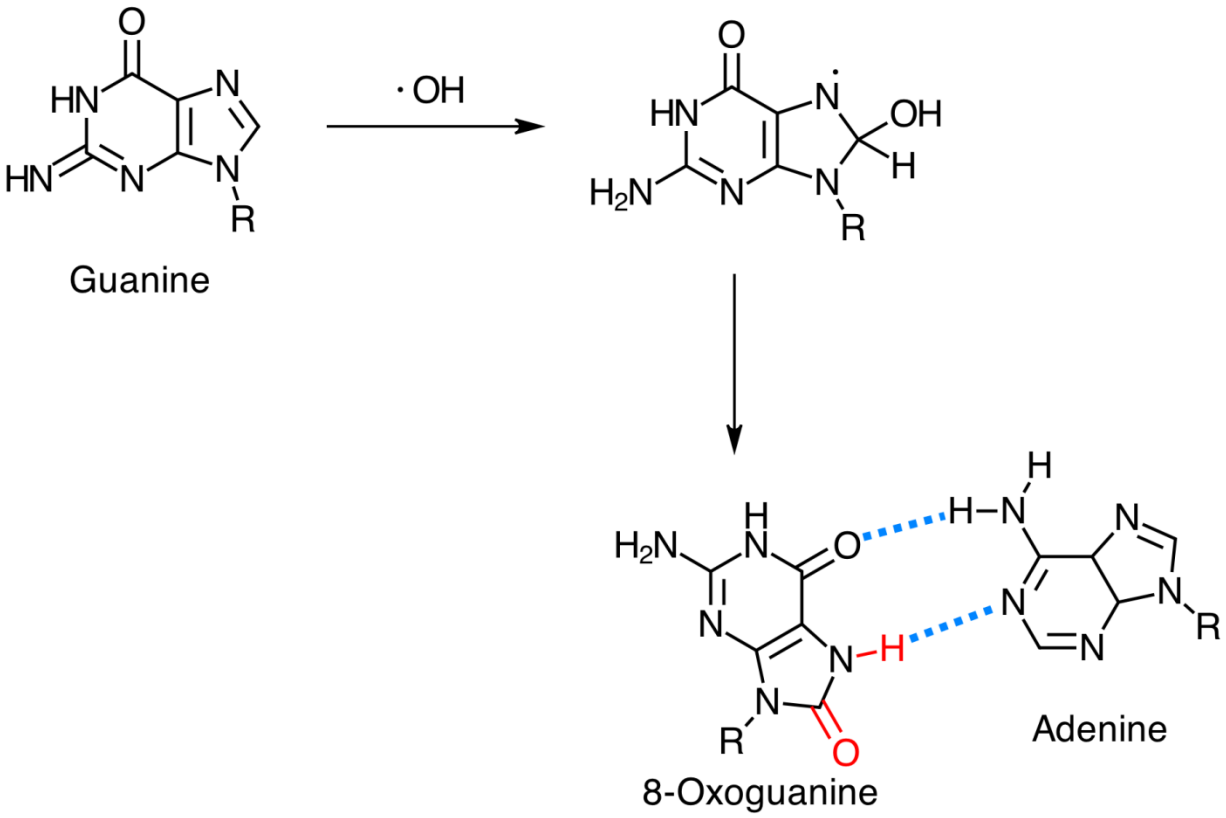

Figure 1.2 Common ROS-induced oxidative lesion resulting in DNA mutation. Oxidation of the double bond of guanine minor ring, leads to 8-oxoguanine, damaged guanine base. If not repaired, this lesion is highly mutagenic through transversion reactions from G-T, as a result of binding to adenine.

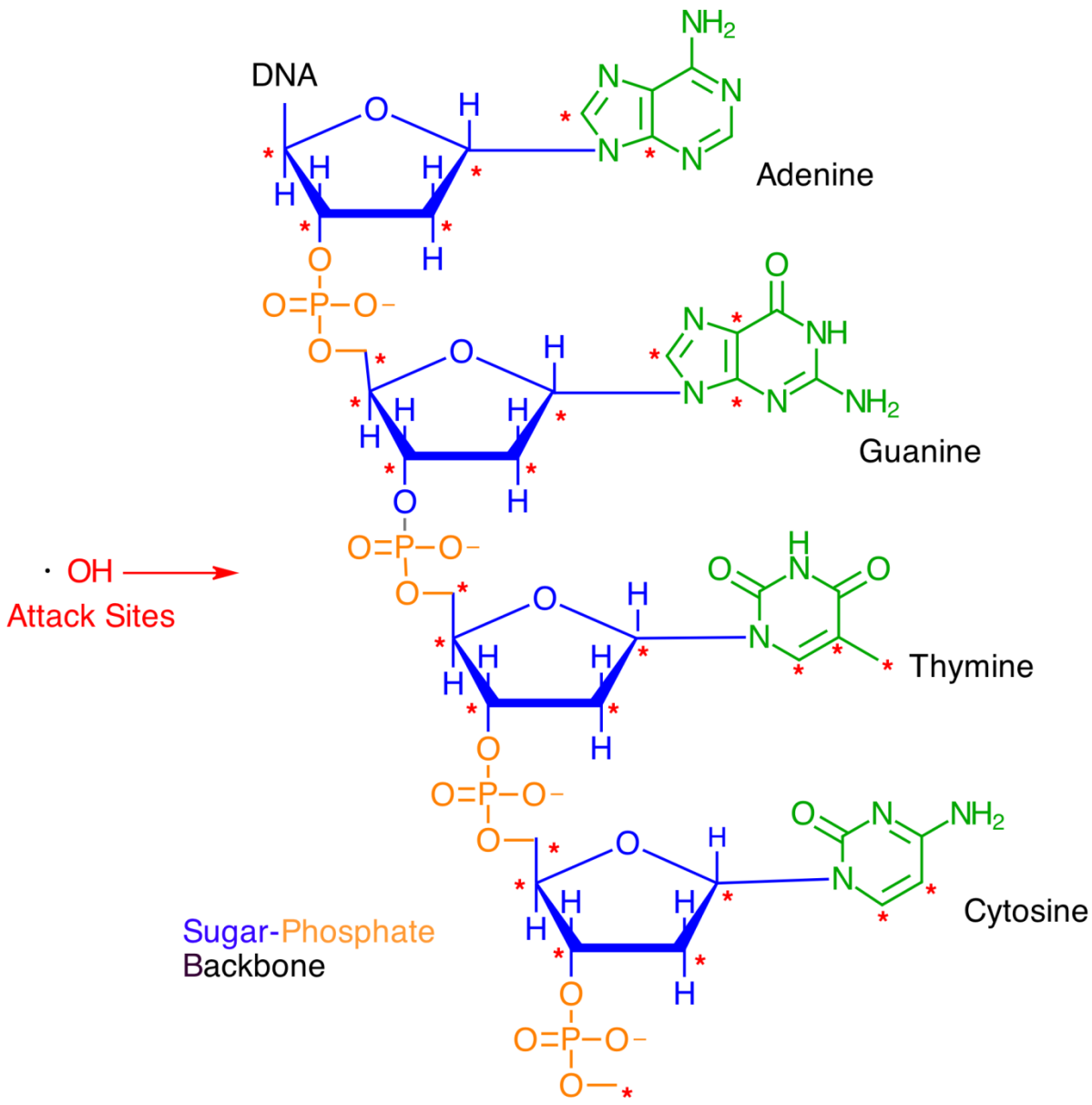

Figure 1.3 Chemical sites where ROS can directly attack sugar-phosphate backbone and/or DNA bases. The red asterisk indicates chemical sites that have been reported to be attacked by oxygen radicals. Along the sugar-phosphate back bone, oxidative damage can result in strand cleavage or base release.

Oxidative stress-induced double strand breaks are far less common than other damage types (70). However, they can occur indirectly when single strand breaks are formed in close proximity on opposite strands, and more so when repair of both lesions occurs simultaneously (71). A common marker of double strand breaks is phosphorylated histone H_2AX (γ-H_2AX). The nucleus has been found to be organized into large nuclear domains known as foci. Upon certain DNA damage insults, γ-H_2AX and DNA repair proteins will accumulate and localize to nuclear foci. Although the direct role of H_2O_2 in inducing double strand breaks is still controversial, there is evidence that this does occur (72). However, more recent reports have attributed oxidative stress induced γ-H_2AX foci to be independent of double strand breaks and instead attributed them to single strand intermediates during DNA break repair or stalled replication forks (73).

1.2.3 Oxidative Stress in Pathological Conditions

Although extensive research has focused on understanding the direct effects of oxidative stress and senescence, how these cellular changes result in vascular disease is less clear. Various recent studies have attempted to elucidate pathways that link oxidative damage to cardiovascular disease development. Altered mitochondrial homeostasis, impaired DNA-repair responses and chronic low-grade inflammation have been identified as underlying contributors to vascular disease development (65).

Within an atherosclerosis disease model, senescent markers have been used to identify senescent endothelial and vascular SMCs associated with atherosclerotic plaques (74, 75). Senescent endothelial cells were observed on the luminal surface of the blood vessels and senescent vascular SMCs were observed in the intima of more advanced plaques (40, 76). Consistently, these cells expressed lower amounts of NO, and had increased pro-inflammatory molecules adhering to the

cells (76). This senescent phenotype has been attributed to DNA damage from chronic oxidative stress or vascular inflammation through a p21 dependent pathway (74, 75).

Impaired mitochondrial biogenesis and function has been well documented in aging populations and implicated in age-associated disease and aging (57) Changes in mitochondrial homeostasis can be attributed to mutations of mitochondrial-specific DNA encoding 13 proteins required for oxidative phosphorylation (77). Interestingly, the cause of mitochondrial DNA mutations is replication errors from low-fidelity polymerases, and less likely attributed to increased ROS or oxidative damage (78, 79). A recent report has also implicated loss of communication to nuclear DNA encoding additional proteins needed for proper mitochondrial function as a contributor (80). In aging, cells will signal for increased biogenesis of mitochondria to overcome functional deficits, resulting in polyclonal expansion of mitochondria with various mutations (77). The pathophysiology of impaired mitochondrial function is metabolic through depleted ATP, altered Ca^{+} homeostasis and increase NAD/NADH ratios (77). In addition to impaired cellular energy production, these mutations impact aged tissue through increase apoptosis and potentially ROS production, although this is under debate (77).

DNA-damaging cellular stressors play a central role by inducing genomic damage to accelerate phenotypic changes that increase risk of vascular disease. Recently, this concept was supported through impaired nucleotide excision DNA repair leading to an accumulation of damage that contributed to vessel stiffness and hypertension often associated with vascular disease (81).

An additional pathological condition, resulting in acute damage through oxidative stress is sepsis, the systemic inflammation as a result of infection within the blood stream. Oxidative stress and associated damage, in parallel with depleted antioxidant systems, have been well reported in sepsis (82). Consequences of increased oxidative stress in sepsis lead to organ failure, caused by

inflammation through NF-κβ activation and mitochondrial dysfunction resulting in impaired energy production (83).

1.2.4 Effects of ANG II on the Vasculature

Angiotensin II (ANGII) is the downstream product of liver-produced angiotensinogen which is initially cleaved to form ANGI by circulating Renin and then by Angiotensin Converting Enzyme to form ANGII. Angiotensin converting enzyme is present in endothelial cells, and thus the bulk of cleavage occurs in the lung where vessel surface area is high to facilitate diffusion, but also in peripheral vasculature. ANGII functions to maintain fluid volume, blood pressure and salt homeostasis via renin-aldosterone system- acting through its own targets and through stimulation of aldosterone secretion from the adrenal cortex. Together these two hormones, ANGII and aldosterone, will increase blood pressure and signal for changes in expression of aquaporin channels within the kidney to influence salt and water retention. Through these actions they will increase vascular resistance and blood volume which can have long-term contribution to hypertension and atherosclerosis (84).

The over-activation of the renin-angiotensin system has been associated with normal aging (85-88). Because of this, delivery of exogenous ANGII could be used to model age-associated changes in vivo. ANGII has been found to down-regulate the *klotho* gene and protein levels, discussed previously as an aging model centered on endothelial dysfunction (89, 90). Reports have identified ANGII as a mediator of myocardial hypertrophy, sustained vascular dysfunction, hypertension and inflammation (91). These ANGII-mediated age-associated phenotypes have further been linked to pathologies including atherosclerosis and congestive heart failure (91).

On a molecular level, ANGII will induce oxidative stress through eNOS uncoupling (92) and NAD(P)H oxidase activation (93, 94). As a consequence of increased NO production (95), ANGII

will indirectly and further cause the deleterious downstream consequences of oxidative stress through peryoxynitrite formation (96). Critically, it has long been known that ANGII acts on endothelial progenitor cells by subjecting them to oxidative stress and lowering telomerase activity to induce a senescent phenotype (97). Thus, infusion or over-expression of ANGII offers an in vivo model for oxidative stress insult.

Aging creates a scenario by which loss of proper enzyme function, such as eNOS introduced in section 1.1, leads to higher levels of endogenous ROS production, creating a vicious feedback cycle. Oxidative stress initiates the key cellular changes that are the foundation for loss of tissue function contributing to aging within an organism and onset of cardiovascular pathologies. *Strategies that promote oxidative stress management could prevent molecular changes predictive of future cardiovascular disease progression.*

1.3 Managing Oxidative Stress Insults

After reviewing the molecular basis of oxidative-stress induced aging and disease progression in the vasculature, H_2O_2 and ANGII were selected as oxidative stressors for experimental work in this thesis. This section will focus on the corresponding stress response pathways to promote vascular viability and maintain optimal cellular function. The cell has in place initial preventative measures to manage oxidative stress and, when free radicals exceed their capacity, repair pathways are initiated. Importantly, age-associated molecular changes interfere with this defence system; targeting these factors may enhance oxidative stress management in aged cells.

1.3.1 Cellular Anti-Oxidant Machinery

Cellular anti-oxidant defence systems are in place to ameliorate the damaging effects of ROS. Superoxide dismutase (SOD) will break down superoxide anions to H_2O_2. This family of proteins includes three isoforms present in vessel walls: a manganese-dependent, mitochondrial enzyme

(SOD2), a cytosolic, copper-zinc-containing enzyme (SOD1) and an extracellular, copper-zinc-containing enzyme (SOD3) (56, 98). H_2O_2 itself is a reactive oxygen specie which is further broken down by mitochondrial ROS scavengers including catalase (to water and oxygen) (99), glutathione peroxidase (to water and reduced glutathione), and peroxiredoxins (100, 101).

SOD2, present in the inner mitochondrial membrane, is the first line of defence against ROS. Expression levels have been reported to decline in aged mice (102). In humans, changes in anti-oxidant enzyme expression have differed between vascular cell types (35). In endothelial progenitor cells, although SOD2 and catalase levels remained unchanged, glutathione peroxidase expression and activity levels decreased (103). In contrast, changes in human SOD2 levels were observed between young endothelial samples compared to sedentary aged endothelial samples (104). In another study, although expression levels of SOD2 were not changed, peroxynitrite-induced inactivation of the enzyme was observed more frequently in aortas of aged mice (24).

The second isoform, SOD1 maintains normal endothelial vasodilation by limiting cytosolic superoxides; its expression and activity levels were reported to decline in aged human samples (105). The third SOD isoform present in the extracellular vasculature, SOD3, protects vascular cells from superoxide-inactivation of endothelial cellular signal NO; SOD3 expression was reported to decrease in aged mice (106). As ROS levels increase in aged tissues, antioxidant machinery becomes even more imperative to manage oxidative stress. However, as discussed here, there are reports of declining antioxidant expression and/or activity in aged tissues.

1.3.2 DNA Repair Pathways

Free radicals that are not addressed by antioxidants will damage protein, and crucially DNA. Within mammals there are five major DNA repair pathways: nucleotide-excision repair (NER), base-excision repair (BER), non-homologous end joining, homologous recombination and mismatch

repair (58). Damage can be induced by both endogenous (repair of which is mediated mostly by BER (66)) and exogenous sources (repair of which is mediated mostly by NER). Both NER and BER involve damage that affects only one strand and generally is repaired by cutting out the damaged nucleoside (BER) or nucleotide (NER) and filling the gap using the complementary strand as a template. Bulky lesions will disrupt the helix structure and thereby restrict relevant repair enzymes which can no longer recognize, transcribe or replicate the DNA strand; these lesions are beyond BER's scope and require NER machinery (66). When repair is incomplete, mutations can occur as transcription or replication proceeds to match the wrong base through minor changes to bases. The decreased expression of components involved in BER and downstream targets implicating reduced efficacy, implicate an age-associated decline in BER (107).

DNA double-strand breaks hold high risk to impede cell function if not repaired, more so than damage affecting only a single strand. The repair pathways are also more complicated, as repair machinery must determine which ends connect together. Homologous recombination and end joining repair pathways overcome double strand breaks, with homologous recombination utilising the sister chromatid when available to ensure fidelity, and end-joining dominating in phases of the cell cycle when the sister chromatid is not present (108).

1.3.3 Role of Poly (ADPribose) Polymerase Mediated DNA Repair

Poly (ADPribose) polymerases (PARPs) family of proteins are recognized for their roles in base excision repair, nucleotide excision repair, and also an alternative form of non-homologous end-joining (double-strand break repair). As such, they play a critical role in attending to genome damage and promoting survival from their nuclear sub localization (109, 110). PARPs will recognize distortion of typical DNA double helix structure and bind to DNA through a zinc finger domain (110). Various types of damage, including photo lesions and single strand breaks induced by ionizing

radiation, methylating agents or topoisomerase inhibitors, are recognized in this fashion. This enzyme will then initiate the repair response, utilizing NAD^+ as a cofactor, to catalyze formation of a poly (ADP-ribose) chain, comprising 50-200 molecules of ADP-ribose, on nuclear proteins including transcription factors and histones. This provides a docking site that attracts DNA repair proteins to the site of damage, stabilizes repair complexes and alters enzymatic activity to promote a repair response. The PARP family consists of 17 members (111), with PARP1 activity accounting for >90% of PAR polymer generation. Thus, PARP1 is the dominant player in initiating DNA repair pathways mediated through NAD^+ consumption.

Importantly, there can be negative consequences of PARP activation. The addition of PAR chains to transcription factors and histones has implications for transcriptional regulation, notably on various inflammatory genes through NF-κB activation (112-114). One report found that PARP1-mediated signalling promoted apoptosis resistance, through STAT3-dependent activation of NFAT and HIF-1α. Taken together, this suggests that PARP1 can promote prolonged survival and proliferation in cells sustaining chronic inflammation and consequently constitutive DNA damage (115). Excessive PAR chain formation is also an initiator of PARP-mediated cell death discussed later. These various faces of PARP enable it to respond to oxidative stress through PAR chain formation, signaling for downstream repair pathways or regulating the carful balance between repair and cell death (Fig. 1.4). However, the adverse consequences of PAR-mediated signalling are also noted.

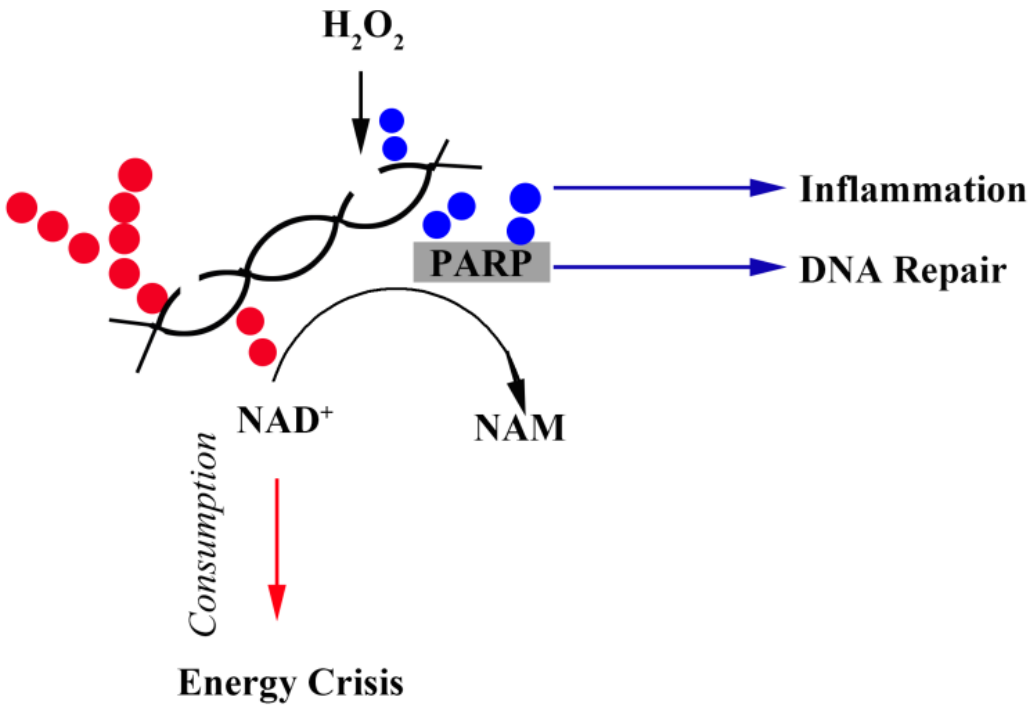

Figure 1.4 The balance between repair and death hinges on PARP activity. In blue, moderate PARP activation will catalyze PAR chain formation on PARP itself, histone and non-histone proteins to promote repair responses. PAR chain accumulation can also signal for an inflammatory response. Shown in red is the consequence of profound PARP activation. Excessive PAR chain formation results in profound NAD^+ consumption that can lead to an energy crisis, and ultimately cell death.

PARP Inhibition

As a consequence of aging, PARP-1 catalytic activity is increased due to an increased presence of DNA strand interruptions (116, 117). PARP activity will increase drastically in response to DNA damage, passing basal levels by 10-500 fold (118). Thus, profound PARP activation will consume NAD^+, and reduce substrate availability for other NAD^+-utilizing enzymes. Extreme PARP1 activation has long been associated with necrotic cell death (114, 119). In response to DNA damage, this excessive up-regulation of PARP-1 activity results in a depletion of metabolic intermediate NAD^+ and subsequently ATP. With low ATP stores, an energy crisis ensues, and cells are no longer able to regulate cell volume leading to cell swelling, and eventually necrosis.

These detrimental side-effects of high-level PARP activity have prompted numerous studies supporting the benefits of PARP inhibition. Previously shown in vascular SMCs and endothelial cells, inhibition of PARP1 protected against H_2O_2-induced cell death. This oxidative insult caused a drastic decrease in NAD^+ stores, blocked by PARP inhibition (120). Further, PARP1 inhibition has been shown to have beneficial effects on models of chemotherapy-induced heart failure through this similar principle of preventing an energy crisis (121-123). Also, PARP inhibition was found to protect against ANGII-induced changes by maintaining NAD^+ stores to enable continued sirt6 function (124). PARP inhibitors have also been linked to protection from hypertrophy and ultimately heart failure in mice through decreased cardiomyocyte death, decreased oxidative stress, inflammation, and prevention of mitochondrial dysfunction (115, 125). Other reports further support the finding that PARP1 inhibition will reduce oxidative stress, since pro-inflammatory gene expression is dependent on PARP1 activation (126).

1.3.4 Caloric Restriction

Endogenous oxidative stress, as a by-product of the metabolic process, links caloric-restriction dietary regimen to prolonged lifespan. Since observing the effects of caloric restriction, scientists have been trying to understand the molecular basis to mimic effects without reducing food intake. Within the cardiovascular system, caloric restriction confers improved risk factors of atherosclerosis, lowered blood pressure, increased bioavailability of NO, improved mitochondrial biogenesis, and lowered inflammation (127). One underlying biochemical change as a result of nutrient depletion is decreased cellular protein acetylation caused by decreased levels of acetyl coenzyme A (AcCoA), which is used as a cofactor for acetylation. This change will stimulate autophagy, the cellular catabolic process of breaking down and recycling dysfunctional or redundant cytosolic components via lysosomes (128). During times of stress, these catabolic actions will provide energy and building blocks for the cell and enable efficient organelle functioning, thus offering protective effects. Accordingly, autophagy itself through overexpression of autophagy-related protein 5 in mice has been shown to be enough to increase longevity (129). Three molecular ways to mimic these changes, ultimately stimulating autophagy, have been reported: decreasing the pool of AcCoA; reducing activity of enzymes that use AcCoA as a cofactor; or upregulating activity of deacetylases (130). The Sirtuin family of proteins have been identified as mediators of the effects of caloric restriction, acting to alter gene expression and prolong lifespan in lower organisms through their deacetylase properties.

1.3.5 The Sirtuin Family of Proteins

The members of this Sirtuin (SIRT) family of enzymes are NAD^+-dependent and have been conserved through evolution for their role in altering gene expression to facilitate regulation of cellular processes (131). SIRTs will consume NAD^+ to generate nicotinamide, which will negatively

feedback to inhibit SIRTs (Fig. 1.7). There are seven known mammalian SIRTs. SIRTs 1, 2, 3, 5 and 7 act as protein deacetylases on histone and non-histone proteins to control the expression of other genes (132). This is consistent with the homologue in lower organisms such as Yeast, known as Sir2. SIRTs 4 & 6 have ADP-ribosyltransferase activity, which also requires NAD^+ (133). Sirtuins have different subcellular localization: SIRT1, SIRT6 & SIRT7 are nuclear (associating with euchromatin, heterochromatin and nucleoli, respectively), SIRT2 is cytoplasmic and SIRT3, SIRT4 & SIRT5 reside in the mitochondria (134). SIRT1 is best characterized and controls various functions including cell differentiation, energy metabolism, circadian rhythm, stress responses and cell survival (135). The roles of remaining SIRTs have not been completely characterized, but have been linked to stress response and regulating lifespan (132). It was shown that by increasing the NAD/NADH ratio within cells, Sir2 activities will be up regulated to extend yeast lifespan (136). This illustrates the importance of NAD^+ homeostasis through its effects on SIRT function.

SIRT1

SIRT1 is abundantly expressed in the cardiovascular system (137-139). General SIRT1 functions have demonstrated cardioprotective abilities in ischemia/reperfusion, aging and atherosclerosis models, but also through promoting vascular development and maintenance (140). More specifically, SIRT1 has beneficial effects on critical factors implicated with aging; it prevents endothelial senescence and dysfunction (through eNOS deacetylation) (141-144) and has anti-oxidative and anti-inflammatory effects in cultured endothelial cells (137, 145). More recently, studies using *Sirt1* KO mice have linked its deacetylation function to protective autophagy through KO mice that exhibited increased cell death and less functional mitochondria (146). KO mouse tissue samples further supported loss of autophagy function through accumulation of p62 and damaged

organelles (147). The direct link between caloric restriction and SIRT1 was shown with these KO mice by losing longevity effects of a calorically restricted diet (148).

SIRT1 over-expression models have had conflicting reports. Some literature has associated SIRT1 over expression with increased oxidative stress, and reduced proper mitochondria and cardiac functions, possibly through an NAD^+ consumption phenomenon (149, 150). In contrast, a mouse study found SIRT1 over expression improved healthy aging through lower DNA damage and senescence, but was not sufficient to affect longevity (151). A recent study supported these findings, reporting that SIRT1 could promote cardiomyocyte cell survival following acute doxorubicin-induced oxidative burden by attenuating ROS production (152). Thus there may be an optimal activity level and time-specific application of sirtuin function to attenuate contributing factors of vascular aging.

Molecular mechanisms behind these SIRT1 findings hinge on managing ROS levels and targeting FOXOs, NF-κB or mTOR pathways (140). SIRT1 will deacetylate FOXOs to exploit their regulatory role, characterized by cellular proliferation, differentiation, genome integrity, cell survival and importantly oxidative stress management. Specifically, DNA damage repair response is initiated (153, 154), cell death is repressed through down-regulation of pro-apoptotic molecules (155) and antioxidant gene expression, including SOD2 and catalase, is upregulated to prevent future oxidative damage (156-158), thereby cohesively managing oxidative stress through SIRT1/FOXO1,3 and 4 complexes. Further supporting these findings, downstream of Sirt1 the formation of FOXO3a/PGC-1α complex has been reported to regulate antioxidant genes including MnSOD, catalase, Prx3, Trx2 and TR2 (157). The importance of these findings was emphasized in the context of the vascular endothelium, which is susceptible to endothelium dysfunction as a result of chronic exposure to oxidative stress. Transcriptional activation of eNOS, also critical to endothelial function, has been

reported to be regulated by the SIRT1/FOXO pathway (159). On another note, SIRT1 has been reported to supress chronic low-grade inflammation associated with aging by deacetylation of NF-κB and AP-1 transcription factors, thus blocking transcription of downstream pro-inflammatory cytokines (160-162). Finally, SIRT1 is considered a contributing promoter of autophagy through down-regulation of the mTOR pathway (140).

Critical to this project, SIRT1 maintains genome integrity by initiating downstream DNA repair pathways during times of stress. Post-translational and post-transcriptional modifications have been reported to regulate these DNA repair functions (163). Acting on SIRT1 during times of stress when transcription is otherwise compromised, HuR was demonstrated to translocate to the cytoplasm and stabilize *SIRT1* mRNA, thereby increasing its presence in the cytoplasm for constitutive expression (164). Recently, ubiquitination post-translational modification of SIRT1 was identified as an essential regulator of downstream DNA damage response pathways (165). Further, SIRT1 itself utilizes post-translational modifications, for example through deacetylation of Nijmegen breakage syndrome protein, an initiator of DNA double strand break repair (166). Thus, during times of stress, SIRT1 is carefully regulated to promote repair pathways.

SIRT6

SIRT6 affects cardiac biology as a regulator of DNA damage repair, telomere maintenance and the metabolism of glucose and lipids (167). These SIRT6 functions have been elucidated through knockout models. For example, genomic instability was identified in mice with SIRT6 deficiency through increased sensitivity to H_2O_2, consistent with deficiency in BER (168). Acting through deacetylation of chromatin, SIRT6 may increase access of repair machinery to sites of DNA damage (169). Alternatively, SIRT6 may be indirectly promoting BER through activation of the PARP family of proteins (170, 171). Double-strand break repair may also be mediated indirectly by

increased PARP activity but also through non-histone deacetylation of CtIP (C-terminal binding protein interacting protein), a key protein involved in DSB end resection (172). Further, it was reported that SIRT6 may form a macromolecular complex to stabilize DNA-dependent protein kinase with chromatin at the site of DSBs to enable repair (173). SIRT6 deficiency may further contribute to genomic instability through impaired telomere capping, normally mediated by SIRT6 deacetylation of telomere chromatin (174).

Contradicting literature has reported SIRT6 to alter both pro-inflammatory and anti-inflammatory signalling pathways. The difference may depend on the cell types studied (167). SIRT6 was found to regulate TNF-α ligand by enhancing its secretion from the cell (175) and increasing its translational efficiency (176). TNF-α is a common pro-inflammatory cytokine that functions to activate NF-κβ. Distinct research conducted in parallel found that SIRT6 physically interacted with an NF-κβ subunit to deacetylate promoter residues of a subset of target genes, thereby attenuating expression (177). This finding indirectly implicates anti-inflammatory effects of SIRT6.

SIRT6 overexpression has also been linked to increasing longevity in male mice (178). Consistent with this, deficiency of SIRT6 has been associated with features of premature aging, likely through its role in genomic instability (168). Additionally, changes in regulation of SIRT6 during the natural aging process may implicate *SIRT6* down-regulation in age-associated phenotypes. Peroxynitrite, which increases during aging, can decrease SIRT6 activity (179). H_2O_2-induced oxidative stress has been reported to push endothelial cells towards a senescent phenotype through *SIRT6* down-regulation (180). Further, a reported increased methylation state of *sirt6* gene in humans with aging (age 20-79) suggests age-related repressed gene expression (181).

1.3.6 Cell Death: Modes and Stimuli

Repair pathways and homeostatic maintenance adaptive responses are linked with signalling pathways that initiate cell death. For example, DNA damage is recognized by the cell and the cell cycle is paused to allow repair or trigger death. Similarly, metabolic checkpoints such as ATP/ADP and NAD/NADH ratios signal metabolic perturbations that if excessively severe can also trigger death (182). As discussed above, PARP can act as a metabolic checkpoint through energetic catastrophe following extensive DNA damage insults, signalling through depleted ATP, NAD^+ and NADH stores (182).

Cell death occurs when any of three events occur: loss of plasma membrane integrity, cell & nuclear disintegration or consumption by a neighbouring cell (183). Numerous stimuli can trigger signalling cascades that push a cell towards various distinct modes of cells death. These modalities can be classified by morphological changes and molecular definitions, yet no single molecular event can uniformly be used as "the point of no return" to determine death.

Traditional classifications describe cell death subroutines based primarily on morphology: describing apoptosis as chromatin condensation, nuclear fragmentation and shrinking and necrosis as cell & organelle swelling and breakdown of intracellular contents in a disorganized manner (183). Incorporating molecular definitions offers more precise classification, as morphological descriptions hide heterogeneity in lethal signalling cascades (184). Currently, apoptosis is classified as caspase-dependent extrinsic apoptosis or caspase-dependent or -independent intrinsic apoptosis, depending on the source of stimuli triggering death (184). Similarly, necrosis can be sub-defined through molecular events as necroptosis, a mode of regulated necrotic cell death (184).

Molecular definitions also open avenues for cell death classifications based on specific lethal stimuli. PARP activation has been linked to a distinct caspase-independent mode of cell death,

known as parthanatos. Accumulation of PAR chains in the nucleus will induce their translocation into the mitochondria. There, the PAR chains bind to and initiate the release of apoptosis-initiating factor (AIF) (185). In turn, AIF will translocate to the nucleus resulting in fragmentation of DNA in distinctly larger segments than that occurring during apoptosis (186, 187). Based solely on morphological changes, this mode of death fell under the broad term necrosis. However, it can be defined as a specific type of regulated necrosis. In fact, several cell death subroutines can arise by PARP over-activation, specifically apoptosis, necrosis, parthanatos or autophagy, depending on extent of damage and resulting molecular events (Fig. 1.5). PARP activation will stabilize p53 to promote apoptosis at moderate damage levels (188) and PARP itself is cleaved during the apoptosis pathway by caspases to conserve ATP (189). However, PARP over-activation may inactivate caspase 8 inhibiting apoptosis (190) or stimulate AMPK and inhibit mTOR pathways to promote autophagy through PARP-mediated ATP depletion (191).

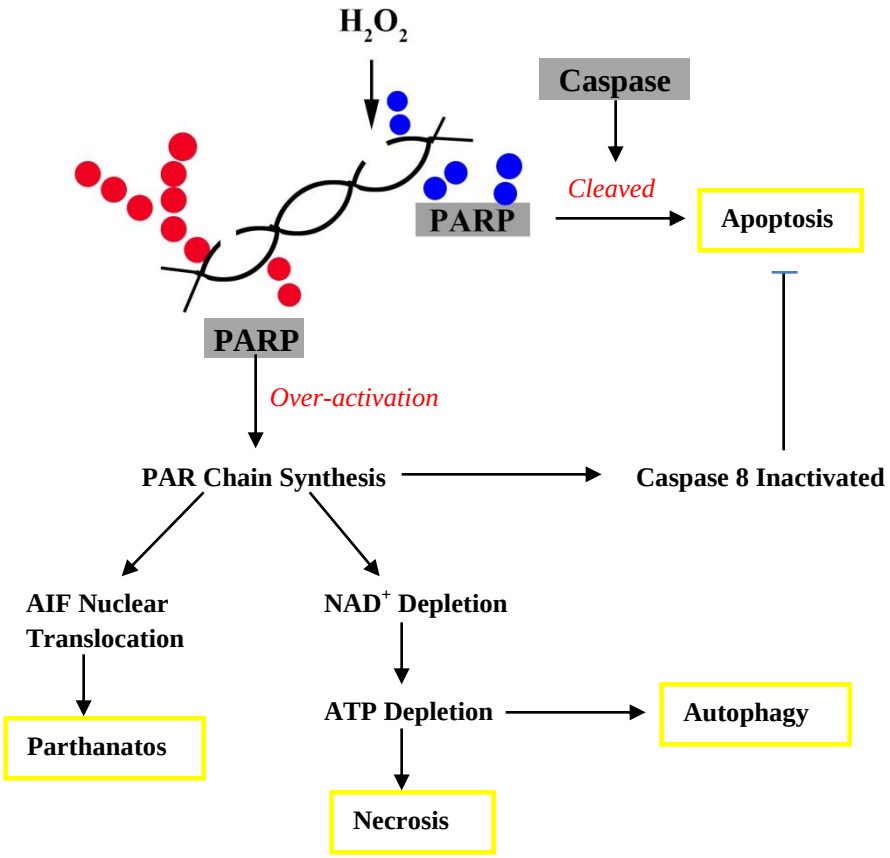

Figure 1.5 Determination of cell death subroutines following oxidative stress. PARP over-activation will catalyze excessive PAR chain synthesis. PAR chain accumulation can induce the nuclear translocation of AIF, initiating pathways leading to parthanatos. Synthesis of PAR chains will consume NAD^+ and the following NAD^+ salvage will consume ATP. Low levels of ATP can stimulate autophagy, or in extreme cases the energy crisis can initiate necrosis. Caspase family of enzymes will regulate cell death by cleaving PARP during times of damage to maintain NAD^+ levels and instead push cells towards apoptosis.

1.3.7 The Central Role of NAD^+ in Managing Oxidative Stress

Nicotinamide adenine dinucleotide (NAD^+) plays a central role as an energy signal, triggering a response to stress insults to assist in determination of cell fate. NAD^+ is more traditionally recognized for its role as a cofactor of the hydride transfer enzymes of cellular redox reactions involved in energy metabolism (133). NAD^+ is a versatile acceptor to compounds that contain hydrogen centers with strong nucleophilic or reducing properties. NAD^+ will utilize its oxidizing properties to transfer electrons and become the reduced dinucleotide NADH (192). Thus, NAD^+ is interconnected between NAD/NADH in various metabolic pathways, ensuring there is no net loss of the molecule to fuel oxidative metabolism by providing reducing equivalents through NADH. However, NAD^+ is also used as a substrate for various NAD^+ consuming reactions (193). This creates a need for the cells to regenerate NAD^+ to maintain proper function of SIRTs and PARPs, but also avoid an energy crisis through loss of ATP synthesis as NAD/NADH stores are depleted.

Oxidative damage can be managed by preventative and/or post-damage response systems. There exists a carefully regulated threshold for cell death initiation based on damage pathways and metabolic signals. Regulation of these pathways centers on NAD^+ levels, which fuel the sirtuin and PARP family of enzymes in both preventative and response measures. Further, the NAD/NADH ratio directly acts as a metabolic signal that can trigger death cascades. However, with aging the supply systems for NAD^+ can be impaired. *Exogenous control of NAD^+ levels may offer a therapeutic intervention to manage better oxidative stress insults.*

1.4 <u>Therapeutic Potential of Exogenous NAD^+ Precursors</u>

The potential for exogenous NAD^+ precursors to regulate NAD^+ homeostasis to promote repair response and avoid an energy crisis induced by active NAD^+-consuming enzymes has important implications to vascular aging. Higher PARP activity as a result of increased oxidative

damage in aged vascular tissue implicates constitutive NAD^+ consumption as a phenomenon of aging (194). This highlights the importance of NAD^+ regeneration. The therapeutic potential of precursor supplementation is however dependent on the expression of proper transporters to bring precursors into the cell, the ability of cells to tolerate changes in cellular NAD^+ levels and tissue specific expression of required salvage enzymes.

1.4.1 Aging as an NAD^+-Deficient System

Increased NAD^+ consumption in aging contributes to the need for salvage pathways. However, impaired salvage as a result of age-associated changes suggests that aging is an NAD^+-deficient system. Lower overall NAD^+ levels have been reported in various aged rat and human tissues (195, 196). Declining levels can be explained by increased consumption such as chronic PARP activation in aged models (194), but also changes in mitochondrial function and salvage enzyme expression. Changes in circadian clock machinery have been reported to lower levels of key salvage enzyme, NAMPT, as well as NAD^+ (192, 197). More directly, NAMPT expression levels have been reported to decline in aged mice (198). Chronic inflammation was implicated as a causative factor of these drops through TNF-α, a major inflammatory cytokine, and oxidative stress both lowing NAMPT and NAD^+ in primary hepatocytes (198, 199). Mitochondria homeostasis is impacted by declining NAD^+ levels, requiring more resource input to generate ATP in less functional mitochondria in aged tissue (80). Taken together, increased consumption, decreased biosynthetic capacity and lower energy production efficiency contribute to an NAD^+-deficient system in aged models.

1.4.2 Uptake Transporter

Cellular uptake transporters that allow nucleosides (such as NAD^+ precursors nicotinamide (Nam), nicotinic acid (NA) or nicotinamide riboside (NR)) to enter cells have been characterized. NR

and NA are brought into the cell through high affinity major facilitator superfamily transporters Nrt1 and Tna-1, respectively; a transporter for Nam has not yet been identified (200, 201). Pathways for NA and NR export have also been identified, although the mechanism and purpose for export are unknown (201). Speculations have suggested precursors are exported to store vitamins extracellularly or cross-feed surrounding cells. Nrt1 and Tna-1 transporters are not bidirectional, as export pathways have been found to be independent of these enzymes. Interestingly, in conditions of high NA or Nam, NR export will increase. Further, NR import remains low when other precursors are plentiful (202). In contrast to nucleoside import mechanisms, nucleotides including NAD^+ and NMN must be degraded extracellularly before being brought into the cell, requiring an additional step and lowering bioavailability (203).

1.4.3 Key Enzymes Involved in NAD^+ Salvage Pathway

NAD^+ can be generated through two broad pathways in mammals: the de novo pathway from L-tryptophan amino acid precursor and the salvage pathway from precursors such as Nam, NA or NR (Fig. 1.6). Nam and NA together are also known as niacin or vitamin B3. Nam and NA are generated in parallel with ADP-ribosyl products following NAD^+ catabolism. Key expression differences in enzymes between cell types and tissues have been identified, revealing tissue-specific pathways for NAD^+ biosynthesis (204).

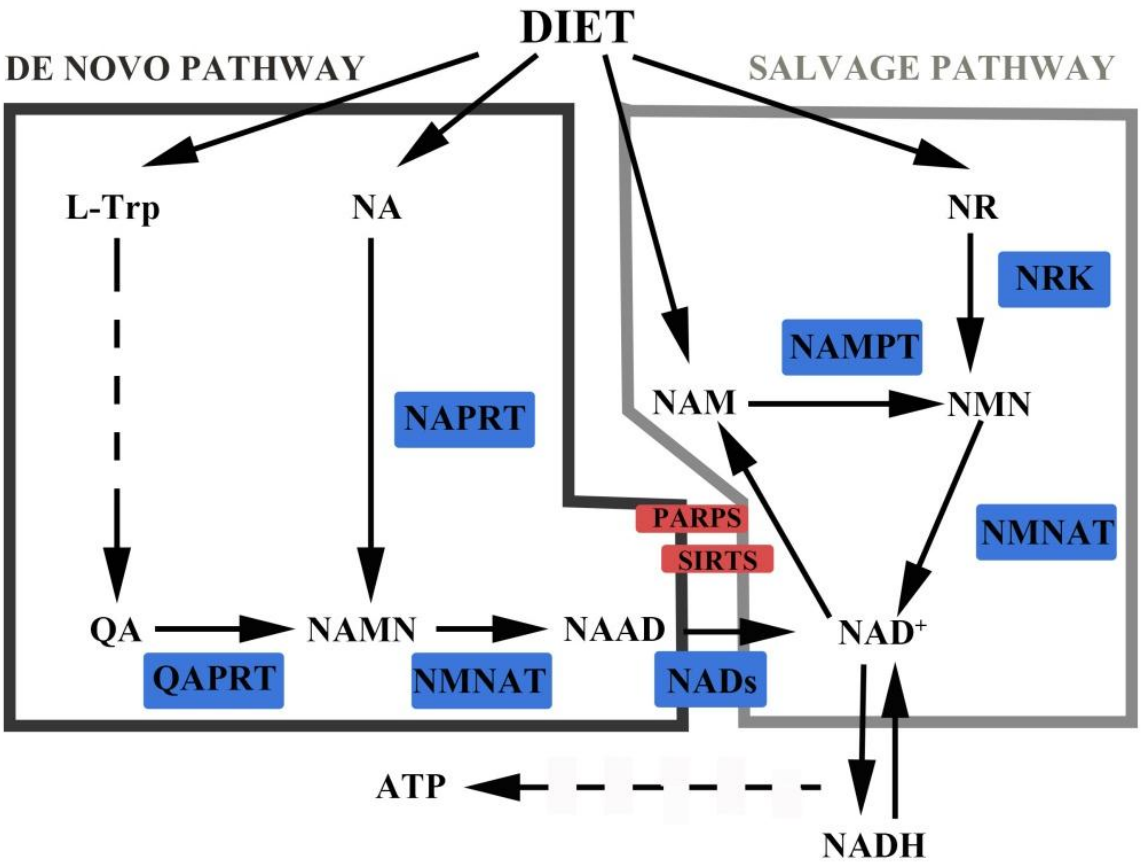

Figure 1.6 Pathways for NAD^+ regeneration. This image illustrates the role of NAMPT (nicotinamide phosphoribosyltransferase), the rate-limiting enzyme in the regeneration pathway, as well as the role of other key enzymes, such as Nrk1 (nicotinamide riboside kinase) and NMNATs (nicotinamide mononucleotide adenylyltransferases), discussed in this report. On the left, the longer, more energy-consuming de novo pathway generates NAD^+ from amino acid precursor L-tryptophan. On the right, key players in the salvage pathway are depicted.

Nicotinamide Phosphoribosyltransferase

Nicotinamide Phosphoribosyltransferase (NAMPT) was initially believed to be a cytokine, and given the name pre-B enhancing colony factor, and later an insulin-mimetic hormone called Visfatin (205-207). The first claim has not been supported and remains inconclusive, while evidence supporting Visfatin has been retracted. It is now known as one of a few enzymes involved in the NAD^+-salvage pathway. NAD^+ is consumed as a substrate by PARPs, cADPR synthases and SIRTs. This thesis focuses on PARPs and SIRTs. Following consumption of NAD^+, NAMPT will convert the nicotinamide by-product to nicotinamide mononucleotide as the first and rate-limiting step to regenerating NAD^+ (205) (Fig. 1.7). Since nicotinamide is a negative inhibitor of SIRTs, this enzyme consequently increases SIRT activity by lowering cellular nicotinamide levels (208). NAMPT is therefore intricately linked within the salvage pathway to maintain cellular NAD^+ levels.

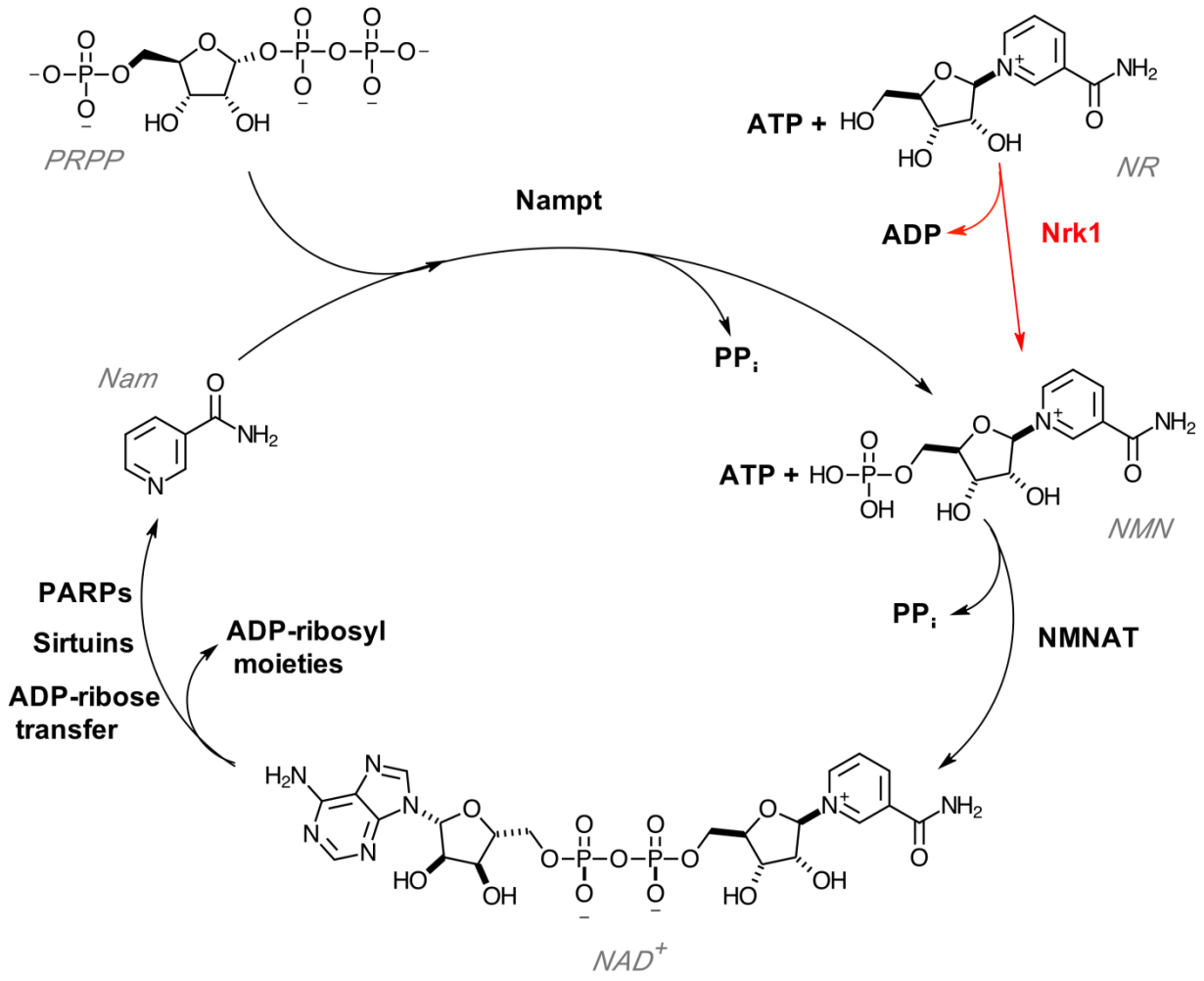

Figure 1.7 A closer look at NAD$^+$ salvage pathway. NAD$^+$ is consumed by PARPs and SIRTs to Nam, which feeds back to inhibit SIRT function. NAMPT catalyzes the addition of a phosphoribosyl group in the first step of salvage. The resulting NMN product then gains a phosphor-adenine group from ATP to form NAD$^+$, catalyzed by the NMNAT family of enzymes. NR enters this two-step salvage pathway by receiving a phosphate group from ATP to form NMN, catalyzed by Nrk1 (shown in red).

Our lab previously isolated a cell line able to undergo differentiation between an immature, proliferative smooth muscle phenotype to a mature, contractile state (209). In this model, NAMPT was identified as a factor up-regulated in the mature SMC phenotype, illustrating dynamic differential expression between phenotypes (210). The role of NAMPT during SMC differentiation presents an additional interest in the enzyme and understanding the link between NAD^+ homeostasis and vascular health.

Within a vascular aging model, NAMPT expression decreases with age (198) and decreases following acquisition of a senescent phenotype in SMCs. Our lab has previously shown that overexpressing NAMPT in SMCs and endothelial cells in culture enhances cell life span through SIRT1 activity and p53 degradation (211). Further, NAMPT overexpression has been shown to increase cellular NAD^+ levels to promote cell survival and resistance to oxidative stress (211-213). Other experiments have further supported these findings by showing that incubating cells with a known NAMPT inhibitor will decrease the ability of cells to withstand genotoxic stress (214).

Nicotinamide Riboside Kinase

Although NAMPT is a major enzyme within the salvage pathway for NAD^+, other enzymes such as Nicotinaminde Riboside Kinase (Nrk) and the Nicotinamide Adenylyltransferase (NMNAT) protein family also play a large role. Salvage of NAD^+ from nicotinamide riboside precursor can occur through two pathways. One of these involves human Nrk1 or Nrk2 phosphorylation of NR and the second pathway, independent of these enzymes, entails using yeast Urh1 and pnp1 enzymes to split NR into a ribosyl product and Nam (215). Nam can then be used to regenerate NAD^+ through alternate salvage pathways. The relevance of pathways involving these two yeast enzymes have not yet been considered in mammalian models.

Nrk1 and Nrk2 differ in both structure and tissue-specific function. They share 57% homology; Nrk1 is a polypeptide of 199 amino acids, whereas Nrk2 is 230 amino acids (216). An additional splice form of 186 amino acids exists for human Nrk2, functionally identified as a muscle integrin β1 binding protein that regulates cell adhesion and laminin deposition in myoblasts (217). This 186 amino acid muscle integrin β1 binding protein lacks enzymatic activity, in contrast to the human and yeast Nrk1 with high specificity for phosphorylation of nictonamide riboside (216). The 230 amino acid human Nrk2 enzyme has a reported 25% enzymatic activity relative to that of Nrk1 (216).

1.4.4 Nicotinamide Riboside Supplementation

For decades niacin (consisting of NAD^+ precursors Nam and NA) has been used to therapeutically treat dyslipidemia by lowering triglycerides circulating in the blood stream and raising HDL levels (218). However, two clinical trials have reported that niacin did not reduce cardiac events in high risk patients (219). Additional studies suggest that niacin's benefits on vascular health act independently of its lipid-lowering effects (220-222). Instead, recent work suggests that niacin can improve endothelial function and reduce oxidative stress (223), thereby enabling stress management in models of ischemia & reperfusion injury or stroke (224). The mechanism of niacin's actions is unclear. It is possible that benefits of niacin are mediated by distinct signalling pathways downstream of the niacin receptor. Alternatively, benefits through niacin supplementation could act in part by increasing NAD^+ levels, although this has yet to be determined.

NMN supplementation has been reported to overcome age-associated NAMPT decline to protect the heart from ischemia & reperfusion injury (225) and to treat diabetes in aged mice (198). Both of these studies identified compromised NAD^+ levels by either ischemic insult or high fat diet. NMN was shown to protect from damage insults and protective effects were mediated by restoring

NAD^+ levels. In two additional studies, NMN was found to overcome NAD^+ decline, induced by age-associated increases in PARP activation (80, 194). As discussed, NMN is degraded to NR or NA and brought into the cell through their respective transporters. Consequently, additional signalling pathways may be involved in the reported protection.

In vascular aging, NAD^+ levels are also compromised. Vascular pathology is associated with chronic oxidative stress (65, 226-228) that can induce NAD^+ depletion (194-196). There are many molecular pathways that may be contributing to decreased NAD^+ levels including PARP activation, declining NAMPT expression, nutritional deficiencies, etc. Notably, all of these pathways centre on vulnerability of NAD^+ supply systems in aged tissues. Currently no studies directly addressed the therapeutic potential of elevating NAD^+ levels in vascular cells or models of vascular aging.

NAD^+ precursor supplementation offers a potential mechanism to elevate NAD^+ levels. Currently, there are limitations to NA, Nam and NMN supplementation. The limitation of NMN is an additional step for uptake; NA results in flushing side effect (229, 230), and Nam inhibits SIRT activity (231). NR has the potential to overcome limitations of these precursors while still providing the benefits of elevated NAD^+. Importantly, only NR has been identified as a nutrient naturally present in the human diet. As a nutrient in milk, NR offers a favourable mechanism of absorption into the cell (216). NR has been observed to stably elevate NAD^+ levels, and increase NAD^+ bioavailability in HEK293, Neuro2a, AB1, C2C 12 and Hepa1.6 mammalian cell lines (232, 233). In addition, NR has potential therapeutic benefits over nicotinamide. Nicotinamide has been reported to negatively affecting SIRT activity, whereas NR increases SIRT activities (233, 234). Further, niacin (consisting of NA and Nam) has been known to induce painful flushing; these side effects may be avoided by instead administering NR (218). The ability of NR delivery to control NAD^+ homeostasis in vascular cells has not been determined.

NR delivery is an emerging field. Within the last decade, it was recognized for facilitating downstream biosynthetic pathways to extend lifespan in yeast (202, 216). Current literature is expanding these findings to determine benefits in vertebras. One of the first in vivo reports identified NR's ability to stably elevate NAD^+ levels in mouse tissue, enhance oxidative metabolism and overcome harmful effects of a high fat diet, mediated by SIRT1 signalling (233). Additionally, this study reported increase mitochondrial biogenesis and increased activity of SIRT3, which resides in the mitochondria. A more recent study reported that NR protected against noise-induced hearing loss in mice, in a SIRT3-dependent pathway (234). Although the mechanism behind this protection was not explored in depth, mitochondrial dysfunction inducing increased ROS is established as a feature of noise-induced hearing loss. Additionally, NR was reported to elevate NAD^+ levels and protect against two distinct models of mitochondrial disease in mice (235, 236). These studies have recently been expanded to human cells; NR delivery and PARP inhibition were reported to restore mitochondrial membrane potential and oxidative activity in human fibroblasts (237). Mitochondrial dysfunction is a hallmark of aging and effective energy metabolism is essential to support repair responses during oxidative insults.

In another study, both PARP inhibition and NR delivery were observed to overcome neurodegeneration-associated phenotypes induced by mutations to DNA repair proteins (238). Interestingly, this study looked at NRs effect on the transcriptome of diseased mice and found that NR normalized gene ontology terms for DNA damage repair, DNA damage response and oxidative stress. Additionally, NR delivery has been reported to prevent DNA damage and tumor formation in a model of mouse hepatocellular carcinoma (239). However, the direct effects of NR on DNA damage repair have yet to be explored. Vascular aging is associated with oxidative-stress-induced

DNA damage and PARP activation. Therefore, these studies support rationale to explore NR delivery in vascular cells and oxidative stress models.

In summary, vascular aging is associated with chronic oxidative stress (65, 226-228). Oxidative-stress-induced DNA damage will activate PARP and NAD^+ consumption pathways (194-196). Thus, there is growing appreciation for the impact of NAD^+ biology in aging to maintain oxidative stress responses. In aging, the supply of NAD^+ is particularly vulnerable due to constitutive PARP activation, declining NAMPT expression, and relative nutritional deficiencies. NR delivery is an emerging intervention to combat this NAD^+ deficiency. Current literature has reported that NR will elevate NAD^+ levels to promote mitochondrial health and protect against metabolic disease (233-237). Some reports have indirectly linked NR to oxidative stress response and DNA damage repair pathways in diseased mouse models (238, 239). However, the role of NR delivery in these pathways remains unclear. Additionally, the potential benefit of NR delivery on vascular cells is currently unknown.

1.5 Aims and Hypothesis

I hypothesize *that control over NAD^+ homeostasis in vascular cells can be obtained by delivery of nicotinamide riboside and that this imparts resistance to oxidative stress insults with enhanced repair of DNA damage.*

To test this hypothesis, I will address two aims:

1. To determine if exogenous delivery of NR increases NAD^+ content in endothelial cells and smooth muscle cells, at baseline and following acute oxidative stress.
2. To determine if NR delivery improves viability of vascular cells subjected to oxidative stress and imparts resistance to DNA damage and premature senescence.

2 – MATERIALS AND METHODS

2.1 Reagents

High capacity cDNA reverse transcription kit and TaqMan real-time quantitative PCR reagents including primer probes were from Applied Biosystems (Streetsville, ON). Qualitative PCR reagents, cell culture reagents, HAEC cell line, SYBR-safe, lipofectamine RNAiMAX Reagent and goat anti-mouse Alexa Fluor 546 were from Life Technologies (Burlington, ON). Agarose was from BioShop (Burlington, ON). Nicotinamide Riboside from High Performance Nutrition (Newport Beach, CA). Anti-PAR polymer mouse monoclonal antibody was from Trevigen (Gaitherburg, MD). Hydrogen peroxide was from VWR International (Mississauga, ON). Comet Assay reagents and EGM-2 SingleQuots were from Cedarlane (Burlington, ON). Triton-X from EMD Millipore (Billerica, MA). Phenazine ethosulfate, Nrk1 (E-13) antibody and Nrk1 (m) 293T lysate were from Santa Cruz Biotechnology (Santa Cruz, CA). RNAeasy Mini Kit and SYBR Green PCR master mix were from QIAgen (Maryland, USA). Anti 8-Hydroxydeoxyguanosine monoclonal antibody was from Northwest Life Science Specialties (Vancouver, WA). Alexa Fluor 488 Phalloidin dye was from Cell Signalling Technology Inc. (Danvers, MA). Primers for qualitative PCR & SYBR Green PCR, lysis buffer and NAD^+ assay reagents were from Sigma-Alderich (St. Louis, MO).

2.2 Global *Nampt* knockout mice

Inducible global *Nampt* knockout (KO) mice were generated on a C57Bl/6 background. *Nampt*$^{flox/flox}$ mice were crossed with a transgenic mouse line expressing Cre recombinase fused to the mutated ligand binding domain of the human estrogen receptor under the control of a chimeric cytomegalovirus immediate-early enhancer/chicken β-actin promoter (Jackson Laboratories, ME). The knockout was induced by injection with 1 mg/10 g body weight of tamoxifen for 5 consecutive days. Animal procedures were approved by the Western University Animal Care Committee.

2.3 mRNA Extraction From Tissue and Cells

Various tissues, including aorta, brain, heart, liver and skeletal muscle, were harvested from 3-month old wildtype or *Nampt* KO mice perfused with PBS. Samples were placed in 1.5 mL tubes and immediately frozen in liquid nitrogen. A small piece of the tissue sample was then homogenized in Trizol using a motorized pestle and stored in the -80°C freezer overnight.

In the case of cells, media was aspirated from confluent plates which were then washed with PBS. Trizol reagent was added to plates and incubated for 5 min at room temperature. The plate was then scrapped and contents were transferred to a 1.5mL tube.

The following protocol was followed for both tissue and cell samples. After trizol was added to the homogenate, tubes were shaken vigorously and then incubated for 3 min at room temperature. Samples were centrifuged for 15 min at 12,200 rpm at 4°C. The aqueous phase was then transferred to a fresh tube. Part two of the protocol followed QIAgen RNeasy kit instructions. The RNA was then eluted using 30 μL of RNase-free water and a 1 min spin at 12,200 rpm.

2.4 High Capacity cDNA Reverse Transcription

The concentrations and integrity (260/280) of RNA samples were determined by Nano-Drop spectrometry (Wilmington, DE). The volume of RNA to be taken from each sample was calculated to obtain 1 μg of RNA for the reaction. Each sample was added to a 1X master mix without RNase inhibitor, including 1X RT buffer, 1X RT random primers, 10 mM dNTP mix, reverse transcriptase and nuclease-free water. Reverse transcription reaction was run using suggested optimized conditions of 10 min at 25°C, 120 min at 37°C and 5 sec at 85°C on a Eppendorf Master cycler Gradient S thermal cycler.

2.5 Qualitative PCR DNA Amplification

Respective primers were used to amplify various genes within the NAD^+ regeneration pathway including *Nampt, Nmnat1-3* and *Nrk1&2* and the sirtuin family *Sirt1-7*. A mastermix including 1 mM dNTP, 1.5 mM $MgCl_2$, 1 µM reverse and forward primer stocks, 1X PCR buffer, Platinum Taq DNA Polymerase and sterile water was aliquoted into PCR nanotubes to which 100 ng of cDNA was added. The thermal cycler ran 30 cycles with a 58°C annealing temperature for 30 sec, 72°C for 30 sec and 95°C for 30 sec. 36B4 housekeeping gene was used as an internal control. Wildtype kidney sample was used as a positive control in the sirtuin expression profile.

2.5.1 Gel Electropheresis

Gels were prepared using 1XTAE buffer (diluted from 50X TAE made with 24% Tris buffer, 10% 0.5M EDTA at pH 8.0 and 6% acetate), 2% agarose and 3µL SYBR-safe per 50mL of buffer. A 100 bp ladder was used to verify the size of PCR products. Following sufficient separation of amplified products through electrophoresis at 500 A and 100 V, gels were imaged with a UV transilluminator (UVP, Upland, CA).

2.6 Quantitative Real Time-PCR Analysis (TaqMan)

Following reverse transcription, 50 ng cDNA was added to RT quantitative PCR reaction mix consisting of 2X PCR master mix and 20X TaqMan Gene Expression assay. Wildtype and knockout tissue samples were probed for *Nampt* primer (Mm00451934_m1) and normalized to *Gapdh* (Mm03302249_g1). Using a 7900HT Fast Real-Time PCR system with Sequence Detection Systems software version 2.3, relative abundance was determined using the threshold cycle at which amplicons generated are sufficiently above background signal. Samples were run in triplicates.

2.7 Cell Culture

Cells were cultured in 37°C conditions with 5% CO_2 atmosphere. Two cell lines were maintained, Human Aortic Endothelial Cells (HAEC, cell passage 13-21) and HITC6 smooth muscle cells (HSMC, cell passage 26-32).

(1) HSMC, a clonal line derived from human internal thoracic aorta, were grown in M199 +10% FBS, streptomycin/penicillin and L-glutamine and passaged at 90% confluence using 2.5% Trypsin-EDTA. When ready for experiments, cells were split and grown in MEM (custom- without nicotinamide) supplemented with 10% FBS, streptomycin/penicillin and L-glutamine.

(2) HAEC were cultured in M199 +EGM-2 SingleQuots, streptomycin/penicillin and L-glutamine and passaged at 90% confluence using 1: 10 2.5% Trypsin-EDTA. When ready for experiments, cells were plated in MEM (custom- without nicotinamide) supplemented with EGM-2 SingleQuots, streptomycin/penicillin and L-glutamine.

2.8 Western Blot of Nrk1

Cells were grown on a 100 mm plate to 80% confluence in MEM (without nicotinamide). Protein was extracted by incubation with 4°C RIPA buffer (with protease inhibitor cocktail and phenylmethanesulfonylfluoride) for 5 min on ice, and scrapped with a cell scrapper. Lysate was agitated during 15 minute incubation on ice, before being stored in the -80°C freezer for no more than 3 weeks. Protein concentration was assessed using Pierce BSA Protein Assay kit and read at 660 nm on a Thermo Electron Corporation microplate reader with Multiskan Ascent software after 20 min incubation. A gel was prepared: top third consisting of 2% polyacrylamide for stacking and the bottom two thirds of 12% polyacrylamide for resolving. Polymerization with initiated with equimolar ammonium persulfate and TEMED. Protein was then diluted with RIPA to 45 μL to obtain 100 μg

protein in samples and 10 μg protein in positive control. 4X loading dye with 10% β-mercaptoethanol was added to bring the final volume to 60 μL. Samples were loaded and gel was run at 80 V for 2 h. Samples were transferred to a 0.45 μm pore membrane at 110 V for 1 h.

Membrane was blocked with 5% skim milk in TBS buffer with 0.1% Tween 20 (TBS/t) for 1 h at room temperature. The primary goat polyclonal Nrk1 antibody was diluted 1:150 in 5% skim milk TBS/t buffer and left on the membrane overnight at 4°C, while rocking. Membrane was washed 4x 5 min with TBS/t, incubated for 1 h with 1:10,000 secondary donkey anti-goat antibody at room temperature, washed with 4x 5 min TBS/t and developed following a 5 min exposure onto high performance chemiluminescence film (Amersha hyperfilm ECL).

2.9 Determination of Commercial NR structure by NMR

One commercial NR capsule was dissolved in 100% D_2O (5 mg/mL) and run through a 0.2 μm HT Tuffryn membrane. Sample was given to Western Biochemistry NMR facility for a One-Dimensional Proton NMR experiment. NR spectrum was acquired at 25 °C on a Varian INOVA 600-MHz spectrometer equipped with a pulse field gradient triple resonance probe.

2.10 NAD^+ Quantification

This enzymatic cycling assay was previously described by K. Umemura and H. Kimura in 2005 (240).

2.10.1 Experimental Set-Up

For dose-response experiments, HAEC and HSMC were pre-treated for 24 h with 0, 50, 100 or 300 μM NR. For NAD^+ quantification, cells were pre-treated for 24 h with 100 μM NR or 1 h with 20 μM 3,4-Dihydro-5-[4-(1-piperidinyl)butoxyl]-1(2H)-isoquinolinone (DPQ) (or respective vehicle controls). Cells were then subjected to 30 min of 0.25 mM H_2O (HAEC) or 0.2 mM H_2O (HSMC)

with respective pre-treatments. Media was then changed and cells were given 0, 2 or 24 h recovery with respective pre-treatments before NAD^+ was quantified as described below.

2.10.2 NAD/NADH isolation from Cells

For cell culture samples, plates were first washed with PBS and 160 μL of 0°C lysis buffer (10 mM nicotinamide, 20 mM NaHCO3, 100 mM Na2CO3 and 0.05% triton X-100) was added to each well of a 6-well plate. A cell scraper was used to detach the cells. Samples were frozen in a -80°C freezer. Samples were then thawed quickly in a 37°C water bath and promptly chilled to 0°C. The tubes were centrifuged at 12,200 g at 4°C for 5 min and transferred to a new tube. Half of the sample was kept at 4°C to quantify NADt. The other half of the aliquots was incubated at 60°C for 30 min to decompose the oxidized forms of NAD^+, to quantify NADH.

2.10.3 NAD/NADH Quantification

Following extraction of NAD/NADH from cells, 25-40 μL of sample were added to a 96 well plate in duplicates diluted with lysis buffer to a maximum volume of 50 μL/well. NAD^+ was used to produce a standard curve. Fresh reagent mix was prepared (100 mM Tris-CL, 5 mM EDTA-Na4, 0.5 mM 3-[4,5-dimethylthiazol-2-yl]-2,5-diphenyltetrazolium bromide (MTT), 0.2 mg/mL alcohol dehydrogenase and 1.66 mM phenazine ethosulfate) and 100 μL was aliquoted to each well immediately after adding 0.5M ethanol. Following 15-20 min of incubation in the dark, total NAD/NADH and decomposed samples with only NADH were measured by reading the absorbance at 550 nm on a Thermo Electron Corporation microplate reader with Multiskan Ascent software. The NAD/NADH levels were then standardized to the protein level. Protein was assessed using BSA Protein Assay kit and read on the same microplate reader after 20 min incubation. NAD^+ was calculated by subtracting NADH levels from total NAD/NADH.

2.11 Immunostaining

2.11.1 8-oxoguanine

HAEC and HSMC were grown on coverslips in 24-well plates to 50% confluence and subjected to 1 h 0.25 mM and 0.2 mM H_2O_2, respectively.

1) HAEC were washed with cold PBS, fixed with 4% paraformaldehyde for 15 min at RT, and permeabilized in 0.4% Triton-X-100 in PBS for 15 min. Slides were then blocked with 5% BSA for 20 min before incubation with 1:1000 mouse anti 8-hydroxydeoxyguanosine (8-OHdG) monoclonal primary antibody overnight at 4°C. Secondary goat polyclonal anti-mouse 546 Alexa Flour antibody diluted to 1:1000 was left on slide for 20 min at RT. HAEC were then counterstained with 2.5 μg/mL DAPI for 10 min at RT. Slides were then mounted with PermaFluor.
2) HSMC were washed with MEM without serum and fixed with 80% ethanol for 20 min at RT, dehydrated with 100% ethanol for 20 min and incubated in 0.5% Triton-X-100 in PBS for 20 min. Slides were then blocked with 5% goat serum for 20 min before incubation with 1:200 mouse anti 8-hydroxydeoxyguanosine (8-OHdG) monoclonal primary antibody overnight at 4°C. Secondary goat polyclonal anti-mouse 546 Alexa Flour antibody diluted to 1:200 was left on slide for 20 min at room temperature. Slides were then mounted with PermaFluor.

2.11.2 PAR chains

HAEC and HSMC were grown on coverslips in 24-well plates to 70% confluence and subjected to 10 min 0.25 mM and 0.2 mM H_2O_2, respectively. Cells were washed with cold PBS, fixed with 4% paraformaldehyde for 15 min at 4°C and permeabilized with 0.4% triton-X in PBS for 15 min at RT. Cells were blocked with 5% BSA and incubated with 1:500 anti-PAR polymer primary mouse monoclonal antibody in 5% BSA overnight at 4°C. Secondary goat anti-mouse Alexa

Fluor 546 antibody diluted to 1:1000 was left on cells for 30 min at room temperature. Cells were counterstained with 2.5 μg/mL DAPI for 10 min. Coverslips were then mounted with PermaFluor onto microscope slides.

Immunostained cells were imaged using with Northern Eclipse software on an Olympus BX51 microscope.

2.12 Cell Shrinkage and Viability

HAEC and HSMC cells were grown to 80% confluence and pre-treated for 24 h with 100 μM NR or 1 h with 20 μM DPQ (or respective vehicle controls). Cells were then subjected to 4 h treatment with 0.25 mM (HAEC) or 0.2 mM (HSMC) H_2O_2 with respective pre-treatments and imaged using time-lapse Leica Application Suite Advanced Fluorescence software on a Leica DMI 6000B microscope. Immediately following image acquisition, cells were incubated for 5 min with 100% Trypan Blue (0.4%), and dead/alive cells were recorded (N=1 represents a full experiment), which was determined by presence of dye within the cytoplasm. Time-lapse videos were quantified using ImageJ to trace the area of cells at time 0, 2 and 4 h (n=1 represents one cell).

2.13 Actin Cytoskeleton Staining

HAEC and HSMC were grown on coverslips in 24-well plates to 50% confluence, pre-treated with 100 μM NR for 24 h (or vehicle control) and then subjected to 1 h 0.25 mM and 0.2 mM H_2O_2, respectively. Cells were rinsed with PBS at room temperature, fixed with 4% paraformaldehyde for 20 min at 37°C, permeabilized for 5 min with 0.5% Triton-X-100 and stained for 20 min with 1:50 phallodin 488. Slides were then counterstained with 2.5 μg/mL DAPI and mounted with PermaFluor. Slides were imaged using with Northern Eclipse software on an Olympus BX51 microscope.

2.14 Alkaline Comet Assay

2.14.1 Experimental Set-Up

For tail moment analysis following H_2O_2, cells were pre-treated for 24 h with 100 μM NR or 1 h with 20 μM DPQ. Cells were then subjected to 30 min or 1 h treatment with 0.25 mM (HAEC) or 0.2 mM (HSMC) H_2O_2 with respective pre-treatments. Media was then changed and cells were given 0-11 h recovery with respective pre-treatments. Experiment time-line is depicted below. Stars represent time-points when CometAssay was run.

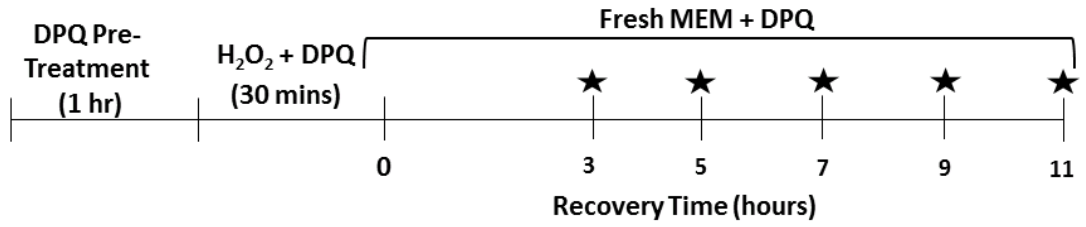

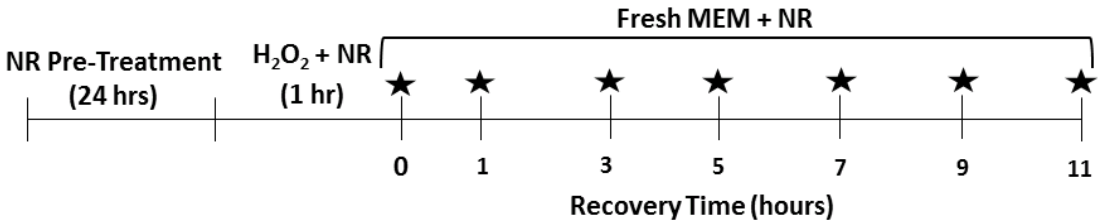

2.14.2 Single Cell Gel Electrophoresis Assay

CometAssay kit was run according to Trevigen's supplied instructions for alkaline comet assay. Briefly, cells were incubated in trypsin for 1 min, neutralized with MEM and spun in a 1.5 mL microtube tube for 5 min at 800 rpm at 4°C in an Eppendorf Centrifuge 5415D. Cells were then re-suspended to $1x10^5$ cells/ mL in cold PBS. Then, 10 μL of cell suspension was plated in 100 μL molten Comet LMAgrose and allowed to chill for 20 min in 4°C fridge. Once chilled, supplied lysis solution was put on gels and incubated overnight in 4°C fridge. Alkaline Unwinding Solution (200 mM NaOH, 1 mM EDTA, pH>13) was left on cells for 20 min at room temperature. Plates were then

transferred to a gel electrophoresis apparatus filled with Alkaline Electrophoresis Solution (300 mM NaOH, 1 mM EDTA, pH>13) on a bed of ice. Samples were run at approximately 300 mA and 17.5 V for 25 min. Plates were then stained for 30 min with 1:10000 SYBR Gold (DMSO vehicle) diluted in TE buffer (10 mM Tris-HCL pH 7.5, 1 mM EDTA). Plates were dried completely and mounted with ProLong Gold Antifade Reagent.

2.14.3 CometAssay Analysis

OpenComet version 1.3 was used for automated analysis of comet assay images (241). This validated open-source software program is a plugin for ImageJ.

2.15 Quantitative Real Time-PCR Analysis (SYBR Green)

The sequences of forward and reverse primers for SIRT1-7 and anti-oxidant genes are listed in appendix A. Expression levels were normalized to the single-copy gene, acidic ribosomal phosphoprotein PO (36B4).The sequence of the 36B4-specific forward (36B4) and reverse (36B4) primers was 5' ACT GGT CTA GGA CCC GAG AAG 3' and 5′TCA ATG GTG CCT CTG GAG ATT 3', respectively.

Each reaction sample contained 5 µL of RT^2 SYBR green master mix with ROX (SAbiosciences, 300 nM of respective primers, 180-500 ng cDNA and nuclease-free water to yield a total volume of 10 µL. Samples were assayed in triplicates on a 384-well plate. The following thermal profile was used 95°C hot start for 10 min, followed by 40 cycles of denaturation at 95°C for 15 sec, and anneal-extension at 60°C for 1 min. The experiment was carried out using a ViiA7 PCR machine (Life Technologies, Burlington, ON). The data were exported to Microsoft Excel and the ΔΔCt was calculated for each sample to compare expression levels changes to control.

2.16 siRNA Transfection to knockdown SIRT1-7

HAEC and HSMC were grown in a 24-well plate (cell-shrinkage, viability and senescence experiments) or 12- well plate (tail moment analysis) to 70% confluence. For 24-well plate, 5 pmol respective siRNA and 1.5 μL Lipofectamine RNAiMAX in 50 μL Opti-MEM Medium was added to each well. These values were doubled per well for 12-well plates. Cells were incubated with transfection reagents for 48 h with 100 μM NR. Media was changed to fresh media with 100 μM NR for 24 h before use in cell shrinkage, viability and tail moment experiments.

2.17 Senescence Associated β-Gal

HAEC and HSMC were grown on coverslips in 24-well plates to 50% confluence, pre-treated with 100 μM NR for 24 h or 1 h 20 μM DPQ (or respective vehicle controls) or siRNA transfection protocol section 2.15. Cells were then subjected to 1 h 0.025 mM (HAEC) and 0.02 mM (HSMC) H_2O_2 and given 48 h recovery in fresh media. Cells were then rinsed with PBS, fixed for 3 min (fixative: 2% formaldehyde & 0.2% gluteraldehyde in PBS) and stained for 6 h at 37°C without CO_2 (staining solution: 5 mM potassium ferrocyanide, 5 mM potassium ferricyanide, 150 mM NaCl, 2 mM MgCl, 40 mM sodium citrate, 1 mg/mL X-Gal (dissolved in DMSO), pH 6.0 with NaH_2PO_4). Coverslips were then mounted with PermaFluor.

Cells were imaged using Northern Eclipse software on Olympus BX51 microscope. Positive cells were determined using threshold function on ImageJ and compared to total cells in each field of view (n=1 represents one field of view).

2.18 Statistical Analyses

Statistical differences ($P < 0.05$) were determined by using Graphpad Prism software version 6.0. One-Way ANOVA was used to assess the effects of one independent variable on a dependent variable. This test was followed by Dunnett's Multiple Comparison Test when all groups were

compared to one control group or Tukey's Multiple Comparison Test when every group was compared to every other group. Two-Way ANOVA was used for grouped analysis when the effects of two independent variables were assessed. This test was then followed by either Tukey's Multiple Comparison Test when every paired group was compared to every other paired group or Sidak's Multiple Comparison Test when sets of paired groups were compared. The statistical test used is outlined in figure legends, corresponding to their respective experiments.

3 - RESULTS

3.1 NAD^+ Deficient Environment Upregulates Nrk1 mRNA Abundance

Previous studies have reported increased uptake and metabolism of NR under NAD^+ deficient conditions caused by low availability of alternative NAD^+ precursors (202, 242). This finding sets the stage for testing the effect of NR delivery in aging models, where NAD^+ levels are reported to decline (195, 196). Our lab has created an NAD^+ deficient environment in mice through a tamoxifen-induced Cre/lox *Nampt* knockout mouse model. Nampt is the rate-limiting enzyme in the NAD^+ salvage pathway (Fig. 1.6), and its knockout leads to a decline of tissue NAD^+ content.

To determine the effect of NAMPT knockout on mRNA abundance of NAD^+ salvage enzymes, I harvested tissue from *Nampt*-deficient mice and their wild-type littermates and isolated the mRNA. To confirm that *Nampt* was in fact depleted, I used real-time PCR. This revealed that *Nampt* levels decreased in aorta, brain, heart and skeletal muscle following injection with 1mg/10g body weight of tamoxifen for 5 consecutive days. The observed changes varied in a tissue-specific manner (Fig. 3.1A). This variability might be attributed to differential tamoxifen accessibility, Cre expression or cell turnover in tissue (243). Next, I compared the abundance of NAD^+ salvage enzyme mRNA transcripts in *Nampt* KO to wild-type littermates using reverse transcription-quantitative PCR (RT PCR). This revealed differential regulation of NAD^+ salvage enzyme expression in low NAD^+ conditions (Fig. 3.1B). Specifically, I observed a striking up-regulation of *Nrk1* expression in aorta, brain and heart, with little to no change in expression of NMNAT 1-3 and Nrk2.

For this vascular focused project, I specifically noted changes in the aorta tissue, comprising endothelial and smooth muscle cells. Following injection with tamoxifen, I used real-time PCR to asses *Nampt* KO and I observed a drop to 70% of baseline aortic *Nampt* mRNA levels (Fig. 3.1A). A distinct up-regulation in *Nrk1* and possibly a decrease in *NMNAT 2* expression are also seen, using quantitative RT PCR (Fig. 3.1B).

In light of previously reported tissue-specific preferential NAD^+ salvage pathways (204), I compared the wild-type expression profile of NAD^+ enzymes between aorta and other tissues. RT PCR was used and I found that aorta tissue expressed a full spectrum of NAD^+ salvage enzymes, however tissue-dependent differences were also revealed (Fig. 3.1B). There was lower expression of *Nrk1*, under normal NAD^+ conditions, as compared with heart, skeletal muscle, liver and kidney. The expression of *Nrk2* in aorta was lower than in heart and skeletal muscle, which is consistent with its identification as a muscle integrin β1 binding protein that regulates cell adhesion and laminin deposition in myoblasts (217). Also interesting to note was the strong expression of NMNAT 2 in wild-type brain tissue, consistent with previous reports (244).

The sirtuin family of enzymes are histone deacetylases that consume NAD^+ to regulate cell survival and stress response pathways (245). To determine if their expression was effected by low NAD^+ conditions, I used the same tamoxifen-induced Cre/lox *Nampt* knockout mouse model used in Fig. 3.1 A&B. Following tamoxifen injection, tissues were isolated and RT PCR was used to assess the levels of *Sirt 1-7* mRNA in tissues from *Nampt* KO mice and their wild-type littermates. I found that the mRNA levels of all seven sirtuins remained unchanged (Fig. 3.1C). Also interesting to note is the ubiquitous expression of *Sirt 1-7* across all of the mouse tissues examined. Specifically, aorta tissue showed robust *Sirt1*, *Sirt2* & *Sirt6* expression and lower levels of *Sirt4*, *Sirt5* & *Sirt7* mRNA.

Figure 3.1 Expression profile of enzymes within the NAD^+ regeneration pathway and sirtuin family of enzymes in *Nampt* knockout mouse tissues and wild-type littermates. RNA transcripts from mouse aorta, brain (frontal cortex), heart, liver, skeletal muscle (hind limb) and kidney tissue were harvested, isolated and reverse transcribed to cDNA. **(A)** The cDNA was amplified by quantitative real-time PCR. *Nampt* mRNA is presented as a ΔΔct comparison of knockout mouse sample transcript expression to wild-type littermates (n=3). **(B)** The cDNA was amplified by RT PCR using primers specific for *Nmnat 1-3*, *Nrk1*, *Nrk2*, *Nampt*, and *36B4*, the latter a housekeeping gene used as an internal control for comparison. Products were resolved on a 2% agorose gel by gel electrophoresis. **(C)** Primers specific for *Sirts 1-7* were used to amplify cDNA by RT PCR. The positive control is mouse wildtype kidney tissue, found to be ubiquitously expressed in all *Sirts* in preliminary data. The negative control is a non-template control. [WT- wildtype, KO- Knockout, Skel. M.- skeletal muscle, NTC- non-template control, +ve- Positive, -ve- Negative]

A

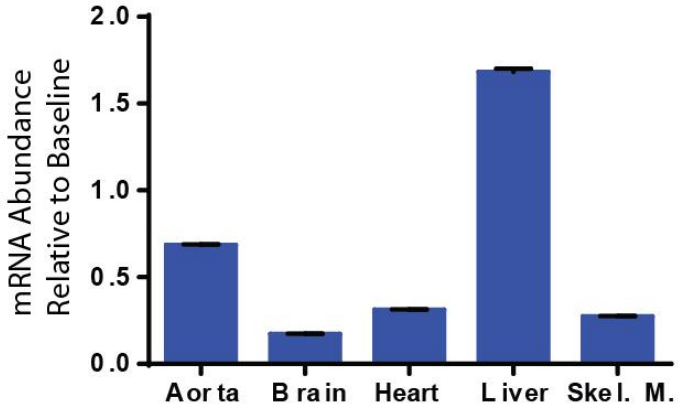
mRNA Abundance
Relative to Baseline
2.0
1.5
1.0
0.5
0.0
Aorta
Brain
Heart
Liver
Skel. M.

B

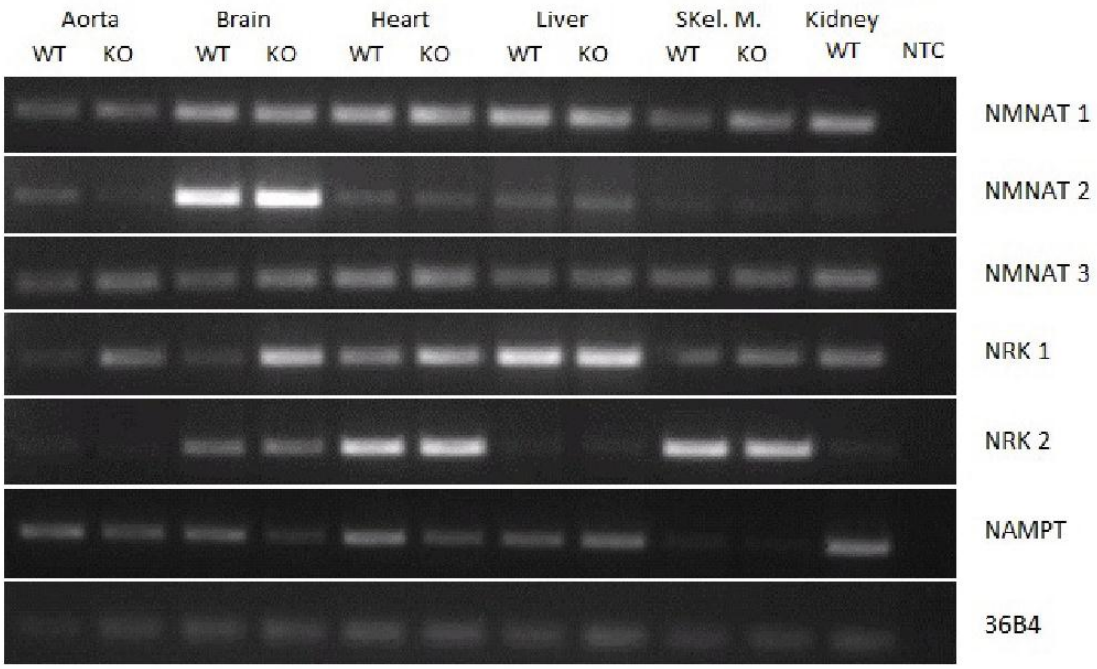
Aorta
Brain
Heart
Liver
SKel. M.
Kidney
WT KO WT KO WT KO WT KO WT KO WT NTC
NMNAT 1
NMNAT 2
NMNAT 3
NRK 1
NRK 2
NAMPT
36B4

C

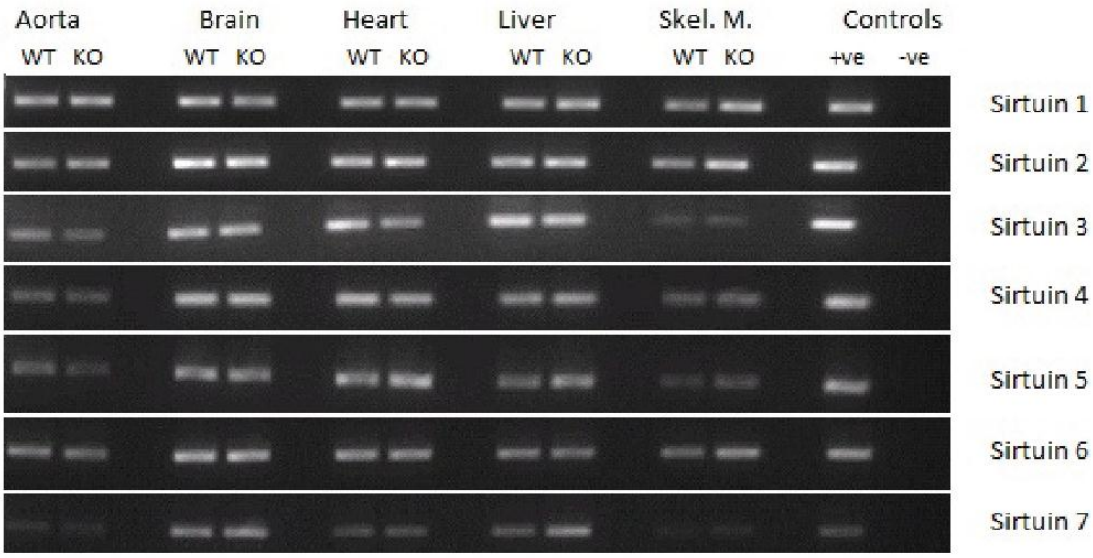
Aorta
Brain
Heart
Liver
Skel. M.
Controls
WT KO WT KO WT KO WT KO WT KO +ve -ve
Sirtuin 1
Sirtuin 2
Sirtuin 3
Sirtuin 4
Sirtuin 5
Sirtuin 6
Sirtuin 7

3.2 NR Delivery Increases NAD^+ Content in a Dose-Dependent Manner

Direct entry of NR into the NAD^+ salvage pathway depends on both a functional uptake transporter to bring NR into the cell and on Nrk1 to catalyze the phosphorylation of NR to NMN (202). I examined NR delivery into vascular cells, using human aortic endothelial cells (HAEC) and human smooth muscle cells (HSMC). Acting on the evidence delineated above for preferential NR salvage in NAD^+-depleted conditions, vascular cells were plated in NAD^+ precursor free MEM media with cell-specific supplements for experiments. However, to maintain normal growth prior to experiments, cells were cultured in regular growth media for passages.

To determine if Nrk1 is expressed in vascular cells, I assessed mRNA and protein abundance. To do this I used quantitative real-time PCR analysis using primer probe for human *Nrk1* and I confirmed that HSMC and HAEC express *Nrk1* mRNA (ct=26.262, 24.823, respectively). To assess Nrk1 protein abundance, I used a Western Blot, which revealed a 23 kDa protein comparable to a positive control of mouse NRK1 transfected whole cell lysate (Fig. 3.2A). The difference in molecular weight of the expressed protein compared to positive control may be accounted for by human versus mouse splice variants. Using protein BLAST, NRK1 Mus musculus sequence was run and found to have significant alignment with NRK1 isoform 1 Homo sapiens (81% identity) and NRK1 isoform 2 Homo sapiens (69% identity). The differences in position and alignment of amino acid residues may account for the observed difference in molecular weight.

Exogenous supplementation of NR has been reported to increase cellular NAD^+ levels in a dose-dependent manner in yeast, mouse myoblast, mouse heptoma and human embryonic kidney cell lines (202, 233). An increase in intracellular NAD^+ levels in response to NR supplementation would confirm that NR could be brought into vascular cell and metabolized to NMN, thereby entering the NAD^+ salvage pathway. To assess these foundations for NR delivery in vascular cells, I incubated

HAEC and HSMC with 50-300 μM NR for 24 h. NAD^+ levels were quantified through an enzymatic cycling assay, developed from a published protocol (240). Intracellular NAD^+ levels in HAEC significantly increased by 26±3%, 35±4% and 41%±2 ($p<0.0001$) in response to 50, 100 and 300 μM NR, respectively (Fig. 2B). In HSMC, an increase of 34±9% ($p=0.33$), 62±9% ($p=0.02$) and 80±30% ($p=0.002$) in NAD^+ levels was observed in response to 50, 100 and 300 μM NR, respectively. These findings suggest a functional Nrk1 was present and established that NR supplementation increased NAD^+ content in vascular endothelial and smooth muscle cells.

3.3 Source for NR Supplementation

When this project began three years ago, there were limited options for acquiring NR. Preliminary dose-response experiments used NR purchased from Toronto Research Chemicals, which was very costly. As the project expanded, a more cost-effective and abundant supply of NR was needed. I partnered with the Shilton Lab to synthesize NR using a previously published protocol (246). The purity of this synthesized NR was confirmed using one dimentional-^{1}H spectrum analysis (data not shown). This source of NR was less costly; however it was labour intensive and time-consuming for the Shilton Lab. Both of these sources of NR were used to generate reproducible dose-response curves, reported in Fig. 3.2. The synthesized NR was then used for preliminary cell shrinkage, viability and NAD^+ quantification experiments, discussed later.

Within the last year, commercially available NR supplements have emerged on the market, offering a cost-effective and abundant source of NR. I decided to switch sources of NR from synthesized NR to the commercial NR capsules to: i) reproduce results using an additional source of NR; ii) use a source of NR readily available to the public; and iii) build foundations for future in vivo work. To determine the purity of commercially available NR, as well as its stability following preparation for experimental use, a sample of NR was given to Western Biochemistry NMR facilities

for one dimentional-^{1}H spectrum analysis. NR extracted from a commercially available capsule (NIAGEN® ChromaDex, purchased from High Performance Nutrition) was dissolved in 100% D_2O to avoid the interfering signal caused by H_2O. According to the spectrum analysis, the purity of NR was found to be 92%, using previous literature for proton assignment (Fig. 3.2D) (232). The calculated integrals of the less intense peaks in the 8.0-9.6 ppm region represent impurity of 8.4±1.4%, possibly arising from nicotinamide. The less intense peaks in the lower ranges may have been caused by debris from the filter, used to prepare NR capsules for experimental use. Speculations on the source of impurity cannot be confirmed by this proton spectrum.

The commercial source of NR was then used to reproduce preliminary data generated by the synthesized NR (Fig. 3.4 and 3.5). Once its protective effects on cell shrinkage and viability were confirmed, the commercial source of NR solely was used for the remaining experiments.

Figure 3.2 Model for NR delivery in vascular cells. (A) Western blot of HSMC and HAEC (40 μg protein) probed with goat polyclonal Nrk1 antibody and compared to positive control from mouse Nrk1 transfected whole cell lysates (10 μg protein). (**B-C)** Graphs show effects of NR supplementation on NAD^+. Cells were cultured in NAD^+-precursor-free MEM media. NAD^+ was extracted from cells and levels were quantified using an enzymatic cycling assay, 24 h following 0-300 μM NR supplement to HAEC, mean ± SEM (n=6) (**B**) and HSMC, mean ± SEM (n=9) **(C)**. *Significant compared to control ($p<0.05$) using One-way ANOVA and Tukey's Multiple Comparison Test of the means. (**D)** One-dimensional proton spectrum of commercially available NR (5 mg/mL) in 100% D_2O. The H's are assigned to the spectrum according to the structure of NR, displayed in the top-right corner of **(D)**. The bonding pattern of each hydrogen to its surrounding atoms determined its resonance in the magnetic field, reported in ppm.

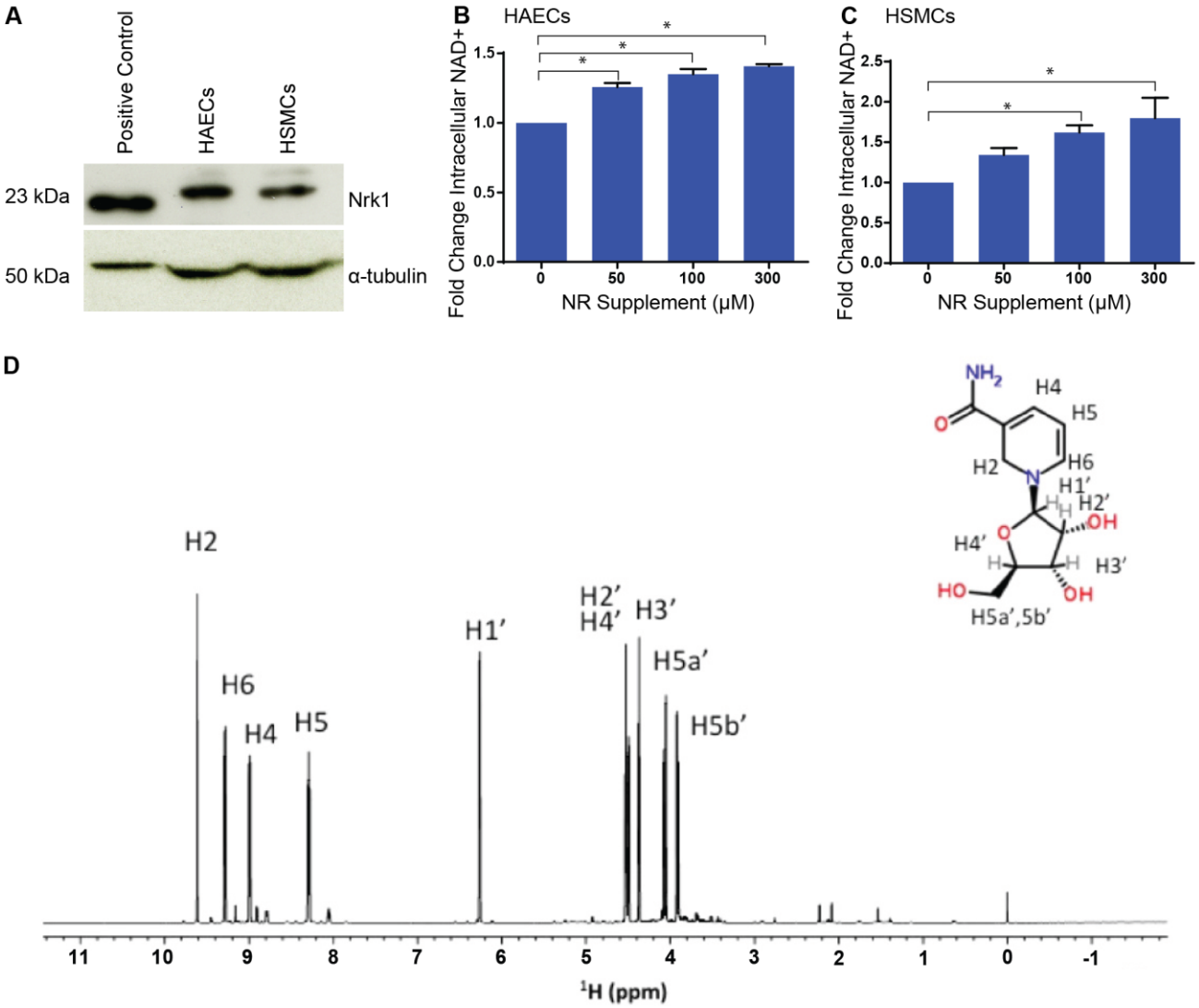
A
Positive Control
HAECs
HSMCs
23 kDa
Nrk1
50 kDa
α-tubulin
B
HAECs
Fold Change Intracellular NAD+
NR Supplement (μM)
C
HSMCs
Fold Change Intracellular NAD+
NR Supplement (μM)
D
H2
H6
H4
H5
H1′
H2′
H4′
H3′
H5a′
H5b′
H5a′,5b′
¹H (ppm)

3.4 Acute Oxidative Stress Induces PARP-Dependent NAD^+ Depletion

To induce oxidative stress in vascular cells, I selected hydrogen peroxide (H_2O_2). This was chosen because it is a physiologically relevant stress, it is increased in aged tissues, and this results in oxidative lesions, NAD^+ consumption and senescence (65). An acute dose was used in sections 3.4-3.10 for proof of concept to assess NRs protective capacity against oxidative stress insults. I used preliminary cell shrinkage dose-response curves to select a dose of H_2O_2 at which the most prominent protection was observed by NR (data not shown). From this preliminary data, HSMC were found to be more sensitive to oxidative stress, requiring a slightly lower H_2O_2 dose to produce a response similar to HAEC. The selected dose of 0.25 mM for HAEC and 0.2 mM for HSMC was in the same range as previous in vitro vascular studies (120).

Previous reports have associated oxidative stress with a decline in NAD^+ levels, attributed to the activation of PARPs, a major NAD^+-consuming enzyme, in response to oxidative DNA lesions (194-196). To determine if an acute oxidative stress insult lead to the formation of oxidative DNA lesions in vascular cells, I used a 1 h H_2O_2 insult. This induced persistent oxidative lesions, assessed by 8-oxo-guanine positive staining in both cell types (Fig. 3.3A,B).

PARP has been reported to recognize DNA lesions and catalyze the formation of PAR chains at the site of damage (111). Next, to assess PARP response to the formation of these oxidative lesions, I used the same acute H_2O_2 insult and immunofluorescence against α-PAR. At 10 min, almost immediately after H_2O_2 insult began, nuclear PAR-chain accumulation was visible in both vascular cell types through immunofluorescence for α-PAR, which was confined to the nucleus (Fig. 3.3C). To confirm that this response was PARP1 dependent, PARP1 specific inhibitor, 3,4-Dihrdro-5-[4-(1-piperidinyl)butoxyl]-1(2H)-isoquinolinone (DPQ) was used. Ten minutes after H_2O_2 insult,

nuclear α-PAR staining was abolished by the presence of DPQ (Fig. 3.3C). Thus, H_2O_2 induced oxidative DNA lesions and PAR-chain formation, in a PARP-dependent manner.

I then examined the NAD^+ levels in this oxidative insult model. By 30 min of H_2O_2 insult, H_2O_2 had induced an 86±8% drop in intracellular NAD^+ levels in HAEC (Fig. 3.3D) and a 55±5% drop in HSMC (Fig. 3.3E). PARP1 has been reported to account for 90% of PARP-dependent NAD^+ consumption (111). To determine if the NAD^+ decline was due to PARP1 activation, cells were pre-treated for 1 h with DPQ and incubated with DPQ for the duration of the experiment. By 30 min, this revealed that PARP1 inhibitor (DPQ) significantly blocked the drop in NAD^+ levels, observed by 68±3% of baseline NAD^+ levels in HAEC (P=0.0002) and 74±7% in HSMC (p=0.03). By 2 and 24 h following H_2O_2 insult, NAD^+ levels in vehicle control group were restored to baseline levels in both cell types in a time-dependent manner. Similarly, DPQ-treated groups also restored NAD^+ levels to baseline. This established H_2O_2-induced oxidative lesions resulting in PARP activation and PAR-chain formation, in parallel with NAD^+ consumption in vascular cells.

Figure 3.3 H_2O_2-induced oxidized DNA lesions, PAR-chain accumulation and NAD^+ depletion in vascular cells. **(A)** HAEC and **(B)** HSMC were exposed to 1 h 0.25 mM and 0.2 mM H_2O_2 insult. Cells were then fixed with 80% EtOH, dehydrated with 100% EtOH and permeabilized with 0.4% Trtion-X in PBS and stained with 1:200 8-oxo guanine primary antibody (red). HAEC, but not HSMC, were counter-stained with 2.5 μg/mL DAPI (blue). Exposure to H_2O_2 induced oxidative lesions within the nuclei, visualized by red fluorescence. **(C)** HAEC and HSMC were exposed for 10 min with 0.25 mM and 0.2 mM H_2O_2, respectively, following pre-treatment for 1 h with 0.8% DMSO or 20 μM DPQ. Cells were then fixed using 4% paraformaldehyde, permeabilized with PBS + 0.4% triton X, immunostained with 1:1000 α-PAR primary antibody (red) and counter-stained with 2.5 μg/mL DAPI (blue). Exposure to H_2O_2 induced PAR-chain accumulation within the nuclei, visualized by red fluorescence. Pre-treatment with DPQ reduced accumulation of PAR-chains and image resembles that of control cells without H_2O_2 treatment. Bar on bottom right of images represents a 50 micron scale. **(D-E)** Cells were grown in NAD^+-precursor-free MEM media. NAD^+ was extracted from cells and levels were quantified using an enzymatic cycling assay. **(D)** HAEC, mean ± SE (n=3) and **(E)** HSMC mean ± SE (n=6) were pre-treated for 1 h with 0.8% DMSO or 0.2 μM DPQ and then exposed to 30 min of 0.25 or 0.2 mM H_2O_2, respectively. At 0, 2 or 24 h after H_2O_2 insult, cells were harvested and NAD^+ content was analyzed. *Significantly different than corresponding vehicle control group ($p<0.05$, using Two-Way ANOVA and Sidak's Multiple Comparison Test of the means). ** Blue bars only, significant differences between indicated groups ($p<0.05$, using Two-Way ANOVA and Sidak's Multiple Comparison Test of the means). There were no significant differences between 0 h and 2 h time points for both red and blue bars.

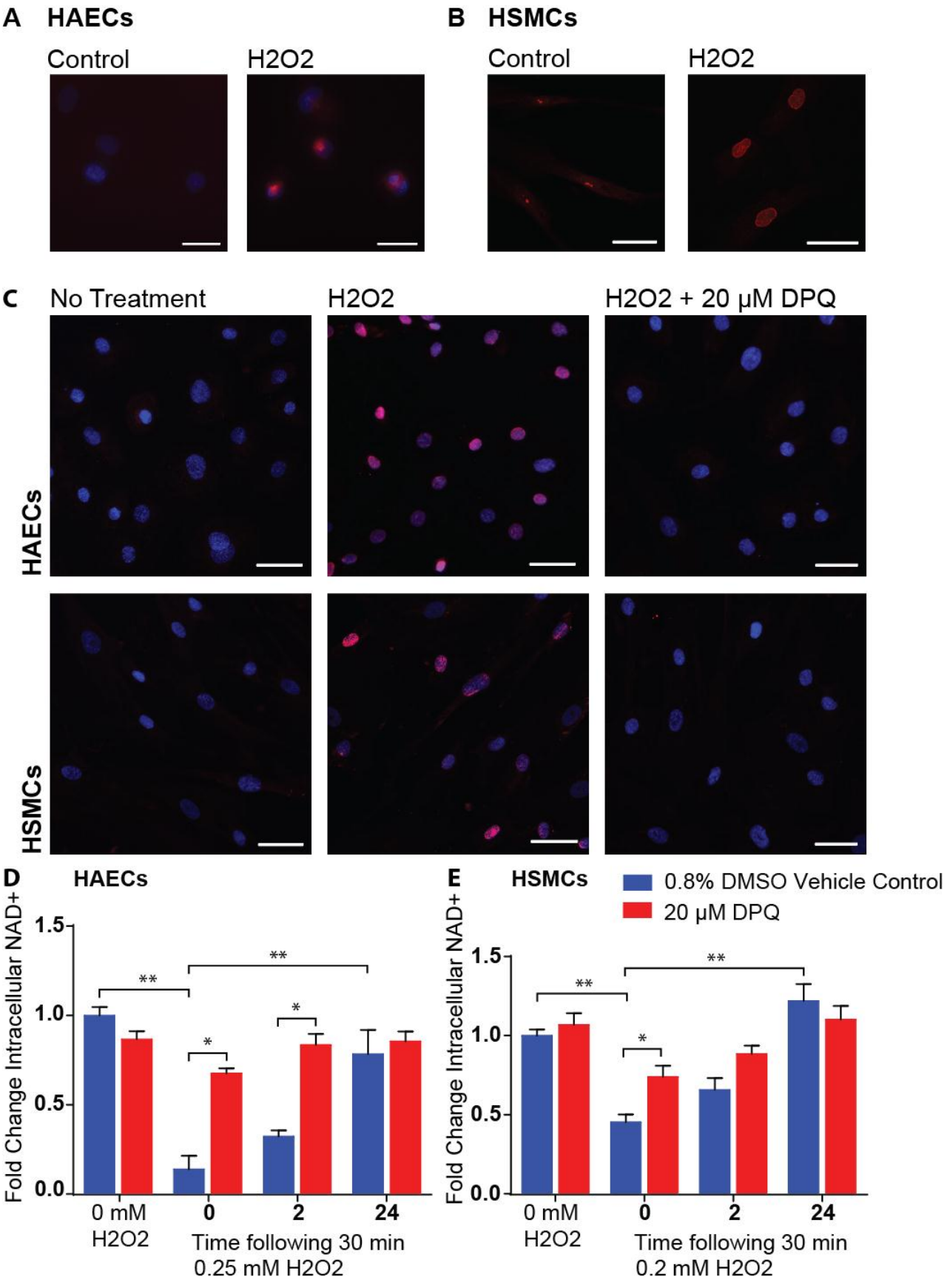
A HAECs
Control
H2O2
B HSMCs
Control
H2O2
C
No Treatment
H2O2
H2O2 + 20 μM DPQ
HAECs
HSMCs
D HAECs
Fold Change Intracellular NAD+
1.5
1.0
0.5
0.0
**
**
*
*
0 mM H2O2
0
2
24
Time following 30 min 0.25 mM H2O2
E HSMCs
0.8% DMSO Vehicle Control
20 μM DPQ
Fold Change Intracellular NAD+
1.5
1.0
0.5
0.0
**
**
*
0 mM H2O2
0
2
24
Time following 30 min 0.2 mM H2O2

3.5 NR buffers NAD^+ content, preserves morphology integrity and increases cell survival after oxidative stress insult

To determine if NR could provide vascular cells with a reserve of NAD^+ to sustain the NAD^+ consumption associated with acute oxidative insults, I pre-treated cells for 24 h with NR and quantified NAD^+ levels. Consistent with Fig. 3.2B&C, pre-treatment with NR supplements provided a reserve of intracellular NAD^+ by significantly increasing baseline levels by 38±8% in HAEC ($p=0.0006$) and 40±7% in HSMC ($p=0.0014$) (Fig. 3.4A). Next, I confirmed that the response to H_2O_2 was similar to previous experiments. I exposed cells to 30 min H_2O_2 and quantified NAD^+ levels at 0, 2 and 24 h after the insult. Consistent with Fig. 3.3A&B, NAD^+ levels again declined in response to H_2O_2 by 87±4% in HAEC (Fig. 3.4A) and 68±6% in HSMC (Fig. 3.4B).

Next I assessed NRs effect on NAD^+ consumption and regeneration following an oxidative stress insult. NR-treated groups dropped a similar absolute value compared to vehicle controls of 73% in HAEC and 55% in HSMC. The NAD^+ reserve from NR supplements provided a buffer following H_2O_2 insult, with NAD^+ levels immediately following the insult being higher than vehicle control by 3-fold in HAEC ($p=0.051$) and 2-fold in HSMC ($p=0.02$). During the following 2 h and 24 h repair, NAD^+ levels returned to their baseline levels in both cell types in a time-dependent manner. Importantly, the increase in NAD^+ content above baseline conferred by NR in a given treatment group remained higher than untreated groups throughout the time-course experiment.

To further assess NR's protective capacity, cells were subjected to H_2O_2 for 4 h, and their morphology and viability was tracked. In preliminary experiments, I found that this more prolonged exposure to H_2O_2 was required to compromise morphology and viability. The longer exposure likely sufficiently depleted NAD^+ stores, which resulted in notable NR protection in this model. Time-lapse video microscopy was used to track individual cells and changes in area were quantified at 0, 2 and 4

h. Following exposure to H_2O_2, both HAEC and HSMC appeared to shrink and cytoplasmic blebs were visible in vehicle-exposed cells (Fig. 3.5 A,B&G,H). However, following NR supplementation, many cells maintained their shape and size. A small subset of cells still strikingly shrunk (Fig. 3.5 C,D&I,J). Quantification of cell area using image J revealed a two-fold reduction in cell-shrinkage at 4 h of H_2O_2 exposure, as compared to baseline in HAEC and HSMC ($p<0.0001$) (Fig. 3.5 F&L).

To determine NRs ability to protect cell viability, vascular cells pre-treated with NR were exposed to 4 h acute H_2O_2 insult and viability was quantified through trypan blue exclusion assay. This assay was chosen because it could be used immediately following the time-lapse experiment to assess cell death on the same population of cells used for morphology and cell shrinkage analysis. This revealed significantly greater viability in the presence of NR- 60±10% versus 35±8% in vehicle control in HAEC ($p=0.039$) and 84±6% compared to 63±9% in vehicle control in HSMC ($p=0.049$) (Fig. 3.5E&K).

Figure 3.4 NR buffers H_2O_2-induced consumption of intracellular NAD^+ levels. Cells were grown in NAD^+-precursor-free MEM media. NAD^+ was extracted from cells and levels were quantified using an enzymatic cycling assay. **(A)** HAEC mean ± SE, (n=12) and **(B)** HSMC mean ± SE, (n=15) were pre-treated for 24 h with 100 μM NR supplement or vehicle and then given 0, 2 or 24 h recovery following treatment with 30 min 0.25 or 0.2 mM H_2O_2, respectively. * Significantly different than corresponding vehicle control group ($p<0.05$, using Two-Way ANOVA and Sidak's Multiple Comparison Test of the means). ** Blue bars only, significant differences between indicated groups ($p<0.05$, using Two-Way ANOVA and Sidak's Multiple Comparison Test of the means).

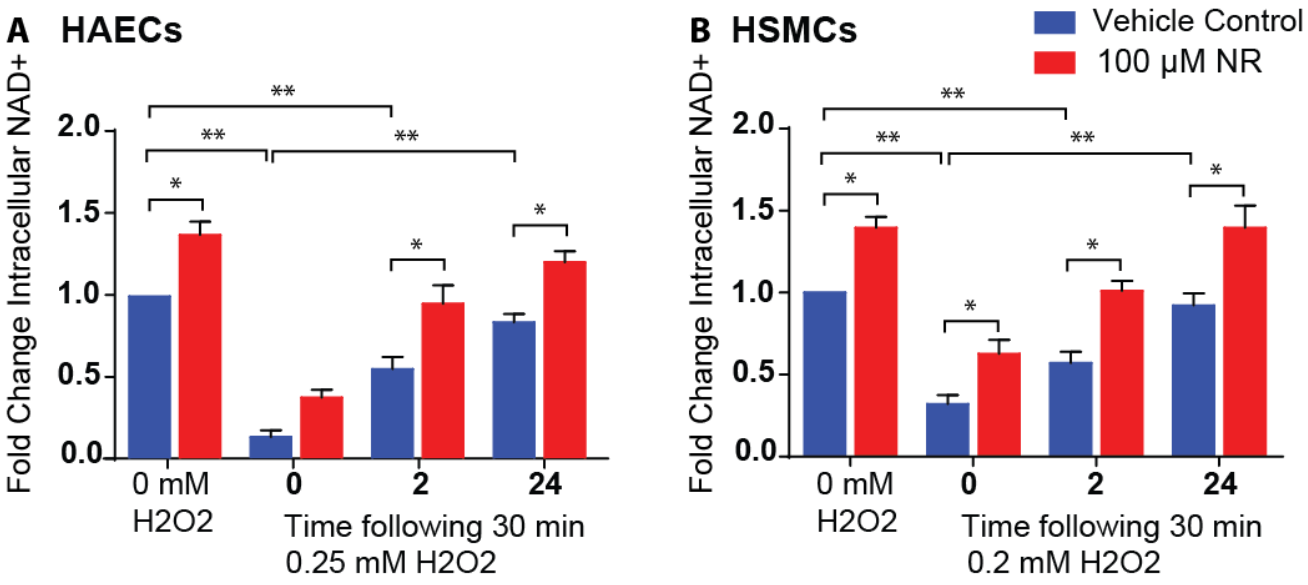
A HAECs
Fold Change Intracellular NAD+
2.0
1.5
1.0
0.5
0.0
**
**
**
*
*
*
0 mM H2O2
0
2
24
Time following 30 min 0.25 mM H2O2
B HSMCs
Vehicle Control
100 μM NR
Fold Change Intracellular NAD+
2.0
1.5
1.0
0.5
0.0
**
**
**
*
*
*
*
0 mM H2O2
0
2
24
Time following 30 min 0.2 mM H2O2

Figure 3.5 H_2O_2-induced cell shrinkage and cell death is attenuated by NR delivery in vascular cells. HAEC and HSMC, pre-treated for 24 h with NR, were exposed to 0.25 and 0.2 mM H_2O_2, respectively, and imaged live using time-lapse Hoffman modulated contrast microscopy for 4 h. **(A-D)** HAEC and **(G-J)** HSMC images corresponding to baseline (0 h) and 4 h after respective H_2O_2 dose was added (4 h), with NR pre-treatment or vehicle. Fold change in area (±SE), measured by tracking cells and tracing border in Image J was recorded for **(E)** HAEC (n=192-224) and **(K)** HSMC (n=128). * Shows significantly higher cell shrinkage than untreated control and significantly less cell shrinkage than cells not pre-treated with NR ($p<0.05$, using Two-Way ANOVA and Tukey's Multiple Comparison Test of the means). Trypan Blue exclusion (viability ±SE) was quantified in cells 4 h post-insult for **(F)** HAEC (N=10) and **(L)** HSMC (N=8). * Shows significantly lower viability than untreated control and significantly greater viability than cells not pre-treated with NR ($p<0.05$, using One-Way ANOVA and Tukey's Multiple Comparison Test of the means).

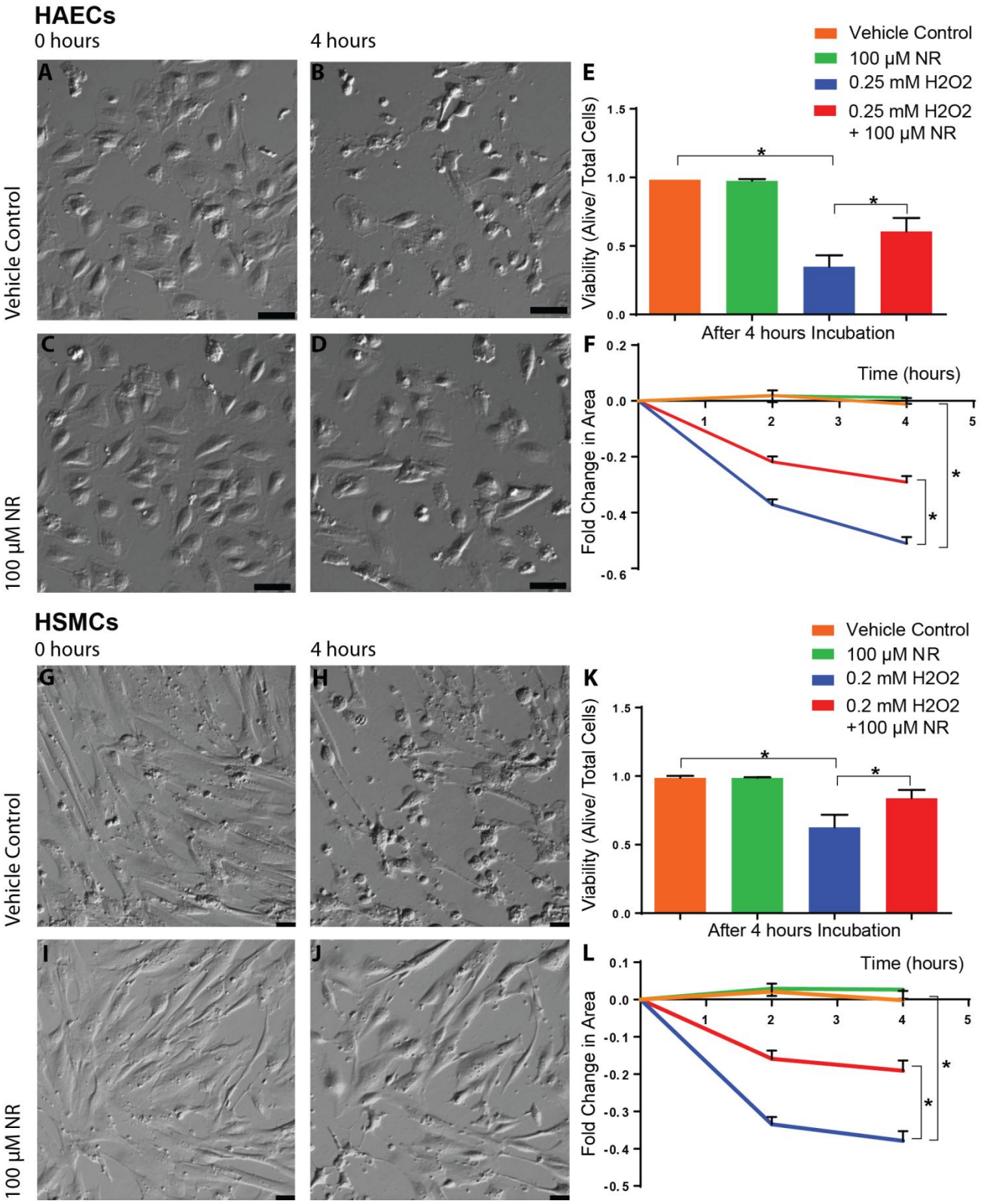
HAECs
0 hours
4 hours
A
B
C
D
Vehicle Control
100 µM NR
E
Vehicle Control
100 µM NR
0.25 mM H2O2
0.25 mM H2O2
+ 100 µM NR
Viability (Alive/ Total Cells)
1.5
1.0
0.5
0.0
*
*
After 4 hours Incubation
F
Time (hours)
Fold Change in Area
0.2
0.0
-0.2
-0.4
-0.6
1
2
3
4
5
*
*
HSMCs
0 hours
4 hours
G
H
I
J
Vehicle Control
100 µM NR
K
Vehicle Control
100 µM NR
0.2 mM H2O2
0.2 mM H2O2
+100 µM NR
Viability (Alive/ Total Cells)
1.5
1.0
0.5
0.0
*
*
After 4 hours Incubation
L
Time (hours)
Fold Change in Area
0.1
0.0
-0.1
-0.2
-0.3
-0.4
-0.5
1
2
3
4
5
*
*

3.6 NR Preserves Morphology by Maintaining Cytoskeletal Integrity

Morphological shrinkage, in response to oxidative damage, suggests possible cytoskeletal collapse. Actin is a vital component of the cytoskeleton that acts as a linker protein to focal adhesions, thereby maintaining cell shape (247-249). Therefore, NR's effects on actin cytoskeletal structures against oxidative damage were examined using immunostaining with fluorescent phalloidan, a bicyclic heptapeptide specifically binding to F-actin, following H_2O_2. By observing cells at 1 h, a snap-shot of cytoskeletal changes was possible, avoiding the full-collapse at 4 h, likely associated with cell death. Consistent with Fig. 3.4, a prominent change in shape and size was observed following 1 h H_2O_2 exposure in both cell types (Fig. 3.6). Stress fibres, running length wise through the cytoplasm, degraded into short segments, aggregated into puncta or completely collapsed in some cells treated with vehicle control. NR treatment enabled cells to maintain stress fibre integrity and resist the shrinking effect.

Surprisingly, NR treatment led to notable actin reorganization at baseline. This was particularly evident in the HAEC, which revealed a shift in actin structures from cortical bundle and filopodia to stress fibres upon NR treatment (Fig. 3.6). NR-treated HAEC at baseline exhibited dense stress fibre networks, possibly acting to maintain cell morphology under episode of oxidative insult. Similar effects of NR to stress fibre networks were also noted in HSMC, but to a milder extent.

Figure 3.6 NR delivery results in actin re-organization and protects from H_2O_2-induced cytoskeletal collapse in vascular cells. Cells were pre-treated with 100 μM NR for 24 h. Immediately following 60 min 0.25 mM or 0.2 mM H_2O_2, **(A)** HAEC and **(B)** HSMC, respectively, were fixed using 4% paraformaldehyde, permeabilized with PBS + 0.4% triton X, stained with 1:50 Alexa Fluor 488 phalloidin (green) and counter-stained with 2.5 μg/mL DAPI (blue). Bar on bottom right of images represents a 50 micron scale.

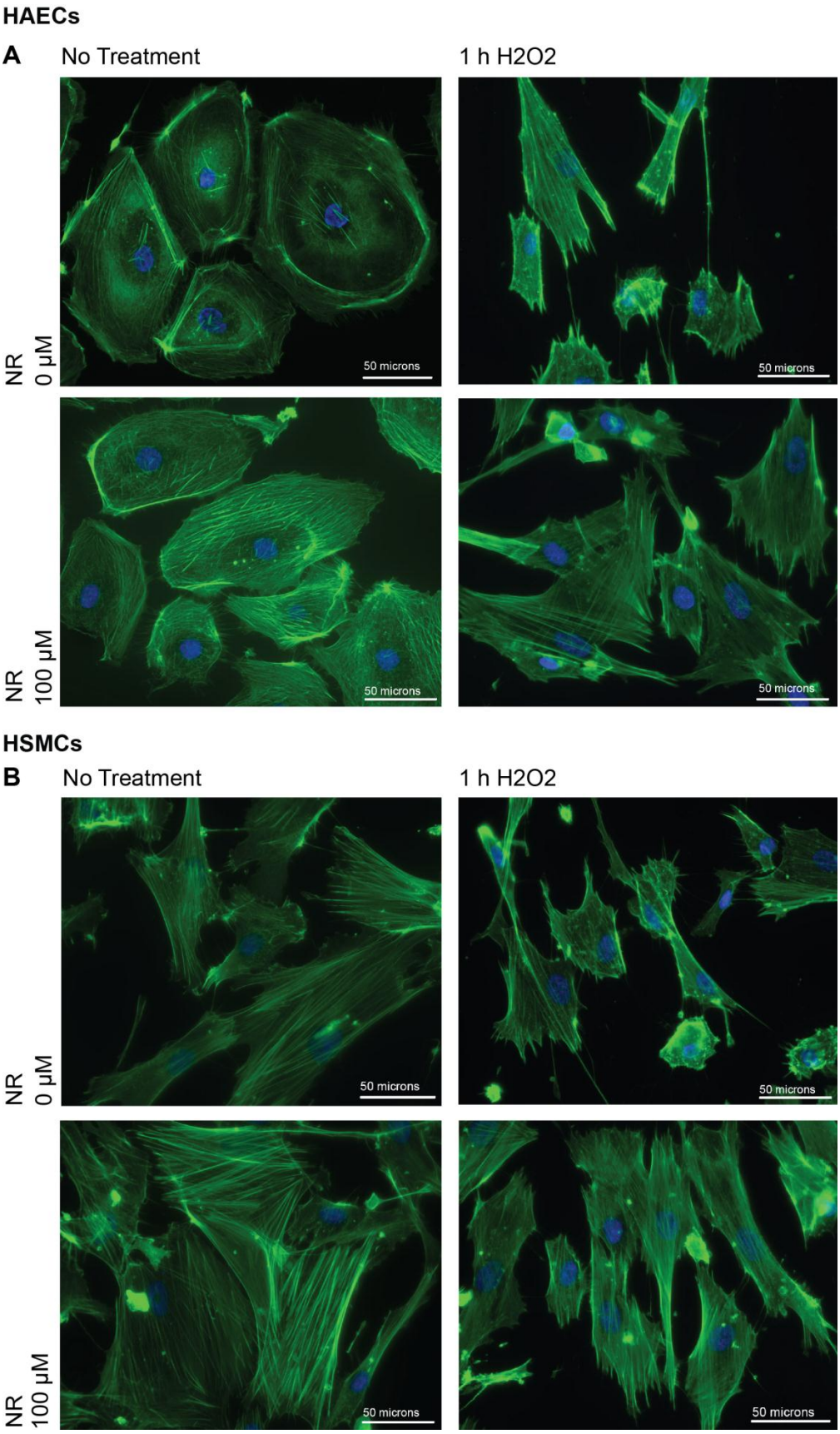
HAECs
A
No Treatment
1 h H2O2
NR 0 µM
NR 100 µM
50 microns
HSMCs
B
No Treatment
1 h H2O2
NR 0 µM
NR 100 µM
50 microns

3.7 NR delivery promotes DNA repair efficiency.

The previous data indicates that NR delivery augments NAD^+ reserves in vascular cells and that these reserves enable the cells to better maintain morphology and viability in response to H_2O_2 stress. The PARP family of enzymes rely heavily on NAD^+ stores to fuel their highly NAD^+-consuming role in recruiting DNA repair machinery to sites of damage (111). Additionally, the sirtuin family of enzymes consume NAD^+ for their cellular function, including maintaining genome integrity, stress response, and up-regulating anti-oxidant pathways to name a few (140, 245). Therefore, I next considered if NR played a role in promoting DNA repair responses.

To explore the potential effects of NR on DNA repair, a delicately-controlled insult sufficient to induce damage, so as to deplete NAD^+, but not kill the cell was needed. The 4 h oxidative insult in the previous experiment (section 3.5) induced approximately 50% death in untreated groups. The remaining live cells, from which DNA damage and repair would be studied, do not represent the entire population. The new model chosen to investigate DNA repair used the same dose of H_2O_2, but only a 1 h insult. Cells were then washed with fresh media and given variable recovery times to allow DNA repair. An alkaline comet assay was used to quantify both single- and double- strand DNA breaks. In this assay, broken DNA fragments are pulled out of the confines of the nucleus by an electrical current and damage is quantified by tail length, shape and intensity, compared to the size and intensity of the nucleus.

One such measure is tail moment:

$$Tail\ Moment = \frac{(Tail\ Length\ \times Tail\ \%DNA)}{100}$$

In cells not exposed to H_2O_2, DNA remained within the confines of the nuclei. Upon oxidative damage induced by H_2O_2, a tail representing damaged DNA species arose, was evident within 1 h of H_2O_2 exposure and then gradually diminished, indicating DNA repair (Fig. 3.7 C,D).

In HAEC, tail moment was significantly lowered with NR treatment at all times quantified (0-11 h post H_2O_2 withdrawal) ($P<0.001$), indicating less DNA damage (Fig. 3.7A). Similarly, in HSMC tail moment was lower in most groups including 3, 5, 7 and 9 h recovery following the 1 h 0.2 mM H_2O_2 insult ($p<0.0001$) (Fig. 3.7B). At 3 h, the greatest change in DNA damage repair between two independent time-points was observed (damage at 3 h compared to 1 h), with tail moment decreasing by 38 AU in HAEC and 29 AU in HSMC. DNA damage can be visualized in HAEC (Fig. 3.7C) and HSMC (Fig. 3.7D) by the comet tail shape that appeared following H_2O_2 insult, representative images show damage after 3 h recovery.

The above findings suggested that NR delivery enhanced the efficiency of DNA repair in vascular cells. However, it remained possible that NR directly reduced the extent of initial oxidative injury. According to previous publications, sirtuins can upregulate the transcription of anti-oxidant genes (156-158). Therefore, I considered the possibility that NR reduced the initial absolute damage from oxidative insults, by activating the transcription of anti-oxidant genes. Interestingly, at 0 h recovery (immediately after the 1 h H_2O_2 incubation) the HAEC tail moment in NR-treated group was 108±3 AU, significantly lower than that in vehicle-treated control cells (130±5 AU, $p<0.0001$) (Fig. 3.7A) . This difference in tail moment at 0 h recovery in HAEC could be explained by either NR-enhanced DNA repair during the 1 h period of oxidative insult or the up-regulation of anti-oxidant genes. Quantitative real-time PCR was used to determine NR's impact on the regulation of transcript levels of selected anti-oxidant genes. Based on previous reports, I selected anti-oxidant genes downstream of peroxisome proliferator-activated receptor gamma coactivator 1-alpha (PGC-1α), a transcription coactivator known to be upregulated by SIRT1 (157). SIRT1 will bind and activate PGC-1α through deacetylation. I found no statistically discernible increase in PGC-1α, SOD1, SOD2, catalase and Prdx5 gene transcripts in either cell type following NR treatment (Fig.

3.8). In fact, in NR-treated HSMC, SOD1 showed a lower transcript level 70±10% of vehicle control expression and SOD2 showed 51±9%, indicating a subtle, but not significant, decrease in expression of a subset of anti-oxidant genes upon NR treatment ($p=0.56$ and $p=0.68$). Overall, these data provide evidence that NR does not increase the transcript levels of anti-oxidant genes. These results indirectly support that the reduction in oxidative stress-induced DNA damage by NR is attributed to enhanced DNA repair. Such enhanced DNA repair could be so efficient to have induced a noticeable difference as early as 0h, immediately after the cease of oxidative insult in HAEC.

Figure 3.7 NR promotes DNA repair. Comet assay kit, including alkaline agarose gel electrophoresis, was used to pull single- and double-strand DNA breaks from the nuclei of cells to form the characteristic comet tail. HAEC and HSMC, pre-treated with 0 or 100 μM NR for 24 h, were exposed to 0.25 mM or 0.2 mM H_2O_2, respectively, for 60 min and given 3-11 h recovery. Tail Moment (±SE) measured using *Open comet* analysis to evaluate impact of NR delivery on H_2O_2-induced DNA damage on **(A)** HAEC (n=82-723) and **(B)** HSMC (n=79-542). *Pre-treatment with NR had significantly lower DNA damage, as measured by tail moment (see p. 78), than corresponding vehicle control group ($p<0.05$) using Two-Way ANOVA and Sidak's Multiple Comparison Test of the means. **(C-D)** Representative images of comet tails with no treatment or 1 h H_2O_2 with 3 h recovery for **(C)** HAEC and **(D)** HSMC.

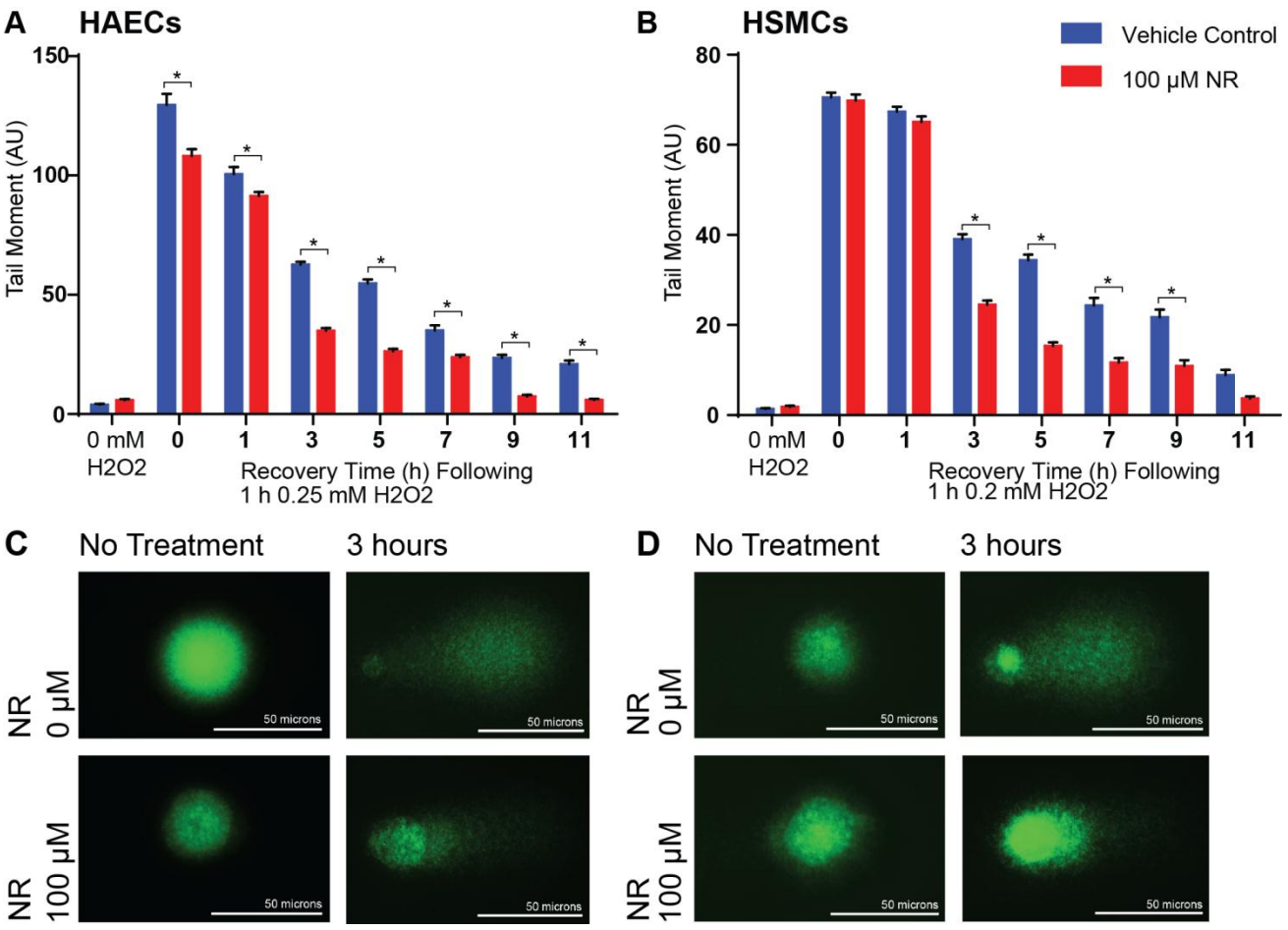
A
HAECs
Tail Moment (AU)
150
100
50
0
0 mM H2O2
0
1
3
5
7
9
11
Recovery Time (h) Following 1 h 0.25 mM H2O2
B
HSMCs
Vehicle Control
100 µM NR
Tail Moment (AU)
80
60
40
20
0
0 mM H2O2
0
1
3
5
7
9
11
Recovery Time (h) Following 1 h 0.2 mM H2O2
C
No Treatment
3 hours
NR 0 µM
NR 100 µM
50 microns
D
No Treatment
3 hours
NR 0 µM
NR 100 µM
50 microns

Figure 3.8 Anti-oxidant gene expression remains unchanged following NR delivery. **(A)** HAEC (n=6-9) and **(B)** HSMC (n=12) expression profile of anti-oxidant genes using SYBR Green Quantitative RT PCR. Primers for *SOD1*, *SOD2*, *catalase*, *Prdx5* and *PGC-1α* were used to amplify mRNA following 24 h treatment with 100 μM NR. Values presented as ΔΔCt comparison of mRNA expression levels with NR treatment to vehicle control, standardized with 18s rRNA housekeeping gene. No significance determined by One-Way ANOVA and Tukey's Multiple Comparison Test of the means.

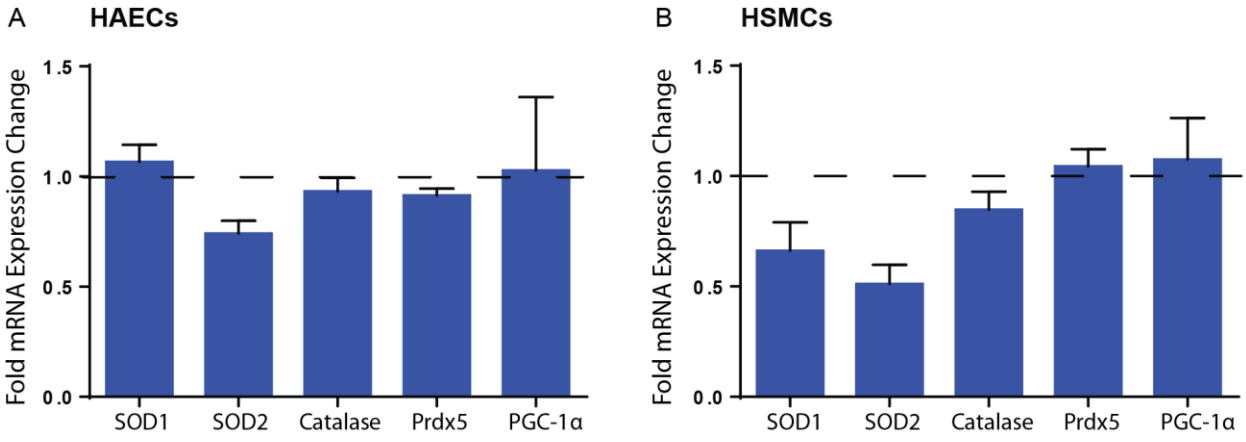
A
HAECs
Fold mRNA Expression Change
1.5
1.0
0.5
0.0
SOD1
SOD2
Catalase
Prdx5
PGC-1α
B
HSMCs
Fold mRNA Expression Change
1.5
1.0
0.5
0.0
SOD1
SOD2
Catalase
Prdx5
PGC-1α

3.8 NAD^+ precursors NA, Nam and NMN similarly protect against H_2O_2-induced cell shrinkage and death.

It has long been known that exogenous supplementation by NAD^+ precursors, NA, Nam and NMN, will increase intracellular NAD^+ levels in cell lines and tissue (250, 251). To determine if this NAD^+ increase would mimic the protection observed by NR supplementation, HAEC and HSMC were incubated for 24 h with 100 μM NA, Nam and NMN and exposed to 4 hr H_2O_2. I then tracked cells and assessed cell shrinkage using image J and viability using trypan blue exclusion. In HAEC, all three precursors significantly protected against H_2O_2-induced cell shrinkage at 4 h (NA $p<0.0001$, Nam $p=0.002$, NMN $p=0.0005$), although not at 2 h (Fig. 3.9A). In HSMC, NMN and Nam significantly protected against shrinkage at 4 h compared to baseline ($p=0.003$, $p=0.005$). Only NA in HSMC exhibited a non-significant trend ($p=0.16$) (Fig. 3.9C). There were no differences observed in viability in HAEC (NA $p=0.49$, NMN $p=0.96$, Nam $p>0.99$) (Fig. 3.9B). A subtle trend towards increased viability was observed for precursor supplementation in HSMCs, although differences were not significant (NA $p=0.76$, NMN $p=0.46$, Nam $p=0.85$) (Fig. 3.9D).

Figure 3.9 NAD^+-precursors similarly protect vascular cells from H_2O_2-induced cell shrinkage. HAEC and HSMC, pre-treated with NA, Nam or NMN for 24 h, were exposed to 0.25 mM H_2O_2 and 0.2 mM H_2O_2, respectively, and imaged through time-lapse Hoffman contrast microscopy for 4 h. Fold change in area (±SE), measured by tracking cells and tracing border in Image J, was recorded for **(A)** HAEC (n=44-48) and **(C)** HSMC (n=48). Trypan Blue exclusion viability data (±SE) was collected 4 h post-insult for **(B)** HAEC (N=3) and **(D)** HSMC (N=3). * Shows significantly less cell shrinkage at 4 h only, compared to cells not treated with precursors ($p<0.05$) using Two-Way ANOVA and Tukey's Multiple Comparison Test of the means.

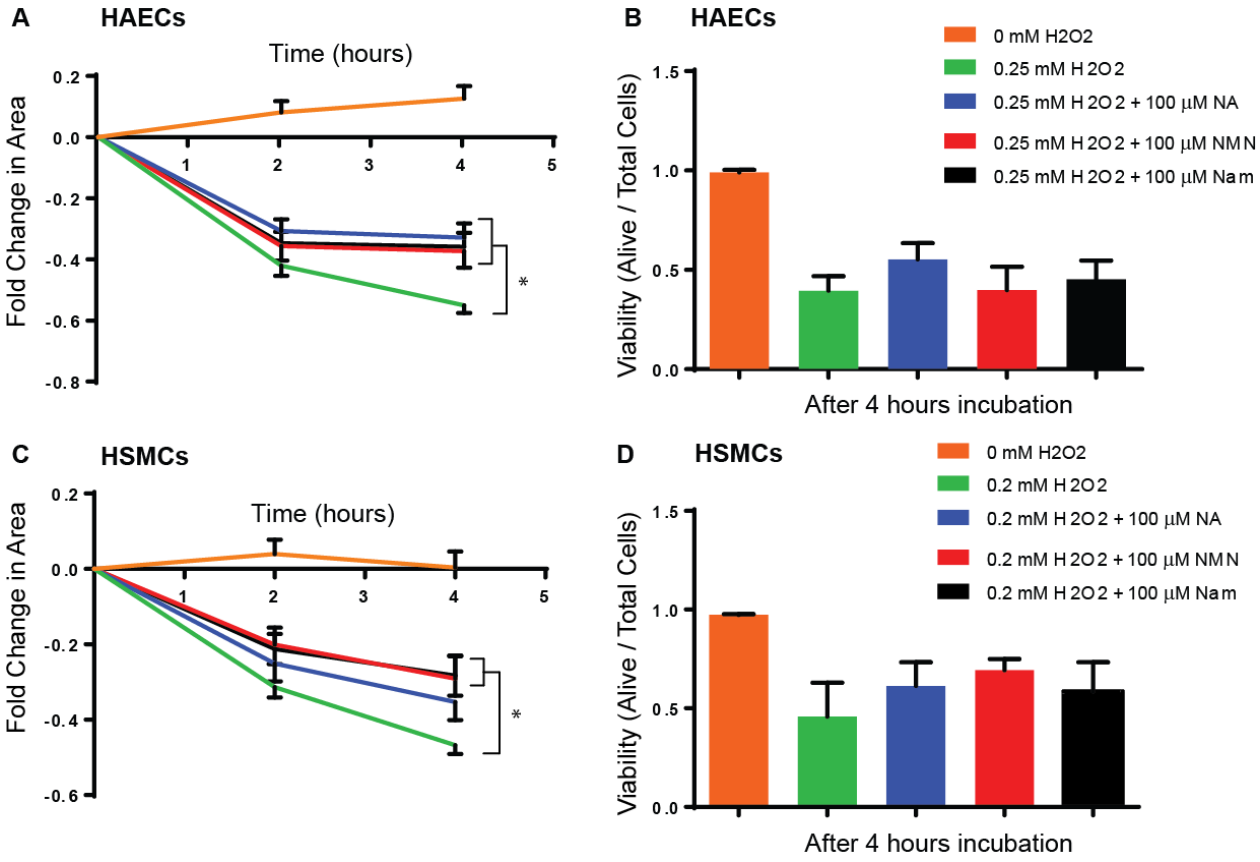
A
HAECs
Time (hours)
Fold Change in Area
0.2
0.0
-0.2
-0.4
-0.6
-0.8
1
2
3
4
5
*
B
HAECs
0 mM H2O2
0.25 mM H2O2
0.25 mM H2O2 + 100 µM NA
0.25 mM H2O2 + 100 µM NMN
0.25 mM H2O2 + 100 µM Nam
Viability (Alive / Total Cells)
1.5
1.0
0.5
0.0
After 4 hours incubation
C
HSMCs
Time (hours)
Fold Change in Area
0.2
0.0
-0.2
-0.4
-0.6
1
2
3
4
5
*
D
HSMCs
0 mM H2O2
0.2 mM H2O2
0.2 mM H2O2 + 100 µM NA
0.2 mM H2O2 + 100 µM NMN
0.2 mM H2O2 + 100 µM Nam
Viability (Alive / Total Cells)
1.5
1.0
0.5
0.0
After 4 hours incubation

3.9 PARP inhibition maintains NAD^+ levels to promote morphology and viability, but impairs DNA repair responses.

Demonstrated by my data, NR will create NAD^+ reserves that support beneficial stress response pathways during times of profound oxidative burden. Building on this principle, blocking NAD^+ consumption to maintain NAD^+ levels during oxidative stress insults should similarly demonstrate beneficial effects. These NAD^+ reserves should maintain sirtuin function and ATP production to fuel stress response pathways. As described above, PARP family of enzymes are a major consumer of NAD^+, thus PARP inhibition through DPQ treatment was tested to determine protection from H_2O_2-induced changes in morphology, viability and DNA integrity.

To determine if DPQ will protect against H_2O_2-induced cell-shrinkage and viability, HAEC and HSMC were pre-treated with 1 hr DPQ and exposed to 4 hr H_2O_2 insult. This revealed that PARP inhibition mimicked NR's beneficial effects on both cell shrinkage and viability. At both 2 and 4 h after H_2O_2 treatment, DPQ-treated HAEC showed significantly less cell shrinkage ($p<0.0001$) compared to DMSO vehicle control (Fig. 3.10 A). Furthermore, HAEC pre-treated with DPQ had almost two-fold higher viability ($p<0.0001$) compared to DMSO vehicle control (Fig. 10B). Similarly, HSMC displayed significantly less cell shrinkage at 2 h ($p=0.009$) and 4 h ($p=0.0002$) with DPQ treatment compared to DMSO vehicle control (Fig. 3.10C). Additionally, viability in HSMC following H_2O_2 with DPQ treatment was 81±7%, significantly higher that DMSO vehicle control of 56±9% ($p=0.02$) (Fig. 3.10D).

In contrast to its benefits over cell morphology and viability, I found that PAPR inhibition delayed DNA repair. This was most evident at 3 h, where HAEC pre-treated with DPQ had 33% higher tail moment and HSMC had 45% higher tail moment compared to vehicle control ($p<0.0001$) (Fig. 3.10 F&H). DNA damage can be visualized by the comet tail shape that gradually loses length and intensity as DNA breaks are repaired during recovery. Representative 3 h and 11 h recovery

images are shown (Fig. 3.10 E&G). DNA remains localized within the confines of the nuclei of untreated cells. DPQ pre-treatment attenuates DNA break repair, shown by longer, more intense comet tail and smaller, less intense comet head at 3 h as compared to DMSO vehicle pre-treatment. These findings are consistent with the fact that PARP functions to catalyze PAR chains on itself, histones and non-histone proteins to recruit DNA repair machinery to the site of damage. PARP inhibition does not mimic the beneficial effects observed by NR delivery because it attenuates DNA repair.

Figure 3.10 PARP inhibition mimics beneficial effects of NR, but at the cost of DNA repair efficiency. HAEC and HSMC were pretreated 1 h with DPQ and incubated for 4 h with 0.25 mM H_2O_2 and 0.2 mM H_2O_2, respectively, and imaged with time-lapse Hoffman modulated contrast microscopy for 4 h. **(A)** HAEC fold change in area (±SE, n=80-112) and **(C)** HSMC (±SE, n=80-96), measured by tracking cells and tracing their borders in Image J. There is less cell shrinkage at 4 h in cells pre-treated for 1 h with 20 μM DPQ. Viability data based on trypan blue exclusion, corresponding to 4 h time point of time-lapse videos showing attenuated cell death upon DPQ delivery in **(B)** HAEC mean (±SE) (N=5) and **(D)** HSMC mean (±SE) (N=6) . Vehicle control group for 0.25 mM H_2O_2 + 0.8% DMSO showed no difference compared to 0.25 mM H_2O_2 for both cell shrinkage and viability (data not shown). *Pre-treatment with DPQ showed significantly higher viability and less shrinkage than corresponding vehicle control group ($p<0.05$, using Two-Way ANOVA and Tukey's Multiple Comparison Test of the means). Comet assay kit, including alkaline agarose gel electrophoresis, was used to pull single- and double-strand DNA breaks from the nuclei of cells to form the characteristic comet tail shape. HAEC, pre-treated with 0 or 20 μM DPQ for 1 h, were exposed to 0.25 mM H_2O_2 for 30 min and given 3-11 h recovery. In **(E)** HAEC and **(G)** HSMC DNA damage can be visualized by the comet tail shape that gradually loses length and intensity as DNA breaks are repaired during subsequent recovery, 3 h and 11 h shown. DNA remains localized within the confines of the nuclei of untreated cells. DPQ pre-treatment attenuates DNA break repair. Tail Moment in **(F)** HAEC (±SE) (n=475-816) and **(H)** HSMC (±SE) (n=738-959) measured using *Open comet* analysis to evaluate impact of DPQ delivery on H_2O_2-induced DNA damage. *Pre-treatment with DPQ had significantly higher DNA damage, as measured by tail moment, than corresponding vehicle control group ($p<0.05$, using Two-Way ANOVA and Sidak's Multiple Comparison Test of the means).

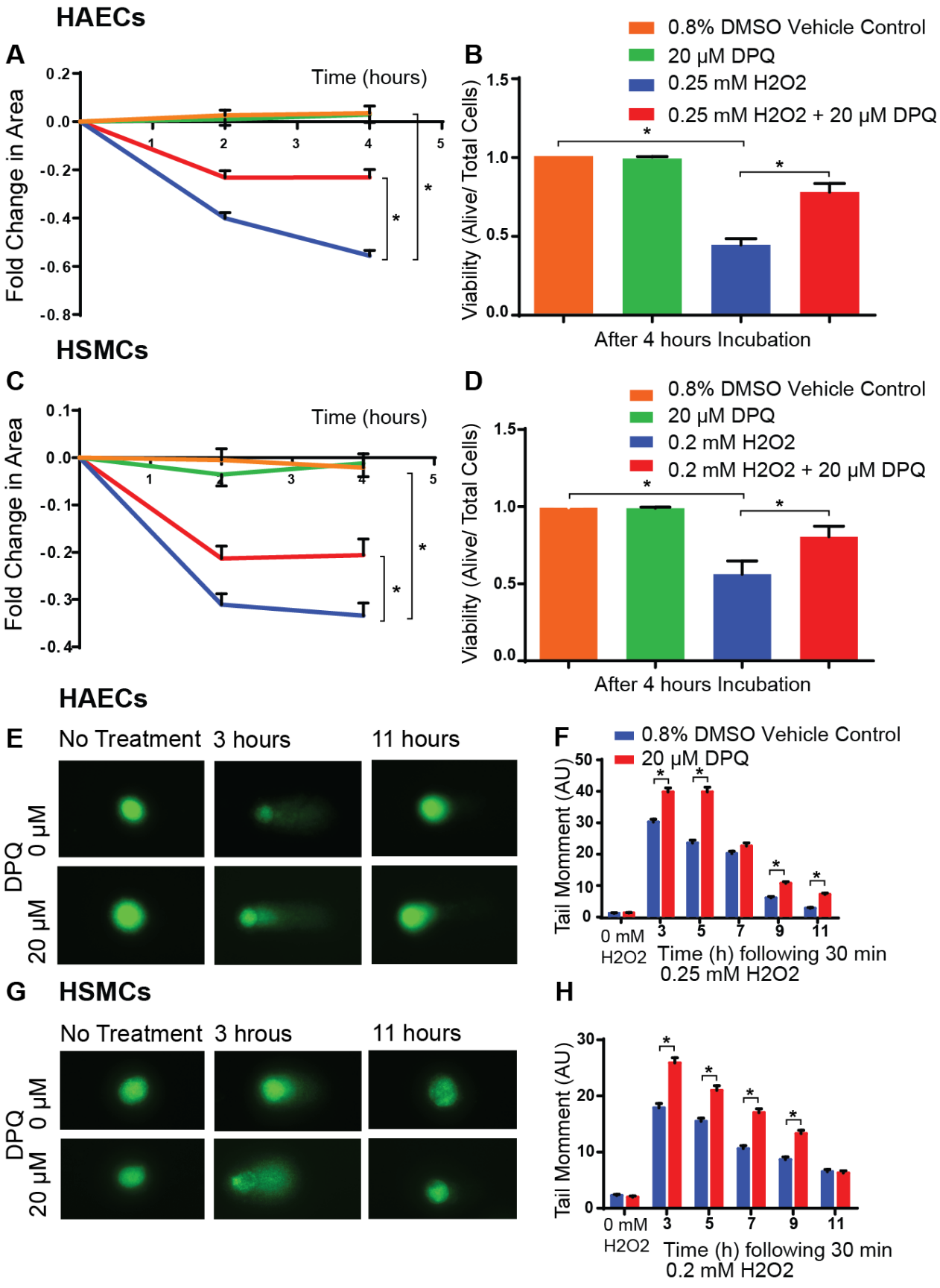
HAECs
A
Time (hours)
Fold Change in Area
0.2
0.0
-0.2
-0.4
-0.6
-0.8
1
2
3
4
5
*
*
B
0.8% DMSO Vehicle Control
20 μM DPQ
0.25 mM H2O2
0.25 mM H2O2 + 20 μM DPQ
Viability (Alive/ Total Cells)
1.5
1.0
0.5
0.0
*
*
After 4 hours Incubation
HSMCs
C
Time (hours)
Fold Change in Area
0.1
0.0
-0.1
-0.2
-0.3
-0.4
1
3
5
*
*
D
0.8% DMSO Vehicle Control
20 μM DPQ
0.2 mM H2O2
0.2 mM H2O2 + 20 μM DPQ
Viability (Alive/ Total Cells)
1.5
1.0
0.5
0.0
*
*
After 4 hours Incubation
HAECs
E
No Treatment
3 hours
11 hours
DPQ
0 μM
20 μM
F
0.8% DMSO Vehicle Control
20 μM DPQ
Tail Momment (AU)
50
40
30
20
10
0
*
*
*
*
0 mM H2O2
3
5
7
9
11
Time (h) following 30 min
0.25 mM H2O2
G
HSMCs
No Treatment
3 hrous
11 hours
DPQ
0 μM
20 μM
H
Tail Momment (AU)
30
20
10
0
*
*
*
*
0 mM H2O2
3
5
7
9
11
Time (h) following 30 min
0.2 mM H2O2

3.10 Role of the sirtuin family of enzymes in oxidative stress responses.

I next speculated that the augmentation of NAD^+ reserves offered by NR might increase the activity of NAD^+-consuming enzymes such as sirtuins. These histone deacetylases consume NAD^+ to regulate transcription of targets implicated in many cellular functions (245). Thus, I hypothesized that the observed NR protective effects may, in part, be attributed to sirtuins. The involvement of SIRTs 1-7 was independently assessed with respect to morphology, viability and DNA repair using siRNA against *SIRT*s 1-7. The objective of this experiment was to build a molecular pathway to explain NRs observed protection beyond providing NAD^+ reserves themselves.

First I determined that SIRT knockdown (KD) could be obtained by siRNA against SIRT 1-7 in vascular cells. HAEC and HSMC were incubated for 48 h with Lipofectamine RNAi max and siRNA against respective SIRTs. KD efficiency was then confirmed through real-time PCR. Upon transfection with gene-specific siRNAs, transcript levels were reduced to 30% or lower, as compared with scrambled negative control siRNA, for all SIRTs in both cell types, except SIRT3 (Fig. 3.11 A&B). Expression of SIRT3 was reduced to 35±3% in HAEC and 42±6% in HSMC.

Next, I wanted to reproduce NRs protection against cell shrinkage and cell death and NRs ability to promote DNA repair, but now under conditions of scrambled negative control siRNA treatment (siscram). This would confirm that procedure of siRNA delivery was not altering NRs beneficial effects. To answer this, I incubated cells with 48 h Lipofectamine RNAi max and scrambled negative control siRNA and pre-treated for 24 h with NR or vehicle. To determine NRs protection against cell shrinkage and cell death, cells were exposed to 4 h H_2O_2 and cell area changes and viability were assessed. This revealed that in HAEC and HSMC siscram with NR compared to siscram without NR had significantly less cell shrinkage ($p=0.007$, $p=0.04$) and significantly higher viability ($p=0.0007$, $p=0.003$) (Fig. 3.12). To determine NRs ability to promote DNA repair, tail moment was assessed at 3 h after cells were exposed to 1 h H_2O_2. This time-point was chosen

because it represented the largest change in damage (between 1 h and 3 h time-points, as seen in Fig. 3.7), thus it offered the most information when assessing impact of interventions on promoting repair. In both HAEC and HSMC, tail moment was significantly less in siscram with NR compared to siscram with vehicle ($p<0.0001$) (Fig. 3.11). Significant differences between siscram with and without NR confirmed that the procedure of siRNA delivery was not altering NRs beneficial effects.

Next, to determine the role of SIRT 1-7 in NRs ability to promote DNA damage repair, cells were incubated with siRNA against one of SIRT 1-7 and then pre-treated with NR for 24 h. Tail moment analysis data for each SIRT KD with NR was then compared to siscram with NR and siscram with vehicle to determine partial, full or not abolished NR protection. If tail moment of SIRT KD with NR was significantly higher than siscram with NR, protection was at least partially abolished. If tail moment of SIRT KD with NR reached a level that was not statistically different from siscram with vehicle, this was considered full loss of protection. This rationale was used in Fig. 3.11 to report the effect of each SIRT KD on NRs ability to promote DNA repair. Analysis of tail moment at 3 h post 1 h H_2O_2-insult revealed partial loss of NRs protection for KD of all SIRT 1-7 in HAEC (Fig. 3.11C) and only SIRT1, SIRT3 &SIRT6 in HSMC (Fig. 3.11D). Data is summarized in a chart displaying mean values ±SE and p-values. From these charts, data for siscram with and without NR, SIRT1 and SIRT6 were displayed in a bar graph with respective controls (Fig. 3.11 E&F).

Finally, to determine the role of SIRT 1-7 in NRs ability to protect against cell shrinkage and death, cells were incubated with siRNA against one of SIRT 1-7 and then pre-treated with NR for 24 h. Cells were then subjected to 4 h H_2O_2 and change in area and viability was assessed. This data was similarly summarized using a chart to report on the full profile of SIRT KD, and a graph is shown representing SIRT1 and SIRT6 data specifically (Fig. 3.12). KD of SIRT 1-7 with NR is compared to

siscram with vehicle, to determine if NRs protection is lost, indicated by no significant difference to siscram with vehicle. Cell shrinkage data revealed that all of the SIRT 1-7 KD with NR treatments were significantly different than siscram with vehicle, suggesting NR protection remains (Fig. 3.12A). However, HSMC showed cell shrinkage return to the level of siscram with vehicle in SIRT 1, SIRT2, SIRT3 and SIRT7 KD with NR (Fig. 3.12B).Viability levels returned to siscram with vehicle in HAEC for SIRT1, SIRT2 and SIRT6 KD with NR (Fig. 3.12E) and in HSMC for SIRT1, SIRT2, SIRT3 and SIRT6 KD with NR (Fig. 3.12F). When damage returned to levels of siscram with vehicle, NRs protection was considered to be abolished.

Figure 3.11 Role of Sirtuin family of enzymes in DNA damage response. **(A)** HAEC (n=3) and **(B)** HSMC (n=3) expression profile of sirtuin genes using SYBR Green Quantitative RT PCR. Primers for sirt 1-7 were used to amplify mRNA following 48 h incubation with Lipofectamine RNAi Max reagents and respective siRNA. Values presented as ΔΔCt comparison of knockdown mRNA to scrambled siRNA control, standardized with 18s rRNA housekeeping gene. **(C)** HAEC and **(D)** HSMC were exposed to 1 h H_2O_2 and given 3 h recovery time before analysis with alkaline comet assay. The profile of sirtuin gene KD was pre-treated with 100 μM NR for 24 h and compared to scrambled siRNA with and without NR treatment. Partially abolished NR protection refers to tail moment significantly different than siscram both with and without NR. No abolished protection refers to tail moment not significantly different than siscram with NR treatment. Tail moment (±SE) of siscram, SIRT1 KD+NR and SIRT6 KD+NR groups from **(C&D)** were graphed with respective controls in **(E)** HAEC (n= 273-482) and **(F)** HSMC (n=613-765). Groups with the same letter are not significantly different from each other using One-Way ANOVA and Dunnett's Multiple Comparison Test of the means ($p<0.05$).

A HAECs

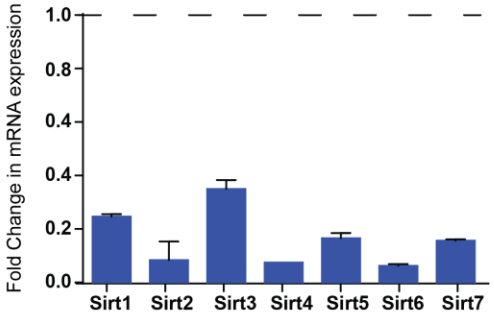

B HSMCs

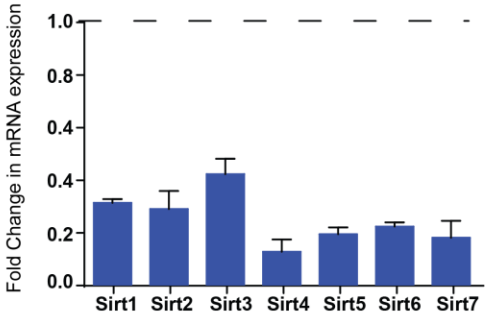

C HAECs

Groups Subjected to 0.25 mM H2O2	Mean Tail Moment at 3 hrs recovery	±SEM	NR Protection Abolished	P Value compared to siscram	P Value compared to siscram+NR
No Treatment	72.01	0.87	N/A	0.9994	< 0.0001
siscram	71.26	1.33	N/A	N/A	< 0.0001
siscram+NR	36.17	1.89	N/A	< 0.0001	N/A
sisirt1+NR	61.88	1.14	Partial	< 0.0001	< 0.0001
sisirt2+NR	59.79	1.18	Partial	< 0.0001	< 0.0001
sisirt3+NR	56.13	1.52	Partial	< 0.0001	< 0.0001
sisirt4+NR	45.24	1.73	Partial	< 0.0001	0.0006
sisirt5+NR	51.15	1.54	Partial	< 0.0001	< 0.0001
sisirt6+NR	57.70	1.89	Partial	< 0.0001	< 0.0001
sisirt7+NR	47.71	1.94	Partial	< 0.0001	< 0.0001

D HSMCs

Groups Subjected to 0.2 mM H2O2	Mean Tail Moment at 3 hrs recovery	±SEM	NR Protection Abolished	P Value compared to siscram	P Value compared to siscram+NR
No Treatment	27.38	1.06	N/A	0.3157	< 0.0001
siscram	30.50	0.96	N/A	N/A	< 0.0001
siscram+NR	15.64	0.89	N/A	< 0.0001	N/A
sisirt1+NR	26.33	1.05	Partial	0.0263	< 0.0001
sisirt2+NR	16.05	0.94	No	< 0.0001	0.9996
sisirt3+NR	19.87	1.19	Partial	< 0.0001	0.0236
sisirt4+NR	14.54	1.17	No	< 0.0001	0.9804
sisirt5+NR	15.56	1.11	No	< 0.0001	> 0.9999
sisirt6+NR	19.77	0.90	Partial	< 0.0001	0.0114
sisirt7+NR	17.40	1.19	No	< 0.0001	0.7744

E HAECs

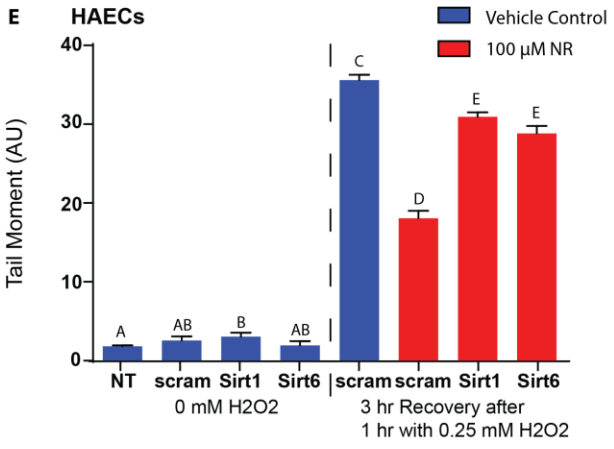

F HSMCs

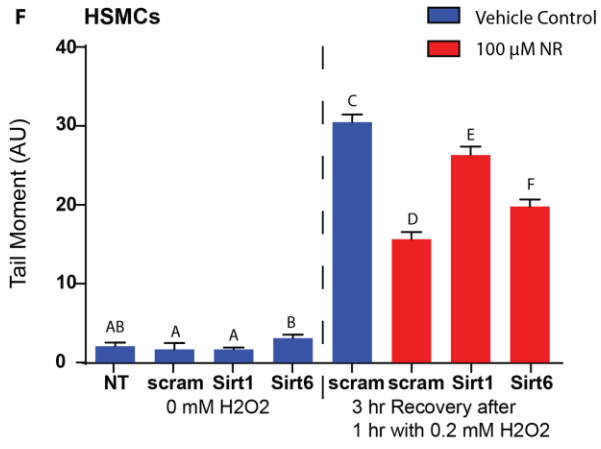

Figure 3.12 Sirtuins mediate NR's protection against H_2O_2-induced cell shrinkage and cell death in vascular cells. SIRT 1-7 knockdown was achieved by 48 h incubation with Lipofectamine RNAi Max reagents and respective siRNA. **(A)** HAEC (n=80-108) and **(B)** HSMC (n=64) fold change in area at four h compared to baseline, measured by tracking cells and tracing border in Image J. **(E)** HAEC (n=7) and **(F)** HSMC (n=7) viability quantified by trypan blue exclusion. No significant differences compared to siscram without NR, suggests abolished NR protection ($p<0.05$) using One-Way ANOVA and Dunnett's Multiple Comparison Test of the means. **(C,D,G,H)** Bars in red were pre-treated for 24 h with 100 μM NR and blue bars correspond to vehicle control. Dotted line separates groups exposed to 0.25 (HAEC) and 0.2 mM (HSMC) for 4 h, from untreated controls. Fold change in area (±SE) of siscram, SIRT1 KD+NR and SIRT6 KD+NR groups from **(A&B)** were graphed with respective controls in **(C)** HAEC and **(D)** HSMC. Viability (±SE) of siscram, SIRT1 KD+NR and SIRT6 KD+NR groups from **(E&F)** were graphed with respective controls in **(G)** HAEC and **(H)** HSMC. Groups with the same letter are not significantly different from each other using One-Way ANOVA and Dunnett's Multiple Comparison Test of the means ($p<0.05$).

A HAECs

Groups Subjected to 0.25 mM H2O2	Mean change in area at 4 hrs	±SEM	Sig.	P Value compared to siscram
No Treatment	-0.45	0.02	No	0.997
siscram	-0.47	0.03	N/A	N/A
siscram+NR	-0.27	0.03	Yes	0.0066
sisirt1+NR	-0.28	0.04	Yes	0.0428
sisirt2+NR	-0.29	0.03	Yes	0.0017
sisirt3+NR	-0.28	0.04	Yes	0.0008
sisirt4+NR	-0.20	0.04	Yes	< 0.0001
sisirt5+NR	-0.19	0.04	Yes	< 0.0001
sisirt6+NR	-0.29	0.03	Yes	0.0022
sisirt7+NR	-0.27	0.04	Yes	0.0006

B HSMCs

Groups Subjected to 0.2 mM H2O2	Mean change in area at 4 hrs	±SEM	Sig.	P Value compared to siscram
No Treatment	-0.44	0.03	No	0.9285
siscram	-0.49	0.05	N/A	N/A
siscram+NR	-0.36	0.03	Yes	0.0407
sisirt1+NR	-0.49	0.02	No	0.9999
sisirt2+NR	-0.53	0.03	No	0.9745
sisirt3+NR	-0.45	0.03	No	0.9714
sisirt4+NR	-0.34	0.04	Yes	0.0096
sisirt5+NR	-0.34	0.03	Yes	0.0172
sisirt6+NR	-0.35	0.03	Yes	0.0269
sisirt7+NR	-0.42	0.03	No	0.6909

C HAECs

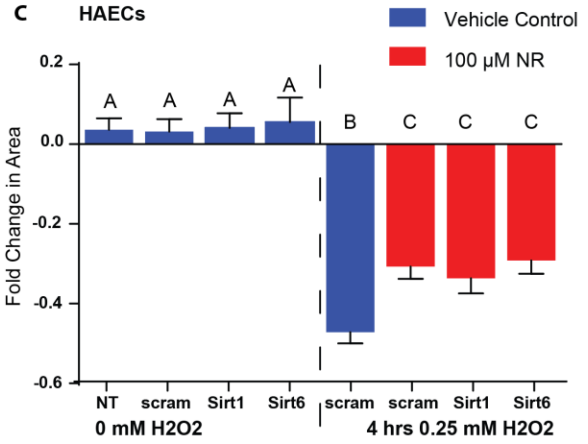

D HSMCs

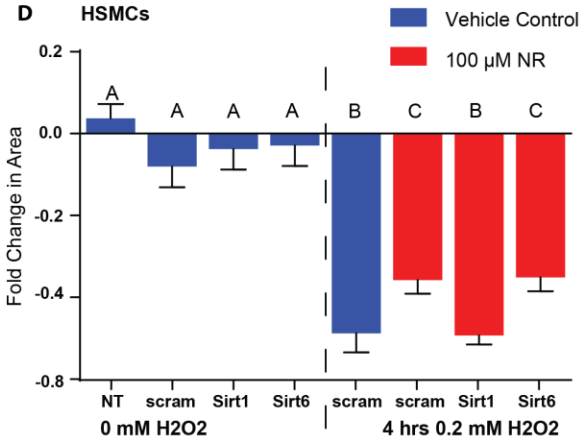

E HAECs

Groups Subjected to 0.25 mM H2O2	Mean viability (alive/totals cells) at 4 hrs	±SEM	Sig.	P Value compared to siscram
No Treatment	0.56	0.09	No	0.6213
siscram	0.59	0.07	N/A	N/A
siscram+NR	0.83	0.06	Yes	0.0007
sisirt1+NR	0.69	0.09	No	0.0532
sisirt2+NR	0.69	0.09	No	0.2123
sisirt3+NR	0.74	0.10	Yes	0.0151
sisirt4+NR	0.82	0.09	Yes	0.0001
sisirt5+NR	0.79	0.10	Yes	0.0009
sisirt6+NR	0.71	0.07	No	0.1115
sisirt7+NR	0.77	0.10	Yes	0.0118

F HSMCs

Groups Subjected to 0.2 mM H2O2	Mean viability (alive/totals cells) at 4 hrs	±SEM	Sig.	P Value compared to siscram
No Treatment	0.62	0.06	No	0.2743
siscram	0.52	0.02	N/A	N/A
siscram+NR	0.77	0.05	Yes	0.0031
sisirt1+NR	0.54	0.07	No	0.995
sisirt2+NR	0.56	0.09	No	0.9344
sisirt3+NR	0.58	0.07	No	0.8505
sisirt4+NR	0.83	0.07	Yes	0.0018
sisirt5+NR	0.80	0.04	Yes	0.0011
sisirt6+NR	0.72	0.07	No	0.0535
sisirt7+NR	0.72	0.06	Yes	0.0349

G HAECs

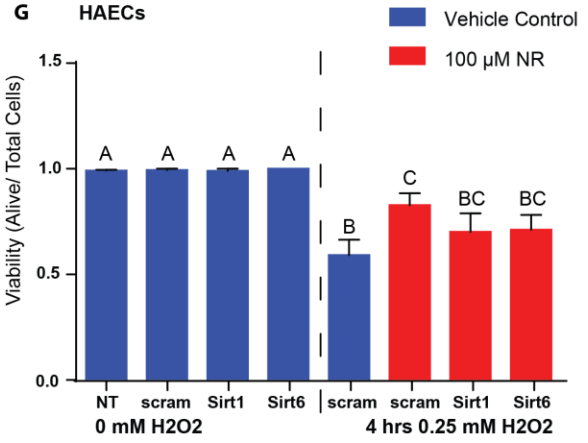

H HSMCs

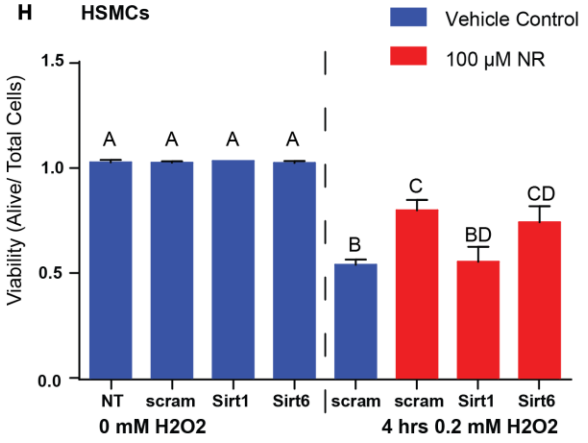

3.11 NR delivery protects vascular cells from chronic H_2O_2-induced senescence, in a partially SIRT1 and SIRT6 dependant manner.

Previous studies have reported SIRT1 implicated in age-associated senescent phenotype in vascular endothelial cells (141-144). Similarly, SIRT6 deficiency has been linked to oxidative stress-induced senescence in endothelial cells (180). In Fig. 3.11 and 3.12, it was revealed that NR acts through SIRT1 and SIRT6 dependent pathways to protect against cell shrinkage, cell death and promote DNA repair. Additionally, accumulation of DNA damage is a key factor in acquiring a senescent phenotype. I therefore speculated that it was possible that NR may protect against senescence in SIRT1 and SIRT6 dependent pathways. The previous acute H_2O_2 dose induced high levels of cell death, which would compound the interpretation of cellular senescence of surviving population. Therefore I selected a milder H_2O_2 insult (25 and 20 μM for HAEC and HSMC, respectively, 1/10 of the dose for cell death and DNA damage insults). This more chronic oxidative insult would also be more relevant to an aging model.

To determine if NR protected against senescence in vascular cells, I used senescence-associated β galactosidase (SA β-Gal) activity assay, a blue colorimetric assay. To assess NR's effect on cell senescence, I pre-treated cell with 100 μM NR for 24 h and subjected them to 1 h H_2O_2. At 48 h following H_2O_2 insult, fewer SA β-Gal positive blue cells were observed in both vascular cell types incubated with NR compared to vehicle (Fig. 3.13 A&B).

Image J was then used to quantify percent positive cells per field of view. Quantification of SA β-Gal positive cells at 48 h following H_2O_2 treatment revealed significantly higher levels than baseline (HAEC $p=0.009$, HSMC $p=0.001$) (Fig. 3.13C,D). Pre-treatment with NR significantly protected against oxidative-stress-induced senescence. Specifically, HAEC vehicle control showed 41±2% positive cells following H_2O_2 insult, with protection by NR showing only 24±3% positive cells ($p=0.007$) (Fig. 3.13C). HSMC vehicle control showed 35±3% positive cells following H_2O_2

insult, and significantly less senescence of 22±3% positive cells in group pre-treated with NR (p=0.039) (Fig. 3.13 D).

To determine if SIRT1 and SIRT6 were implicated in NRs protection against H_2O_2-induced senescence, I used SA β-Gal staining. Cells were exposed to 48 h incubation with Lipofectamine RNAi Max and siRNA against SIRT1 and SIRT6 and pre-treated for 24 h with NR or vehicle. *Sirt1* or *Sirt6* KD with NR revealed a not significant but noticeable increase in senescent cell population compared to H_2O_2-treated cells with vehicle. Interesting, without NR-treatment, *Sirt1* and *Sirt6* KD increased % positive cells to levels above H_2O_2-treated cells with vehicle in HAEC, however this difference was not significant (SIRT1 & SIRT6, p=0.1) These finding suggested a protective role of NR against cellular senescence induced by chronic, non-lethal oxidative stress, and that protection by NR is partially mediated through SIRT1 and SIRT6.

Next, to complete the comparison of NR delivery versus PARP inhibition, I determined if PARP inhibition would protect against senescence. To answer this, I pre-treated cells for 1 h with 20 μM DPQ and subjected cells to 1 h H_2O_2. At 48 h after H_2O_2 insult, no significant difference was observed in cells incubated with PARP inhibitor (DPQ) compared to H_2O_2-treated group with vehicle in both cell types (HAEC & HSMC p=0.99) (Fig. 3.13 C&D). This suggests that PARP inhibition and associated NAD^+ reserve, despite eliciting a similar rescuing effect on cell morphology and viability, could not protect against H_2O_2-induced cell senescence.

Figure 3.13 DPQ and knockdown of SIRT1 or SIRT6 partially abolish NR's protection against H_2O_2-induced senescence. Representative images of senescence –associated β Gal staining in **(A)** HAEC and **(B)** HSMC 48 h after 1 h 0.025 and 0.02 mM H_2O_2 insult, respectively. Pre-treatment with 100 μM NR or no treatment (NT) for 24 h protects against senescence, visible through fewer positive blue cells in both vascular cell types. Quantification of positive senescence-associated β Gal in **(C)** HAEC (n=6-20) and **(D)** HSMC (n=12), analyzed percent positive cells in fields of view using Image J. Cells were pre-treated with 20 μM DPQ, 48 h Lipofectamine RNAi Max reagents & siRNA against SIRT1 or SIRT6, and/or 24 h 100 μM NR. Groups with the same letter are not significantly different ($p<0.05$) using One-Way ANOVA and Dunnett's Multiple Comparison Test of the means.

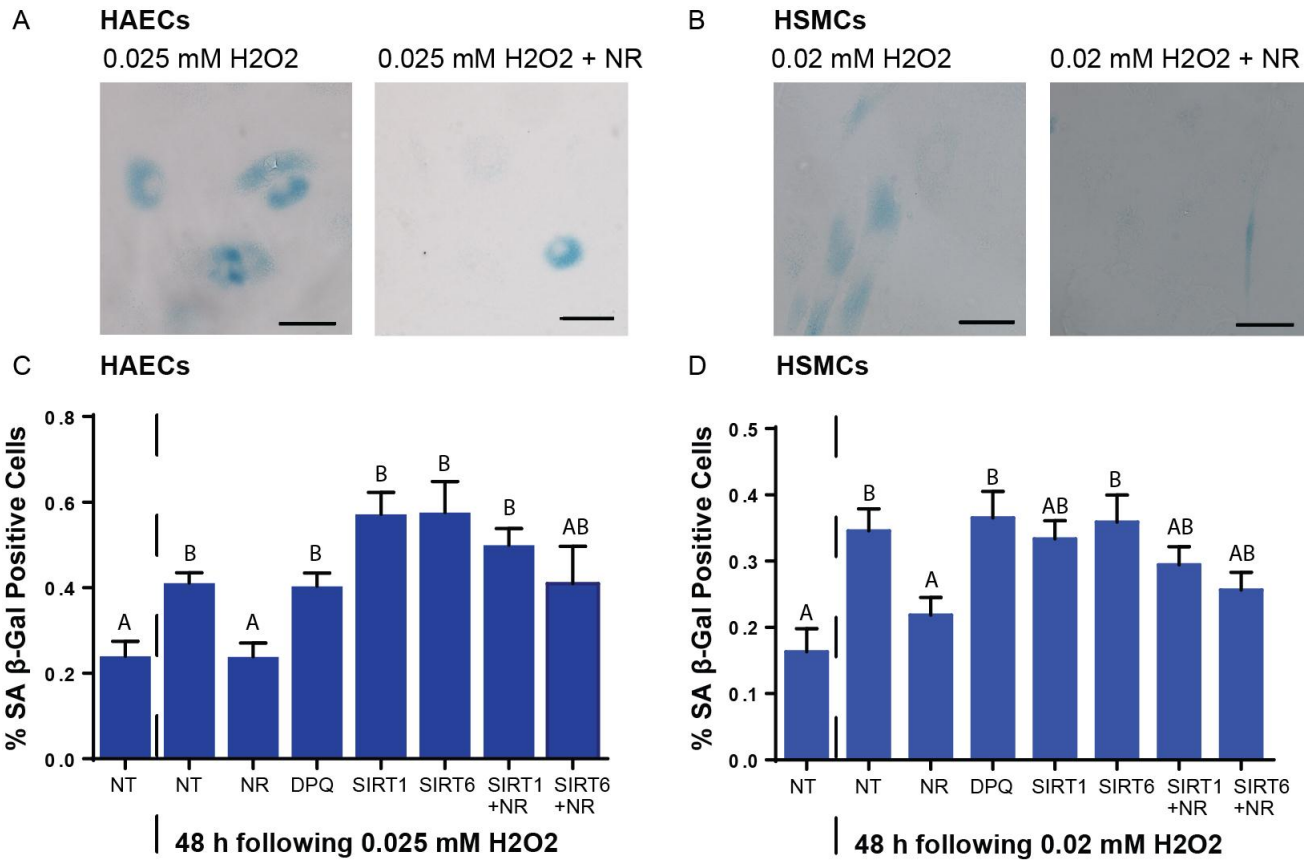
A
HAECs
0.025 mM H2O2
0.025 mM H2O2 + NR
B
HSMCs
0.02 mM H2O2
0.02 mM H2O2 + NR
C
HAECs
% SA β-Gal Positive Cells
0.0
0.2
0.4
0.6
0.8
A
B
A
B
B
B
AB
NT
NT
NR
DPQ
SIRT1
SIRT6
SIRT1 +NR
SIRT6 +NR
48 h following 0.025 mM H2O2
D
HSMCs
% SA β-Gal Positive Cells
0.0
0.1
0.2
0.3
0.4
0.5
A
B
A
B
AB
B
AB
AB
NT
NT
NR
DPQ
SIRT1
SIRT6
SIRT1 +NR
SIRT6 +NR
48 h following 0.02 mM H2O2

4 – DISCUSSION

The major findings of this thesis are summarized:

1. Abundance of Nrk1, a critical enzyme responsible for NR conversion in NAD^+, is upregulated in vivo under conditions of NAD^+ pathway deficiencies in brain, aorta and heart.
2. The human vascular cell lines, HSMC & HAEC, express Nrk1 and NR delivery lead to a dose-dependent increase in cellular NAD^+ content.
3. Oxidative stress insults induced oxidative DNA lesions and activated PARP, resulting in pronounced NAD^+-consumption in vascular cells.
4. NR delivery generated NAD^+ reserves that buffered PARP-mediated NAD^+ consumption during oxidative insults in vascular cells.
5. NR delivery preserved viability and morphology and promoted DNA repair following oxidative stress insult in vascular cells.
6. PARP inhibition generated NAD^+ reserves by blocking consumption. This preserved viability and morphology, but at the cost of impaired DNA damage repair.
7. NR delivery preserved viability, protected against senescence and promoted DNA repair in vascular cells with partial support for SIRT1- and SIRT6- dependent pathways.

4.1 Potential of NR Delivery in Vascular Aging

Vascular pathology and inflammation, arising predominantly in aged vasculature, is associated with chronic oxidative stress (65, 226-228). Current interventions are limited and involve pronounced lifestyle changes in diet and physical activity, which can be challenging. There is growing appreciation for the impact of NAD^+ biology in aging, in part because of increased oxidative stress induces NAD^+ depletion (194-196). There are molecular pathways that may be contributing to these observed changes, including (1) PARP activation, (2) declining NAMPT expression, and (3)

relative nutritional deficiencies. Notably, all of these pathways centre on vulnerability of NAD^+ supply systems in aged tissues. NR delivery is an emerging intervention to combat this NAD^+ deficiency.

In this study I have shown that human vascular endothelial and smooth muscle cells are equipped with the necessary systems to bring NR into the cell and metabolize NR into NAD^+. Vascular cells were able to stably increase intracellular NAD^+ levels. NR delivery is an emerging field and the limited current reports have assessed NR delivery to stably increase intracellular NAD^+ pools in yeast, mouse myoblast, mouse heptoma and human embryonic kidney cell lines (202, 233). This is the first report to my knowledge that assesses NR delivery in vascular cells.

Additionally, I have found that mouse aorta, comprising endothelial and smooth muscle cells, also expressed *Nrk1*. Further, under NAD^+ deficient conditions, characteristic of aged tissue, my preliminary data showed that mouse aorta upregulated *Nrk1*, independent of changes to other NAD^+ salvage enzymes. This suggests that NR delivery may be a preferred pathway to overcome depleted NAD^+ supply in vascular tissues. Previous reports have identified tissue-specific differential expression of NAD^+ salvage enzymes (204). Here, we expand the tissue profile to include aorta and confirm expression of Nrk1. Previous studies in yeast have noted an increased uptake of NR when other precursors are not available (202). Our findings build on this concept and identify selective upregulation of Nrk1 mRNA expression under NAD^+ deficient conditions that we speculate may facilitate NR uptake in the vasculature. Importantly, my findings set the stage for NR delivery in a vascular aging model.

4.2 Intracellular NAD^+ Pools Fuel Oxidative Stress Response

This study established that H_2O_2 induced oxidative DNA lesions in vascular cells. This was associated with PARP activation and profound NAD^+ consumption, in a PARP dependent manner.

Further, we show that PARP inhibition will maintain NAD^+ levels, protect against viability, but also preserve morphology in vascular cells exposed to an acute oxidative stress insults. The role of PARP as a major NAD^+ consumer in response to oxidative damage has been previously established (111). Recognizing the link between NAD^+ consumption and cell death, PARP inhibition studies have emerged reporting protection in models of acute DNA damage caused by chemotherapy drugs (121-123) and ischemia/reperfusion injury (252, 253). In these models, protection can be explained by PARP inhibition preserving NAD^+ levels, thereby preventing an energy crisis and maintaining SIRT function during times of stress. My data supports the principle that maintaining NAD^+ levels will prevent an energy crisis and protect against cell death. Expanding on this, my data also introduced the concept that PARP inhibition preserves cell morphology.

This study further demonstrated that the beneficial effects of increasing NAD^+ reserves can be obtained by NR delivery. My data showed that NR delivery elevated NAD^+ levels, protected against cell death, preserved cell morphology, and importantly increased DNA repair efficiency. Further, NR was observed to protect against H_2O_2-induced senescence. This data supports that NR generated NAD^+ reserves will fuel PARP function while maintaining NAD^+ levels above an energy crisis threshold (Fig. 4.1). Supplementation of other NAD^+ precursors (NA, NMN and Nam) was observed to mimic the effects of NR delivery on maintaining cell shape in these vascular cells. This finding further supports that the benefits of NR delivery are acting through increased intracellular NAD^+ pools.

My data supports that PARP inhibition, NR delivery, and delivery of NAD^+ precursor supplementation will increase NAD^+ supply to protect against oxidative stress insult. As discussed below, I propose that, of these approaches, NR delivery is superior.

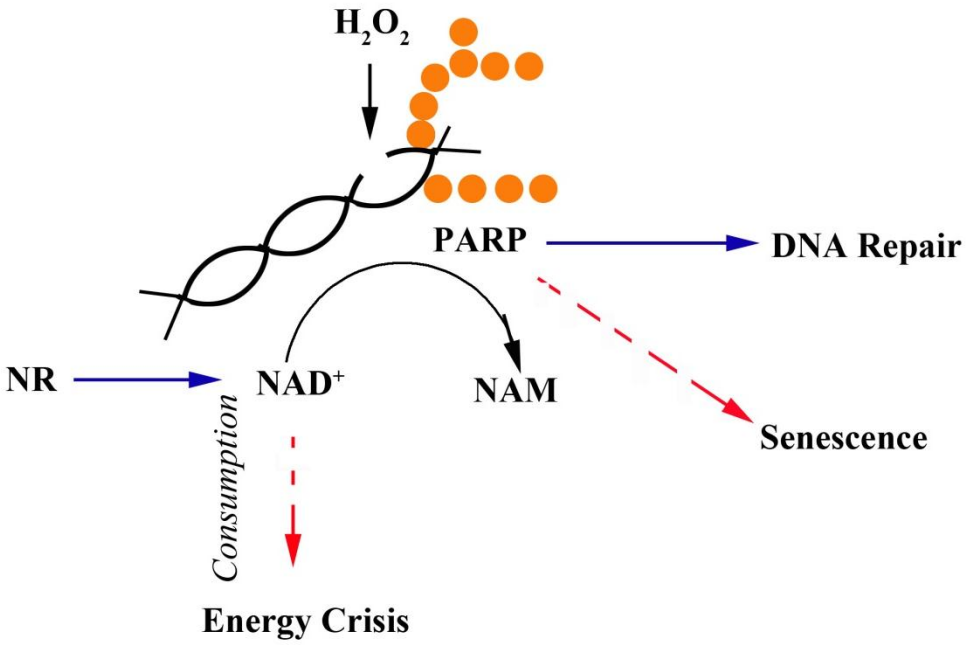

Figure 4.1 NR fuels PARP function to support DNA repair during oxidative insults. NR increases intracellular NAD^+ stores to facilitate cellular oxidative stress response. PARPs consume NAD^+ to catalyze PAR chains, which act to recruit downstream repair proteins. When NAD^+ levels are depleted beyond a threshold, an energy crisis ensues. Similarly, if NAD^+ levels are not sufficient to maintain PARP function or PARP is inhibited, cells may survive but are more likely to take on a senescent phenotype.

4.3 Limitations to PARP Inhibition

Importantly, this study directly addresses the limitations of PARP inhibition. PARP is activated in response to DNA damage to recruit repair enzymes to the site of damage (111). My data reveals that PARP inhibition will delay DNA repair in vascular cells. Additionally, I found that PARP inhibition did not prevent a senescent phenotype following oxidative stress insults. Thus PARP inhibition supports the rationale for increased NAD^+ reserves, but benefits of its intervention are short-term and restricted to acute models.

Since PARP is a nuclear enzyme, it is speculated that this intracellular NAD^+ increase is confined mostly to the nucleus and thus will likely effect only the SIRTs that reside there (SIRT1, SIRT6 and SIRT7). However, NR delivery has the potential to increase intracellular NAD^+ levels in additional subcellular compartments such as mitochondria (SIRT3, SIRT4 and SIRT5) and cytoplasm (SIRT1, SIRT2 and SIRT3) (254). A series of recent reports support this concept of confined subcellular NAD^+ pools. One report revealed that PARP-1 inhibition increased SIRT1 activity levels but not SIRT3, thereby increasing energy expenditure and protecting and against metabolic disease (255). Additional studies reported beneficial effects of NR delivery through SIRT3 activity in metabolic disease (233) and hearing loss (234). This supports the concept that NR delivery may have broader effects of increasing NAD^+ pools compared to PARP inhibition that may be confined to the nucleus. My data showed that despite beneficial effects that PARP-1 inhibition may have through nuclear SIRT activation, the consequences of impaired DNA repair response dominated in this oxidative stress model.

4.4 NR as a Superior NAD^+ Precursor

Despite benefits of other NAD^+ precursors on preserving cell morphology, there are advantages to NR delivery. First, only NR is a nutrient that is naturally present within the human diet

(216). Additionally, NR does not activate GPR109A, a niacin receptor, associated with NA-mediated painful flushing (229, 230). NMN is degraded outside of the cell and brought in as either NA, or NR, creating an additional step for up-take (201). Finally, Nam is a known SIRT inhibitor (256). Consequently, although NAD^+ precursors can similarly elevate NAD^+ levels, NR offers advantages over other NAD^+ precursors.

4.5 NR-mediated SIRT Activation in DNA Damage and Repair

As discussed, NR delivery may offer a more advantageous approach to increase intracellular NAD^+, increase sirtuin activity and thereby enhance oxidative stress response throughout the whole cell. My data showed that NR enhanced the DNA repair response. Through KD studies, I implicated a number of SIRTs in this effect. The identified involvement of SIRTs from various subcellular compartments supports the idea that NR has the ability to broadly increase intracellular NAD^+ levels.

In both cell types, SIRT1 and SIRT6 were implicated in NR-mediated DNA repair. Both of these SIRTs have downstream DNA repair targets (254). To my knowledge, no previous studies have directly looked at benefits of NR delivery in mediating DNA repair efficiency. However, one recent report found that both PARP inhibition and NR delivery were observed to overcome neurodegeneration-associated phenotypes induced by mutations to DNA repair proteins. Interestingly, this study looked at NRs effect on normalizing the transcriptome of diseased mice and found that NR normalized gene ontology terms for DNA damage repair, DNA damage response and oxidative stress. Additionally, a few studies have reported the role of SIRT1 (151, 153, 154, 165, 166) and SIRT6 (169-171) in promoting DNA repair. These reports may offer support for my data, which demonstrated NR-mediated DNA repair efficiency in a partially SIRT1 and SIRT6 dependent manner.

In addition to changes in the DNA repair response, SIRT1, 3, 5 and 6 have downstream targets on anti-oxidant machinery (257). Specifically, previous reports have identified SIRT1 as a regulator of anti-oxidant gene transcription in vascular endothelial cells (157, 158). A single study in human embryonic kidney cells did report an increase in SOD2 mRNA expression following NR delivery (233). However, my data showed that NR delivery did not induce transcriptional changes of anti-oxidant genes. Additionally, changes in transcription do not always mean changes in protein translation or activity, which were not assessed in this thesis.

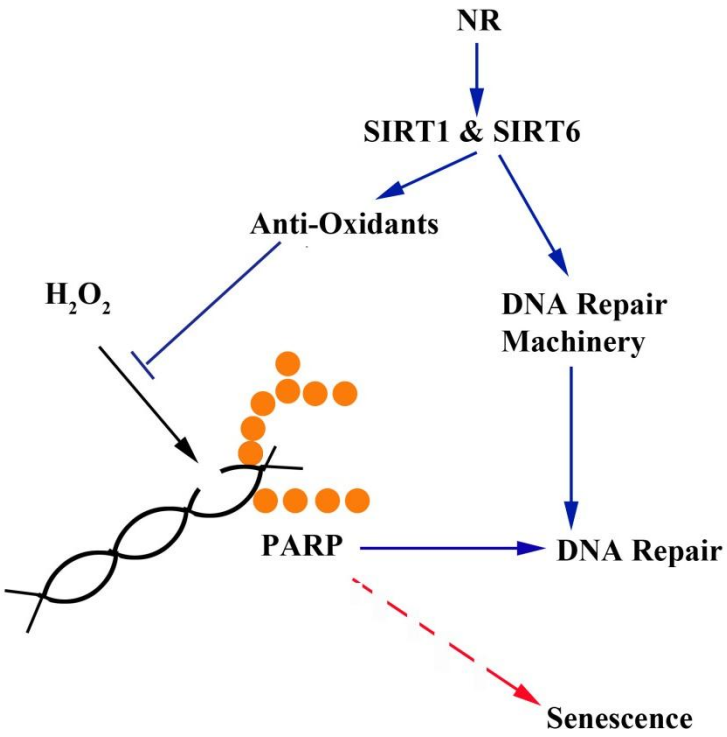

Figure 4.2 Increased SIRT1 & SIRT6 activity may enhance NRs protection through improved defence systems and repair responses. Intracellular NAD^+ reserves will fuel NAD^+-consuming SIRT activity. SIRT1 and SIRT6 have been reported to target regulators of anti-oxidant genes transcription and directly target enzymes involved in DNA repair. During times of oxidative stress, both of these pathways would contribute to improved outcomes with respect to maintaining genome integrity and evading senescence.

4.6 SIRT Involvement in Enhanced Viability

We observe improved cell viability with PARP inhibition and NR delivery following acute oxidative damage. I interpret these viability experiments in the context of an NAD^+-consumption model. Through NR delivery, or PARP inhibition, NAD^+ levels are maintained above an energy crisis threshold while cells continue to consume NAD^+ in their response to the oxidative stress insult.

In this study, I also revealed that NR-mediated protection from cell death was partially lost when SIRTs were knocked-down. Accordingly, an additional interpretation to explain protection from cell death is that NR and PARP inhibition increased NAD^+ levels and activated SIRT1 to partially promote viability. SIRT1 will deacetylate downstream targets such as FOXOs, which can signal for cell survival and promote stress responses (140). The deacetylation activities of SIRT1 have also been reported to increase autophagy (130). By inducing autophagy, the catabolic process to break-down inefficient organelles, additional energy stores are created and cellular energy metabolism is enhanced by healthier mitochondria (258). Both of these pathways could explain why NR protection from cell death was found to be partially SIRT1-dependent in both vascular cell types.

4.7 Role of SIRTs in Maintaining Cytoskeleton Integrity

Our data showed that NR supported cell morphology during times of oxidative stress by preventing cell shrinkage. Actin structures are essential to cell shape and our closer look at actin structures during the oxidative insult support the concept that NR supplementation maintains cytoskeleton integrity.

This link between NR enhancing actin structures has not yet been established. NR may be acting through anti-oxidant up-regulation to protect the cytoskeleton during the oxidative insult; however this concept was not fully explored in this thesis. Downstream target of sirtuins that regulate actin structures have not been well studied.

4.8 Implications of SIRTs in Vascular Aging

I found that SIRT1 and SIRT6 were observed to be abundantly expressed in aorta tissue. I also found that SIRT1 and SIRT6 were implicated in NR-mediated DNA repair in both cell types and protection to viability in HAECs. Importantly, by also studying senescence, I examined oxidative stress response in a model arguably more relevant to vascular aging compared to acute cell damage. Within this model, SIRT1 and SIRT6 were again implicated in NR's protection against senescence. This is consistent with previous literature that has implicated SIRT1 in preventing senescence and sirt6 decline associated with increased senescence (180, 259). In addition to expanding NR delivery interventions to include vascular tissues, we have shown that NR delivery will act through these two identified SIRTs to regulate vascular cell health during oxidative stress.

4.9 Limitations

My study revealed no changes in anti-oxidant gene expression following NR delivery. However, their potential involvement should not be ruled out. For my experiments, real-time PCR was used to analyze a small subset of the entire expression profile. A far more complete approach would be transcriptome sequencing and even this approach requires careful interpretation since data is compositional (constrained to relative values). Further, changes in transcription do not always mean changes in translation or activity, which would additionally need to be assessed.

SIRT-mediated changes in anti-oxidant gene regulation and cytoskeleton changes assume that higher NAD^+ levels are increasing SIRT activity. Currently, interpretations of downstream effects of SIRTs are based on this assumption. Support for NR-mediated increase in SIRT activity is currently limited. Two previous NR studies that observed beneficial effects of NR delivery reported SIRT-dependent mechanisms (233, 234). Only one of those two studies directly looked at SIRT1 and SIRT3 activity changes following NR delivery in human embryonic kidney cells (233). To overcome

this limitation, SIRT activity assays would be required to confirm that SIRT activity is increased in response to NR in human vascular cells.

Interpretation of SIRT KD with NR in determining if NR protection is abolished is limited by the fact that SIRTs themselves consume NAD^+. By inhibiting their NAD^+ consumption through KD, the interpretation is complicated by the possibility that SIRT KD alone is increasing NAD^+ levels. However, according to my results, higher NAD^+ levels should promote viability and DNA damage repair. Instead, I found that SIRT KD with NR delivery showed increased cell death and higher tail moment. Ultimately this implicates SIRT KD in detrimental effects on viability and DNA damage repair, despite any benefits that may be induced by additional NAD^+ supply.

Currently, interpretation of DNA damage repair experiments is confounded by potential differences in initial DNA damage insults. If NR delivery induced differences in anti-oxidant expression, NR-treated groups may have started with lower absolute DNA damage. This limitation could be overcome by using DNA damaging agents (doxorubicin, methy-methane sulphonate or paraquat) to induce DNA strand breaks instead of H_2O_2. This would eliminate any role that anti-oxidants may be playing and instead allow for interpretation of solely DNA damage repair.

Chronic vascular models such as atherosclerosis (120), ANGII infusion (124) and hypertension (115, 125) have been reported to benefit by PARP inhibition. PARP inhibition-induced beneficial effects in these models may be explained by blocking deleterious effects of down-stream PAR signalling, which has been associated with increased inflammation, oxidative stress and cell death (260). In our model of generating NAD^+ to fuel PARPs in a chronic setting, the adverse consequences of increased PAR signalling are not addressed. However, the final experiment of this study did show that NR was able to protect against H_2O_2-induced senescence whereas PARP inhibition was not. Additionally, my data suggests that NR may be acting partially through SIRTs.

Although the downstream SIRT-dependent pathways were not explored in this thesis, reduced oxidative damage or activated stress response pathways may have mitigated the deleterious effects of PAR chain formation.

4.10 Future Directions

Mode of cell death differences, following H_2O_2 stress, between NR-treated cells and vehicle control was not considered. Likely, a form of necrosis is occurring, initiated by an energy crisis following profound NAD^+ consumption (114, 119). More specifically, parthanatos may be occurring. Parthanatos is a necrotic mode of cell death, characterized by profound nuclear PAR chain accumulation, translocation of PAR to the mitochondria and release of apoptosis initiating factor (AIF). It is possible that NR is enabling a subset of cells to resist necrosis and instead initiate a mode of cell death less damaging to surrounding cells, such as apoptosis or necroptosis. Determination of necrosis versus apoptosis would be possible through a cell death kit using Ethidium Homodimer III to signal necrosis and Annexin-V on the plasma membrane to signal apoptosis. Additional mode of death considerations would include TUNEL assay, assessing DNA fragmentation, or Western blot of the caspase family of enzymes, to determine if cell death is caspase-dependent.

Additional cytoskeletal structures may be maintaining morphology during oxidative insults. Tubulin will act to maintain cell shape, but they also form networks for intracellular organelle and protein transport (261). Dynamic instability is crucial to tubulin function, as it will polymerize and de-polymerize continuously to transport across the cell. Post-translational modification, such as acetylation, is one regulator of tubulin dynamics. SIRT2 has been reported to deacetylate α-tubulin, in an NAD^+ dependent manner (262, 263). Changes in SIRT2 activity have been linked to altered microtubule dynamics (264). Further, agents that alter tubulin-mediated intracellular transport of

DNA repair proteins worsen DNA damage repair (265). Thus, an interesting next step would be to observe if NR is acting through SIRT2 to regulate cell shape and DNA repair via tubulin regulation.

Additionally, to strengthen the interpretation of the effects of SIRT KD on NRs protection to viability, cell shrinkage and tail moment end-points, an additional control of SIRT 1-7 KD without NR should be added. This would strengthen the argument that increased cell death and higher tail moment as a result of SIRT KD with NR is in fact demonstrating abolished NR protection. Currently, it is possible that SIRT KD is causing detrimental effects through a distinct pathway, occurring in parallel to NR-mediated signalling pathways.

My encouraging in vitro results have led to the design of in vivo experiments in our lab. The over-activation of the renin-angiotensin system has been associated with normal aging (85-88). Because of this, delivery of exogenous ANGII could be used to model age-associated changes of the vasculature in vivo. On a molecular level, ANGII will induce oxidative stress through eNOS uncoupling (92) and NAD(P)H oxidase activation (93, 94). Thus, ANGII infusion offers an in vivo model for oxidative stress insults. Experimental design for next steps was determined. Middle aged mice will be given NR (400 mg/kg/day) or vehicle control for seven weeks, including a three week pre-treatment with NR. Following this pre-treatment, oxidative stress will be induced by 4-weeks continuous ANGII infusion (1.44 mg/kg/day). Acting on evidence of enhanced oxidative stress response in vascular cells, this project will include an analysis of 8-oxoganine staining in the arteries of the heart of NR pre-treated mice following ANGII infusion. This study is currently underway and preliminary data are being generated.

4.11 Conclusion

In summary, I have found that PARP will consume NAD^+ to recruit repair proteins to the site of oxidative-stress-induced DNA damage. Through this pathway, depleted NAD^+ levels as a result of

PARP activity are speculated to contribute to vascular dysfunction in aging (65). My findings suggest that NR delivery will generate NAD^+ reserves to fuel oxidative stress responses. These NAD^+ reserves maintain PARP function during times of stress, but importantly continue to fuel SIRT function and energy metabolism. This intervention has the potential to overcome age-associated NAD^+ supply deficiencies to combat chronic oxidative stress insults.

5 –REFERENCES

1. Lakatta EG, Levy D. Arterial and cardiac aging: Major shareholders in cardiovascular disease enterprises: Part I: Aging arteries: A "set up" for vascular disease. Circulation. 2003 Jan 7;107(1):139-46.

2. Carmeliet P. Mechanisms of angiogenesis and arteriogenesis. Nat Med. 2000 Apr;6(4):389-95.

3. Stenmark KR, Yeager ME, El Kasmi KC, Nozik-Grayck E, Gerasimovskaya EV, Li M, et al. The adventitia: Essential regulator of vascular wall structure and function. Annu Rev Physiol. 2013;75:23-47.

4. Govers R, Rabelink TJ. Cellular regulation of endothelial nitric oxide synthase. Am J Physiol Renal Physiol. 2001 Feb;280(2):F193-206.

5. Qian J, Fulton D. Post-translational regulation of endothelial nitric oxide synthase in vascular endothelium. Front Physiol. 2013 Dec 13;4:347.

6. Hirata K, Miki N, Kuroda Y, Sakoda T, Kawashima S, Yokoyama M. Low concentration of oxidized low-density lipoprotein and lysophosphatidylcholine upregulate constitutive nitric oxide synthase mRNA expression in bovine aortic endothelial cells. Circ Res. 1995 Jun;76(6):958-62.

7. Drummond GR, Cai H, Davis ME, Ramasamy S, Harrison DG. Transcriptional and posttranscriptional regulation of endothelial nitric oxide synthase expression by hydrogen peroxide. Circ Res. 2000 Feb 18;86(3):347-54.

8. Kuboki K, Jiang ZY, Takahara N, Ha SW, Igarashi M, Yamauchi T, et al. Regulation of endothelial constitutive nitric oxide synthase gene expression in endothelial cells and in vivo : A specific vascular action of insulin. Circulation. 2000 Feb 15;101(6):676-81.

9. Matsushita H, Chang E, Glassford AJ, Cooke JP, Chiu CP, Tsao PS. eNOS activity is reduced in senescent human endothelial cells: Preservation by hTERT immortalization. Circ Res. 2001 Oct 26;89(9):793-8.

10. Tanabe T, Maeda S, Miyauchi T, Iemitsu M, Takanashi M, Irukayama-Tomobe Y, et al. Exercise training improves ageing-induced decrease in eNOS expression of the aorta. Acta Physiol Scand. 2003 May;178(1):3-10.

11. Woodman CR, Price EM, Laughlin MH. Aging induces muscle-specific impairment of endothelium-dependent dilation in skeletal muscle feed arteries. J Appl Physiol (1985). 2002 Nov;93(5):1685-90.

12. Hoffmann J, Haendeler J, Aicher A, Rossig L, Vasa M, Zeiher AM, et al. Aging enhances the sensitivity of endothelial cells toward apoptotic stimuli: Important role of nitric oxide. Circ Res. 2001 Oct 12;89(8):709-15.

13. Kilic U, Gok O, Erenberk U, Dundaroz MR, Torun E, Kucukardali Y, et al. A remarkable age-related increase in SIRT1 protein expression against oxidative stress in elderly: SIRT1 gene variants and longevity in human. PLoS One. 2015 Mar 18;10(3):e0117954.

14. Berkowitz DE, White R, Li D, Minhas KM, Cernetich A, Kim S, et al. Arginase reciprocally regulates nitric oxide synthase activity and contributes to endothelial dysfunction in aging blood vessels. Circulation. 2003 Oct 21;108(16):2000-6.

15. Ungvari Z, Buffenstein R, Austad SN, Podlutsky A, Kaley G, Csiszar A. Oxidative stress in vascular senescence: Lessons from successfully aging species. Front Biosci. 2008 May 1;13:5056-70.

16. Sun D, Huang A, Yan EH, Wu Z, Yan C, Kaminski PM, et al. Reduced release of nitric oxide to shear stress in mesenteric arteries of aged rats. Am J Physiol Heart Circ Physiol. 2004 Jun;286(6):H2249-56.

17. Csiszar A, Labinskyy N, Smith K, Rivera A, Orosz Z, Ungvari Z. Vasculoprotective effects of anti-tumor necrosis factor-alpha treatment in aging. Am J Pathol. 2007 Jan;170(1):388-98.

18. Csiszar A, Ungvari Z, Koller A, Edwards JG, Kaley G. Proinflammatory phenotype of coronary arteries promotes endothelial apoptosis in aging. Physiol Genomics. 2004 Mar 12;17(1):21-30.

19. Rivard A, Fabre JE, Silver M, Chen D, Murohara T, Kearney M, et al. Age-dependent impairment of angiogenesis. Circulation. 1999 Jan 5-12;99(1):111-20.

20. Jacobson A, Yan C, Gao Q, Rincon-Skinner T, Rivera A, Edwards J, et al. Aging enhances pressure-induced arterial superoxide formation. Am J Physiol Heart Circ Physiol. 2007 Sep;293(3):H1344-50.

21. Csiszar A, Ungvari Z, Edwards JG, Kaminski P, Wolin MS, Koller A, et al. Aging-induced phenotypic changes and oxidative stress impair coronary arteriolar function. Circ Res. 2002 Jun 14;90(11):1159-66.

22. Donato AJ, Eskurza I, Silver AE, Levy AS, Pierce GL, Gates PE, et al. Direct evidence of endothelial oxidative stress with aging in humans: Relation to impaired endothelium-dependent dilation and upregulation of nuclear factor-kappaB. Circ Res. 2007 Jun 8;100(11):1659-66.

23. Adler A, Messina E, Sherman B, Wang Z, Huang H, Linke A, et al. NAD(P)H oxidase-generated superoxide anion accounts for reduced control of myocardial O2 consumption by NO in old fischer 344 rats. Am J Physiol Heart Circ Physiol. 2003 Sep;285(3):H1015-22.

24. van der Loo B, Labugger R, Skepper JN, Bachschmid M, Kilo J, Powell JM, et al. Enhanced peroxynitrite formation is associated with vascular aging. J Exp Med. 2000 Dec 18;192(12):1731-44.

25. Jablonski KL, Seals DR, Eskurza I, Monahan KD, Donato AJ. High-dose ascorbic acid infusion abolishes chronic vasoconstriction and restores resting leg blood flow in healthy older men. J Appl Physiol (1985). 2007 Nov;103(5):1715-21.

26. Pacher P, Beckman JS, Liaudet L. Nitric oxide and peroxynitrite in health and disease. Physiol Rev. 2007 Jan;87(1):315-424.

27. Kuro-o M, Matsumura Y, Aizawa H, Kawaguchi H, Suga T, Utsugi T, et al. Mutation of the mouse klotho gene leads to a syndrome resembling ageing. Nature. 1997 Nov 6;390(6655):45-51.

28. Xu Y, Sun Z. Molecular basis of klotho: From gene to function in aging. Endocr Rev. 2015 Apr;36(2):174-93.

29. Martin-Nunez E, Donate-Correa J, Muros-de-Fuentes M, Mora-Fernandez C, Navarro-Gonzalez JF. Implications of klotho in vascular health and disease. World J Cardiol. 2014 Dec 26;6(12):1262-9.

30. Ravikumar P, Ye J, Zhang J, Pinch SN, Hu MC, Kuro-o M, et al. Alpha-klotho protects against oxidative damage in pulmonary epithelia. Am J Physiol Lung Cell Mol Physiol. 2014 Oct 1;307(7):L566-75.

31. Chen J, Goligorsky MS. Premature senescence of endothelial cells: Methusaleh's dilemma. Am J Physiol Heart Circ Physiol. 2006 May;290(5):H1729-39.

32. Vasa M, Breitschopf K, Zeiher AM, Dimmeler S. Nitric oxide activates telomerase and delays endothelial cell senescence. Circ Res. 2000 Sep 29;87(7):540-2.

33. Campisi J. Senescent cells, tumor suppression, and organismal aging: Good citizens, bad neighbors. Cell. 2005 Feb 25;120(4):513-22.

34. Campisi J. The role of cellular senescence in skin aging. J Investig Dermatol Symp Proc. 1998 Aug;3(1):1-5.

35. Wu J, Xia S, Kalionis B, Wan W, Sun T. The role of oxidative stress and inflammation in cardiovascular aging. Biomed Res Int. 2014;2014:615312.

36. Blasco MA. Telomeres and human disease: Ageing, cancer and beyond. Nat Rev Genet. 2005 Aug;6(8):611-22.

37. Aviv H, Khan MY, Skurnick J, Okuda K, Kimura M, Gardner J, et al. Age dependent aneuploidy and telomere length of the human vascular endothelium. Atherosclerosis. 2001 Dec;159(2):281-7.

38. Chang E, Harley CB. Telomere length and replicative aging in human vascular tissues. Proc Natl Acad Sci U S A. 1995 Nov 21;92(24):11190-4.

39. Minamino T, Mitsialis SA, Kourembanas S. Hypoxia extends the life span of vascular smooth muscle cells through telomerase activation. Mol Cell Biol. 2001 May;21(10):3336-42.

40. Minamino T, Miyauchi H, Yoshida T, Komuro I. Endothelial cell senescence in human atherosclerosis: Role of telomeres in endothelial dysfunction. J Cardiol. 2003 Jan;41(1):39-40.

41. Mayr M, Hu Y, Hainaut H, Xu Q. Mechanical stress-induced DNA damage and rac-p38MAPK signal pathways mediate p53-dependent apoptosis in vascular smooth muscle cells. FASEB J. 2002 Sep;16(11):1423-5.

42. Di Leonardo A, Linke SP, Clarkin K, Wahl GM. DNA damage triggers a prolonged p53-dependent G1 arrest and long-term induction of Cip1 in normal human fibroblasts. Genes Dev. 1994 Nov 1;8(21):2540-51.

43. Shaltiel IA, Krenning L, Bruinsma W, Medema RH. The same, only different - DNA damage checkpoints and their reversal throughout the cell cycle. J Cell Sci. 2015 Feb 15;128(4):607-20.

44. Voghel G, Thorin-Trescases N, Farhat N, Mamarbachi AM, Villeneuve L, Fortier A, et al. Chronic treatment with N-acetyl-cystein delays cellular senescence in endothelial cells isolated from a subgroup of atherosclerotic patients. Mech Ageing Dev. 2008 May;129(5):261-70.

45. Kurz DJ, Decary S, Hong Y, Trivier E, Akhmedov A, Erusalimsky JD. Chronic oxidative stress compromises telomere integrity and accelerates the onset of senescence in human endothelial cells. J Cell Sci. 2004 May 1;117(Pt 11):2417-26.

46. Erusalimsky JD. Vascular endothelial senescence: From mechanisms to pathophysiology. J Appl Physiol (1985). 2009 Jan;106(1):326-32.

47. Imanishi T, Hano T, Nishio I. Angiotensin II accelerates endothelial progenitor cell senescence through induction of oxidative stress. J Hypertens. 2005 Jan;23(1):97-104.

48. Minamino T, Komuro I. Vascular aging: Insights from studies on cellular senescence, stem cell aging, and progeroid syndromes. Nat Clin Pract Cardiovasc Med. 2008 Oct;5(10):637-48.

49. Walter DH, Rittig K, Bahlmann FH, Kirchmair R, Silver M, Murayama T, et al. Statin therapy accelerates reendothelialization: A novel effect involving mobilization and incorporation of bone marrow-derived endothelial progenitor cells. Circulation. 2002 Jun 25;105(25):3017-24.

50. Vasa M, Fichtlscherer S, Aicher A, Adler K, Urbich C, Martin H, et al. Number and migratory activity of circulating endothelial progenitor cells inversely correlate with risk factors for coronary artery disease. Circ Res. 2001 Jul 6;89(1):E1-7.

51. Hill JM, Zalos G, Halcox JP, Schenke WH, Waclawiw MA, Quyyumi AA, et al. Circulating endothelial progenitor cells, vascular function, and cardiovascular risk. N Engl J Med. 2003 Feb 13;348(7):593-600.

52. Thum T, Hoeber S, Froese S, Klink I, Stichtenoth DO, Galuppo P, et al. Age-dependent impairment of endothelial progenitor cells is corrected by growth-hormone-mediated increase of insulin-like growth-factor-1. Circ Res. 2007 Feb 16;100(3):434-43.

53. Shantsila E, Watson T, Lip GY. Endothelial progenitor cells in cardiovascular disorders. J Am Coll Cardiol. 2007 Feb 20;49(7):741-52.

54. Hasty P, Campisi J, Hoeijmakers J, van Steeg H, Vijg J. Aging and genome maintenance: Lessons from the mouse? Science. 2003 Feb 28;299(5611):1355-9.

55. Lambeth JD. NOX enzymes and the biology of reactive oxygen. Nat Rev Immunol. 2004 Mar;4(3):181-9.

56. Balaban RS, Nemoto S, Finkel T. Mitochondria, oxidants, and aging. Cell. 2005 Feb 25;120(4):483-95.

57. Lanza IR, Nair KS. Mitochondrial function as a determinant of life span. Pflugers Arch. 2010 Jan;459(2):277-89.

58. Hoeijmakers JH. Genome maintenance mechanisms for preventing cancer. Nature. 2001 May 17;411(6835):366-74.

59. Ungvari Z, Labinskyy N, Gupte S, Chander PN, Edwards JG, Csiszar A. Dysregulation of mitochondrial biogenesis in vascular endothelial and smooth muscle cells of aged rats. Am J Physiol Heart Circ Physiol. 2008 May;294(5):H2121-8.

60. Burns EM, Kruckeberg TW, Comerford LE, Buschmann MT. Thinning of capillary walls and declining numbers of endothelial mitochondria in the cerebral cortex of the aging primate, macaca nemestrina. J Gerontol. 1979 Sep;34(5):642-50.

61. Masoro EJ, Austad SN. The evolution of the antiaging action of dietary restriction: A hypothesis. J Gerontol A Biol Sci Med Sci. 1996 Nov;51(6):B387-91.

62. Dada LA, Chandel NS, Ridge KM, Pedemonte C, Bertorello AM, Sznajder JI. Hypoxia-induced endocytosis of na,K-ATPase in alveolar epithelial cells is mediated by mitochondrial reactive oxygen species and PKC-zeta. J Clin Invest. 2003 Apr;111(7):1057-64.

63. Nemoto S, Takeda K, Yu ZX, Ferrans VJ, Finkel T. Role for mitochondrial oxidants as regulators of cellular metabolism. Mol Cell Biol. 2000 Oct;20(19):7311-8.

64. Ungvari Z, Orosz Z, Labinskyy N, Rivera A, Xiangmin Z, Smith K, et al. Increased mitochondrial H2O2 production promotes endothelial NF-kappaB activation in aged rat arteries. Am J Physiol Heart Circ Physiol. 2007 Jul;293(1):H37-47.

65. Ungvari Z, Kaley G, de Cabo R, Sonntag WE, Csiszar A. Mechanisms of vascular aging: New perspectives. J Gerontol A Biol Sci Med Sci. 2010 Oct;65(10):1028-41.

66. Brenerman BM, Illuzzi JL, Wilson DM,3rd. Base excision repair capacity in informing healthspan. Carcinogenesis. 2014 Dec;35(12):2643-52.

67. Shigenaga MK, Aboujaoude EN, Chen Q, Ames BN. Assays of oxidative DNA damage biomarkers 8-oxo-2'-deoxyguanosine and 8-oxoguanine in nuclear DNA and biological fluids by high-performance liquid chromatography with electrochemical detection. Methods Enzymol. 1994;234:16-33.

68. Grollman AP, Moriya M. Mutagenesis by 8-oxoguanine: An enemy within. Trends Genet. 1993 Jul;9(7):246-9.

69. Dizdaroglu M. Oxidatively induced DNA damage: Mechanisms, repair and disease. Cancer Lett. 2012 Dec 31;327(1-2):26-47.

70. Dahm-Daphi J, Sass C, Alberti W. Comparison of biological effects of DNA damage induced by ionizing radiation and hydrogen peroxide in CHO cells. Int J Radiat Biol. 2000 Jan;76(1):67-75.

71. Sedelnikova OA, Redon CE, Dickey JS, Nakamura AJ, Georgakilas AG, Bonner WM. Role of oxidatively induced DNA lesions in human pathogenesis. Mutat Res. 2010 Apr-Jun;704(1-3):152-9.

72. Driessens N, Versteyhe S, Ghaddhab C, Burniat A, De Deken X, Van Sande J, et al. Hydrogen peroxide induces DNA single- and double-strand breaks in thyroid cells and is therefore a potential mutagen for this organ. Endocr Relat Cancer. 2009 Sep;16(3):845-56.

73. Katsube T, Mori M, Tsuji H, Shiomi T, Wang B, Liu Q, et al. Most hydrogen peroxide-induced histone H2AX phosphorylation is mediated by ATR and is not dependent on DNA double-strand breaks. J Biochem. 2014 Aug;156(2):85-95.

74. Matthews C, Gorenne I, Scott S, Figg N, Kirkpatrick P, Ritchie A, et al. Vascular smooth muscle cells undergo telomere-based senescence in human atherosclerosis: Effects of telomerase and oxidative stress. Circ Res. 2006 Jul 21;99(2):156-64.

75. Kunieda T, Minamino T, Nishi J, Tateno K, Oyama T, Katsuno T, et al. Angiotensin II induces premature senescence of vascular smooth muscle cells and accelerates the development of atherosclerosis via a p21-dependent pathway. Circulation. 2006 Aug 29;114(9):953-60.

76. Minamino T, Yoshida T, Tateno K, Miyauchi H, Zou Y, Toko H, et al. Ras induces vascular smooth muscle cell senescence and inflammation in human atherosclerosis. Circulation. 2003 Nov 4;108(18):2264-9.

77. Park CB, Larsson NG. Mitochondrial DNA mutations in disease and aging. J Cell Biol. 2011 May 30;193(5):809-18.

78. Kujoth GC, Hiona A, Pugh TD, Someya S, Panzer K, Wohlgemuth SE, et al. Mitochondrial DNA mutations, oxidative stress, and apoptosis in mammalian aging. Science. 2005 Jul 15;309(5733):481-4.

79. Trifunovic A, Hansson A, Wredenberg A, Rovio AT, Dufour E, Khvorostov I, et al. Somatic mtDNA mutations cause aging phenotypes without affecting reactive oxygen species production. Proc Natl Acad Sci U S A. 2005 Dec 13;102(50):17993-8.

80. Gomes AP, Price NL, Ling AJ, Moslehi JJ, Montgomery MK, Rajman L, et al. Declining NAD(+) induces a pseudohypoxic state disrupting nuclear-mitochondrial communication during aging. Cell. 2013 Dec 19;155(7):1624-38.

81. Durik M, Kavousi M, van der Pluijm I, Isaacs A, Cheng C, Verdonk K, et al. Nucleotide excision DNA repair is associated with age-related vascular dysfunction. Circulation. 2012 Jul 24;126(4):468-78.

82. Galley HF. Oxidative stress and mitochondrial dysfunction in sepsis. Br J Anaesth. 2011 Jul;107(1):57-64.

83. Duran-Bedolla J, Montes de Oca-Sandoval MA, Saldana-Navor V, Villalobos-Silva JA, Rodriguez MC, Rivas-Arancibia S. Sepsis, mitochondrial failure and multiple organ dysfunction. Clin Invest Med. 2014 Apr 1;37(2):E58-69.

84. Rautureau Y, Paradis P, Schiffrin EL. Cross-talk between aldosterone and angiotensin signaling in vascular smooth muscle cells. Steroids. 2011 Aug;76(9):834-9.

85. Baylis C, Engels K, Hymel A, Navar LG. Plasma renin activity and metabolic clearance rate of angiotensin II in the unstressed aging rat. Mech Ageing Dev. 1997 Aug;97(2):163-72.

86. Thompson MM, Oyama TT, Kelly FJ, Kennefick TM, Anderson S. Activity and responsiveness of the renin-angiotensin system in the aging rat. Am J Physiol Regul Integr Comp Physiol. 2000 Nov;279(5):R1787-94.

87. Wang M, Takagi G, Asai K, Resuello RG, Natividad FF, Vatner DE, et al. Aging increases aortic MMP-2 activity and angiotensin II in nonhuman primates. Hypertension. 2003 Jun;41(6):1308-16.

88. Groban L, Pailes NA, Bennett CD, Carter CS, Chappell MC, Kitzman DW, et al. Growth hormone replacement attenuates diastolic dysfunction and cardiac angiotensin II expression in senescent rats. J Gerontol A Biol Sci Med Sci. 2006 Jan;61(1):28-35.

89. Ishizaka N, Mitani H, Nagai R. Angiotensin II regulates klotho gene expression. Nihon Rinsho. 2002 Oct;60(10):1935-9.

90. Lin SD, Zhou QL, Zhan F, Chen DJ, Li WN. Fosinopril up-regulates and ameliorates the ang II induced down-expression of klotho gene in NRK-52E. Zhongguo Ying Yong Sheng Li Xue Za Zhi. 2010 Aug;26(3):348-51.

91. Mehta PK, Griendling KK. Angiotensin II cell signaling: Physiological and pathological effects in the cardiovascular system. Am J Physiol Cell Physiol. 2007 Jan;292(1):C82-97.

92. Mollnau H, Wendt M, Szocs K, Lassegue B, Schulz E, Oelze M, et al. Effects of angiotensin II infusion on the expression and function of NAD(P)H oxidase and components of nitric oxide/cGMP signaling. Circ Res. 2002 Mar 8;90(4):E58-65.

93. Griendling KK, Ushio-Fukai M. Reactive oxygen species as mediators of angiotensin II signaling. Regul Pept. 2000 Jul 28;91(1-3):21-7.

94. Kimura S, Zhang GX, Nishiyama A, Shokoji T, Yao L, Fan YY, et al. Role of NAD(P)H oxidase- and mitochondria-derived reactive oxygen species in cardioprotection of ischemic reperfusion injury by angiotensin II. Hypertension. 2005 May;45(5):860-6.

95. Pueyo ME, Arnal JF, Rami J, Michel JB. Angiotensin II stimulates the production of NO and peroxynitrite in endothelial cells. Am J Physiol. 1998 Jan;274(1 Pt 1):C214-20.

96. Touyz RM. Activated oxygen metabolites: Do they really play a role in angiotensin II-regulated vascular tone? J Hypertens. 2003 Dec;21(12):2235-8.

97. Imanishi T, Hano T, Nishio I. Angiotensin II accelerates endothelial progenitor cell senescence through induction of oxidative stress. J Hypertens. 2005 Jan;23(1):97-104.

98. Faraci FM, Didion SP. Vascular protection: Superoxide dismutase isoforms in the vessel wall. Arterioscler Thromb Vasc Biol. 2004 Aug;24(8):1367-73.

99. Radi R, Turrens JF, Chang LY, Bush KM, Crapo JD, Freeman BA. Detection of catalase in rat heart mitochondria. J Biol Chem. 1991 Nov 15;266(32):22028-34.

100. Chang TS, Cho CS, Park S, Yu S, Kang SW, Rhee SG. Peroxiredoxin III, a mitochondrion-specific peroxidase, regulates apoptotic signaling by mitochondria. J Biol Chem. 2004 Oct 1;279(40):41975-84.

101. Taylor SW, Fahy E, Zhang B, Glenn GM, Warnock DE, Wiley S, et al. Characterization of the human heart mitochondrial proteome. Nat Biotechnol. 2003 Mar;21(3):281-6.

102. Wenzel P, Schuhmacher S, Kienhofer J, Muller J, Hortmann M, Oelze M, et al. Manganese superoxide dismutase and aldehyde dehydrogenase deficiency increase mitochondrial oxidative stress and aggravate age-dependent vascular dysfunction. Cardiovasc Res. 2008 Nov 1;80(2):280-9.

103. He T, Joyner MJ, Katusic ZS. Aging decreases expression and activity of glutathione peroxidase-1 in human endothelial progenitor cells. Microvasc Res. 2009 Dec;78(3):447-52.

104. Pierce GL, Donato AJ, LaRocca TJ, Eskurza I, Silver AE, Seals DR. Habitually exercising older men do not demonstrate age-associated vascular endothelial oxidative stress. Aging Cell. 2011 Dec;10(6):1032-7.

105. Thangaswamy S, Bridenbaugh EA, Gashev AA. Evidence of increased oxidative stress in aged mesenteric lymphatic vessels. Lymphat Res Biol. 2012 Jun;10(2):53-62.

106. Lund DD, Chu Y, Miller JD, Heistad DD. Protective effect of extracellular superoxide dismutase on endothelial function during aging. Am J Physiol Heart Circ Physiol. 2009 Jun;296(6):H1920-5.

107. Xu Z, Zhang L, Zhang W, Meng D, Zhang H, Jiang Y, et al. SIRT6 rescues the age related decline in base excision repair in a PARP1-dependent manner. Cell Cycle. 2015;14(2):269-76.

108. Takata M, Sasaki MS, Sonoda E, Morrison C, Hashimoto M, Utsumi H, et al. Homologous recombination and non-homologous end-joining pathways of DNA double-strand break repair have overlapping roles in the maintenance of chromosomal integrity in vertebrate cells. EMBO J. 1998 Sep 15;17(18):5497-508.

109. King BS, Cooper KL, Liu KJ, Hudson LG. Poly(ADP-ribose) contributes to an association between poly(ADP-ribose) polymerase-1 and xeroderma pigmentosum complementation group A in nucleotide excision repair. J Biol Chem. 2012 Nov 16;287(47):39824-33.

110. Drew Y, Calvert H. The potential of PARP inhibitors in genetic breast and ovarian cancers. Ann N Y Acad Sci. 2008 Sep;1138:136-45.

111. Rouleau M, Patel A, Hendzel MJ, Kaufmann SH, Poirier GG. PARP inhibition: PARP1 and beyond. Nat Rev Cancer. 2010 Apr;10(4):293-301.

112. Hassa PO, Hottiger MO. A role of poly (ADP-ribose) polymerase in NF-kappaB transcriptional activation. Biol Chem. 1999 Jul-Aug;380(7-8):953-9.

113. Carrillo A, Monreal Y, Ramirez P, Marin L, Parrilla P, Oliver FJ, et al. Transcription regulation of TNF-alpha-early response genes by poly(ADP-ribose) polymerase-1 in murine heart endothelial cells. Nucleic Acids Res. 2004 Feb 3;32(2):757-66.

114. Ha HC, Snyder SH. Poly(ADP-ribose) polymerase is a mediator of necrotic cell death by ATP depletion. Proc Natl Acad Sci U S A. 1999 Nov 23;96(24):13978-82.

115. Meloche J, Pflieger A, Vaillancourt M, Paulin R, Potus F, Zervopoulos S, et al. Role for DNA damage signaling in pulmonary arterial hypertension. Circulation. 2014 Feb 18;129(7):786-97.

116. Pacher P, Vaslin A, Benko R, Mabley JG, Liaudet L, Hasko G, et al. A new, potent poly(ADP-ribose) polymerase inhibitor improves cardiac and vascular dysfunction associated with advanced aging. J Pharmacol Exp Ther. 2004 Nov;311(2):485-91.

117. Burkle A, Beneke S, Muiras ML. Poly(ADP-ribosyl)ation and aging. Exp Gerontol. 2004 Nov-Dec;39(11-12):1599-601.

118. Simonin F, Hofferer L, Panzeter PL, Muller S, de Murcia G, Althaus FR. The carboxyl-terminal domain of human poly(ADP-ribose) polymerase. overproduction in escherichia coli, large scale purification, and characterization. J Biol Chem. 1993 Jun 25;268(18):13454-61.

119. Berger NA. Poly(ADP-ribose) in the cellular response to DNA damage. Radiat Res. 1985 Jan;101(1):4-15.

120. Hans CP, Zerfaoui M, Naura AS, Catling A, Boulares AH. Differential effects of PARP inhibition on vascular cell survival and ACAT-1 expression favouring atherosclerotic plaque stability. Cardiovasc Res. 2008 Jun 1;78(3):429-39.

121. Szanto M, Rutkai I, Hegedus C, Czikora A, Rozsahegyi M, Kiss B, et al. Poly(ADP-ribose) polymerase-2 depletion reduces doxorubicin-induced damage through SIRT1 induction. Cardiovasc Res. 2011 Dec 1;92(3):430-8.

122. Shah GM, Robu M, Purohit NK, Rajawat J, Tentori L, Graziani G. PARP inhibitors in cancer therapy: Magic bullets but moving targets. Front Oncol. 2013 Nov 14;3:279.

123. Pacher P, Liaudet L, Mabley JG, Cziraki A, Hasko G, Szabo C. Beneficial effects of a novel ultrapotent poly(ADP-ribose) polymerase inhibitor in murine models of heart failure. Int J Mol Med. 2006 Feb;17(2):369-75.

124. Liu M, Li Z, Chen GW, Li ZM, Wang LP, Ye JT, et al. AG-690/11026014, a novel PARP-1 inhibitor, protects cardiomyocytes from AngII-induced hypertrophy. Mol Cell Endocrinol. 2014 Jul 5;392(1-2):14-22.

125. Kaur G, Singh N, Lingeshwar P, Siddiqui HH, Hanif K. Poly (ADP-ribose) polymerase-1: An emerging target in right ventricle dysfunction associated with pulmonary hypertension. Pulm Pharmacol Ther. 2014 Dec 3.

126. Brunyanszki A, Hegedus C, Szanto M, Erdelyi K, Kovacs K, Schreiber V, et al. Genetic ablation of PARP-1 protects against oxazolone-induced contact hypersensitivity by modulating oxidative stress. J Invest Dermatol. 2010 Nov;130(11):2629-37.

127. Ungvari Z, Parrado-Fernandez C, Csiszar A, de Cabo R. Mechanisms underlying caloric restriction and lifespan regulation: Implications for vascular aging. Circ Res. 2008 Mar 14;102(5):519-28.

128. Rubinsztein DC, Codogno P, Levine B. Autophagy modulation as a potential therapeutic target for diverse diseases. Nat Rev Drug Discov. 2012 Sep;11(9):709-30.

129. Pyo JO, Yoo SM, Ahn HH, Nah J, Hong SH, Kam TI, et al. Overexpression of Atg5 in mice activates autophagy and extends lifespan. Nat Commun. 2013;4:2300.

130. Madeo F, Pietrocola F, Eisenberg T, Kroemer G. Caloric restriction mimetics: Towards a molecular definition. Nat Rev Drug Discov. 2014 Oct;13(10):727-40.

131. Yu J, Auwerx J. The role of sirtuins in the control of metabolic homeostasis. Ann N Y Acad Sci. 2009 Sep;1173 Suppl 1:E10-9.

132. Kelly G. A review of the sirtuin system, its clinical implications, and the potential role of dietary activators like resveratrol: Part 1. Altern Med Rev. 2010 Sep;15(3):245-63.

133. Sauve AA. NAD+ and vitamin B3: From metabolism to therapies. J Pharmacol Exp Ther. 2008 Mar;324(3):883-93.

134. Michishita E, Park JY, Burneskis JM, Barrett JC, Horikawa I. Evolutionarily conserved and nonconserved cellular localizations and functions of human SIRT proteins. Mol Biol Cell. 2005 Oct;16(10):4623-35.

135. Zhang T, Kraus WL. SIRT1-dependent regulation of chromatin and transcription: Linking NAD(+) metabolism and signaling to the control of cellular functions. Biochim Biophys Acta. 2010 Aug;1804(8):1666-75.

136. Lin SJ, Ford E, Haigis M, Liszt G, Guarente L. Calorie restriction extends yeast life span by lowering the level of NADH. Genes Dev. 2004 Jan 1;18(1):12-6.

137. Csiszar A, Labinskyy N, Podlutsky A, Kaminski PM, Wolin MS, Zhang C, et al. Vasoprotective effects of resveratrol and SIRT1: Attenuation of cigarette smoke-induced oxidative stress and proinflammatory phenotypic alterations. Am J Physiol Heart Circ Physiol. 2008 Jun;294(6):H2721-35.

138. Shinmura K, Tamaki K, Bolli R. Impact of 6-mo caloric restriction on myocardial ischemic tolerance: Possible involvement of nitric oxide-dependent increase in nuclear Sirt1. Am J Physiol Heart Circ Physiol. 2008 Dec;295(6):H2348-55.

139. Mattagajasingh I, Kim CS, Naqvi A, Yamamori T, Hoffman TA, Jung SB, et al. SIRT1 promotes endothelium-dependent vascular relaxation by activating endothelial nitric oxide synthase. Proc Natl Acad Sci U S A. 2007 Sep 11;104(37):14855-60.

140. Luo XY, Qu SL, Tang ZH, Zhang Y, Liu MH, Peng J, et al. SIRT1 in cardiovascular aging. Clin Chim Acta. 2014 Nov 1;437:106-14.

141. Donato AJ, Magerko KA, Lawson BR, Durrant JR, Lesniewski LA, Seals DR. SIRT-1 and vascular endothelial dysfunction with ageing in mice and humans. J Physiol. 2011 Sep 15;589(Pt 18):4545-54.

142. Zarzuelo MJ, Lopez-Sepulveda R, Sanchez M, Romero M, Gomez-Guzman M, Ungvary Z, et al. SIRT1 inhibits NADPH oxidase activation and protects endothelial function in the rat aorta: Implications for vascular aging. Biochem Pharmacol. 2013 May 1;85(9):1288-96.

143. Zu Y, Liu L, Lee MY, Xu C, Liang Y, Man RY, et al. SIRT1 promotes proliferation and prevents senescence through targeting LKB1 in primary porcine aortic endothelial cells. Circ Res. 2010 Apr 30;106(8):1384-93.

144. Ota H, Akishita M, Eto M, Iijima K, Kaneki M, Ouchi Y. Sirt1 modulates premature senescence-like phenotype in human endothelial cells. J Mol Cell Cardiol. 2007 Nov;43(5):571-9.

145. Csiszar A, Labinskyy N, Jimenez R, Pinto JT, Ballabh P, Losonczy G, et al. Anti-oxidative and anti-inflammatory vasoprotective effects of caloric restriction in aging: Role of circulating factors and SIRT1. Mech Ageing Dev. 2009 Aug;130(8):518-27.

146. Ou X, Lee MR, Huang X, Messina-Graham S, Broxmeyer HE. SIRT1 positively regulates autophagy and mitochondria function in embryonic stem cells under oxidative stress. Stem Cells. 2014 May;32(5):1183-94.

147. Lee IH, Cao L, Mostoslavsky R, Lombard DB, Liu J, Bruns NE, et al. A role for the NAD-dependent deacetylase Sirt1 in the regulation of autophagy. Proc Natl Acad Sci U S A. 2008 Mar 4;105(9):3374-9.

148. Guarente L. Calorie restriction and sirtuins revisited. Genes Dev. 2013 Oct 1;27(19):2072-85.

149. Kawashima T, Inuzuka Y, Okuda J, Kato T, Niizuma S, Tamaki Y, et al. Constitutive SIRT1 overexpression impairs mitochondria and reduces cardiac function in mice. J Mol Cell Cardiol. 2011 Dec;51(6):1026-36.

150. Alcendor RR, Gao S, Zhai P, Zablocki D, Holle E, Yu X, et al. Sirt1 regulates aging and resistance to oxidative stress in the heart. Circ Res. 2007 May 25;100(10):1512-21.

151. Herranz D, Munoz-Martin M, Canamero M, Mulero F, Martinez-Pastor B, Fernandez-Capetillo O, et al. Sirt1 improves healthy ageing and protects from metabolic syndrome-associated cancer. Nat Commun. 2010 Apr 12;1:3.

152. Ruan Y, Dong C, Patel J, Duan C, Wang X, Wu X, et al. SIRT1 suppresses doxorubicin-induced cardiotoxicity by regulating the oxidative stress and p38MAPK pathways. Cell Physiol Biochem. 2015;35(3):1116-24.

153. van der Horst A, Tertoolen LG, de Vries-Smits LM, Frye RA, Medema RH, Burgering BM. FOXO4 is acetylated upon peroxide stress and deacetylated by the longevity protein hSir2(SIRT1). J Biol Chem. 2004 Jul 9;279(28):28873-9.

154. Kobayashi Y, Furukawa-Hibi Y, Chen C, Horio Y, Isobe K, Ikeda K, et al. SIRT1 is critical regulator of FOXO-mediated transcription in response to oxidative stress. Int J Mol Med. 2005 Aug;16(2):237-43.

155. Brunet A, Sweeney LB, Sturgill JF, Chua KF, Greer PL, Lin Y, et al. Stress-dependent regulation of FOXO transcription factors by the SIRT1 deacetylase. Science. 2004 Mar 26;303(5666):2011-5.

156. Daitoku H, Hatta M, Matsuzaki H, Aratani S, Ohshima T, Miyagishi M, et al. Silent information regulator 2 potentiates Foxo1-mediated transcription through its deacetylase activity. Proc Natl Acad Sci U S A. 2004 Jul 6;101(27):10042-7.

157. Olmos Y, Sanchez-Gomez FJ, Wild B, Garcia-Quintans N, Cabezudo S, Lamas S, et al. SirT1 regulation of antioxidant genes is dependent on the formation of a FoxO3a/PGC-1alpha complex. Antioxid Redox Signal. 2013 Nov 1;19(13):1507-21.

158. Cheng Y, Takeuchi H, Sonobe Y, Jin S, Wang Y, Horiuchi H, et al. Sirtuin 1 attenuates oxidative stress via upregulation of superoxide dismutase 2 and catalase in astrocytes. J Neuroimmunol. 2014 Apr 15;269(1-2):38-43.

159. Xia N, Strand S, Schlufter F, Siuda D, Reifenberg G, Kleinert H, et al. Role of SIRT1 and FOXO factors in eNOS transcriptional activation by resveratrol. Nitric Oxide. 2013 Aug 1;32:29-35.

160. Xie J, Zhang X, Zhang L. Negative regulation of inflammation by SIRT1. Pharmacol Res. 2013 Jan;67(1):60-7.

161. Yeung F, Hoberg JE, Ramsey CS, Keller MD, Jones DR, Frye RA, et al. Modulation of NF-kappaB-dependent transcription and cell survival by the SIRT1 deacetylase. EMBO J. 2004 Jun 16;23(12):2369-80.

162. Stein S, Matter CM. Protective roles of SIRT1 in atherosclerosis. Cell Cycle. 2011 Feb 15;10(4):640-7.

163. Gorospe M, de Cabo R. AsSIRTing the DNA damage response. Trends Cell Biol. 2008 Feb;18(2):77-83.

164. Wilusz CJ, Wilusz J. HuR-SIRT: The hairy world of posttranscriptional control. Mol Cell. 2007 Feb 23;25(4):485-7.

165. Peng L, Yuan Z, Li Y, Ling H, Izumi V, Fang B, et al. Ubiquitinated sirtuin 1 (SIRT1) function is modulated during DNA damage-induced cell death and survival. J Biol Chem. 2015 Feb 10.

166. Yuan Z, Zhang X, Sengupta N, Lane WS, Seto E. SIRT1 regulates the function of the nijmegen breakage syndrome protein. Mol Cell. 2007 Jul 6;27(1):149-62.

167. Kugel S, Mostoslavsky R. Chromatin and beyond: The multitasking roles for SIRT6. Trends Biochem Sci. 2014 Feb;39(2):72-81.

168. Mostoslavsky R, Chua KF, Lombard DB, Pang WW, Fischer MR, Gellon L, et al. Genomic instability and aging-like phenotype in the absence of mammalian SIRT6. Cell. 2006 Jan 27;124(2):315-29.

169. Toiber D, Erdel F, Bouazoune K, Silberman DM, Zhong L, Mulligan P, et al. SIRT6 recruits SNF2H to DNA break sites, preventing genomic instability through chromatin remodeling. Mol Cell. 2013 Aug 22;51(4):454-68.

170. Mao Z, Hine C, Tian X, Van Meter M, Au M, Vaidya A, et al. SIRT6 promotes DNA repair under stress by activating PARP1. Science. 2011 Jun 17;332(6036):1443-6.

171. Xu Z, Zhang L, Zhang W, Meng D, Zhang H, Jiang Y, et al. SIRT6 rescues the age related decline in base excision repair in a PARP1-dependent manner. Cell Cycle. 2015;14(2):269-76.

172. Kaidi A, Weinert BT, Choudhary C, Jackson SP. Human SIRT6 promotes DNA end resection through CtIP deacetylation. Science. 2010 Sep 10;329(5997):1348-53.

173. McCord RA, Michishita E, Hong T, Berber E, Boxer LD, Kusumoto R, et al. SIRT6 stabilizes DNA-dependent protein kinase at chromatin for DNA double-strand break repair. Aging (Albany NY). 2009 Jan 15;1(1):109-21.

174. Michishita E, McCord RA, Berber E, Kioi M, Padilla-Nash H, Damian M, et al. SIRT6 is a histone H3 lysine 9 deacetylase that modulates telomeric chromatin. Nature. 2008 Mar 27;452(7186):492-6.

175. Jiang H, Khan S, Wang Y, Charron G, He B, Sebastian C, et al. SIRT6 regulates TNF-alpha secretion through hydrolysis of long-chain fatty acyl lysine. Nature. 2013 Apr 4;496(7443):110-3.

176. Van Gool F, Galli M, Gueydan C, Kruys V, Prevot PP, Bedalov A, et al. Intracellular NAD levels regulate tumor necrosis factor protein synthesis in a sirtuin-dependent manner. Nat Med. 2009 Feb;15(2):206-10.

177. Kawahara TL, Michishita E, Adler AS, Damian M, Berber E, Lin M, et al. SIRT6 links histone H3 lysine 9 deacetylation to NF-kappaB-dependent gene expression and organismal life span. Cell. 2009 Jan 9;136(1):62-74.

178. Kanfi Y, Naiman S, Amir G, Peshti V, Zinman G, Nahum L, et al. The sirtuin SIRT6 regulates lifespan in male mice. Nature. 2012 Feb 22;483(7388):218-21.

179. Hu S, Liu H, Ha Y, Luo X, Motamedi M, Gupta MP, et al. Posttranslational modification of Sirt6 activity by peroxynitrite. Free Radic Biol Med. 2015 Feb;79:176-85.

180. Liu R, Liu H, Ha Y, Tilton RG, Zhang W. Oxidative stress induces endothelial cell senescence via downregulation of Sirt6. Biomed Res Int. 2014;2014:902842.

181. Sahin K, Yilmaz S, Gozukirmizi N. Changes in human sirtuin 6 gene promoter methylation during aging. Biomed Rep. 2014 Jul;2(4):574-8.

182. Green DR, Galluzzi L, Kroemer G. Cell biology. metabolic control of cell death. Science. 2014 Sep 19;345(6203):1250256.

183. Galluzzi L, Aaronson SA, Abrams J, Alnemri ES, Andrews DW, Baehrecke EH, et al. Guidelines for the use and interpretation of assays for monitoring cell death in higher eukaryotes. Cell Death Differ. 2009 Aug;16(8):1093-107.

184. Galluzzi L, Vitale I, Abrams JM, Alnemri ES, Baehrecke EH, Blagosklonny MV, et al. Molecular definitions of cell death subroutines: Recommendations of the nomenclature committee on cell death 2012. Cell Death Differ. 2012 Jan;19(1):107-20.

185. Wang Y, Kim NS, Haince JF, Kang HC, David KK, Andrabi SA, et al. Poly(ADP-ribose) (PAR) binding to apoptosis-inducing factor is critical for PAR polymerase-1-dependent cell death (parthanatos). Sci Signal. 2011 Apr 5;4(167):ra20.

186. David KK, Andrabi SA, Dawson TM, Dawson VL. Parthanatos, a messenger of death. Front Biosci (Landmark Ed). 2009 Jan 1;14:1116-28.

187. Wang Y, Dawson VL, Dawson TM. Poly(ADP-ribose) signals to mitochondrial AIF: A key event in parthanatos. Exp Neurol. 2009 Aug;218(2):193-202.

188. Wesierska-Gadek J, Ranftler C, Schmid G. Physiological ageing: Role of p53 and PARP-1 tumor suppressors in the regulation of terminal senescence. J Physiol Pharmacol. 2005 Mar;56 Suppl 2:77-88.

189. Soldani C, Scovassi AI. Poly(ADP-ribose) polymerase-1 cleavage during apoptosis: An update. Apoptosis. 2002 Aug;7(4):321-8.

190. Yuan K, Sun Y, Zhou T, McDonald J, Chen Y. PARP-1 regulates resistance of pancreatic cancer to TRAIL therapy. Clin Cancer Res. 2013 Sep 1;19(17):4750-9.

191. Virag L, Robaszkiewicz A, Rodriguez-Vargas JM, Oliver FJ. Poly(ADP-ribose) signaling in cell death. Mol Aspects Med. 2013 Dec;34(6):1153-67.

192. Imai S, Guarente L. NAD+ and sirtuins in aging and disease. Trends Cell Biol. 2014 Aug;24(8):464-71.

193. Berger F, Ramirez-Hernandez MH, Ziegler M. The new life of a centenarian: Signalling functions of NAD(P). Trends Biochem Sci. 2004 Mar;29(3):111-8.

194. Mouchiroud L, Houtkooper RH, Moullan N, Katsyuba E, Ryu D, Canto C, et al. The NAD(+)/sirtuin pathway modulates longevity through activation of mitochondrial UPR and FOXO signaling. Cell. 2013 Jul 18;154(2):430-41.

195. Braidy N, Guillemin GJ, Mansour H, Chan-Ling T, Poljak A, Grant R. Age related changes in NAD+ metabolism oxidative stress and Sirt1 activity in wistar rats. PLoS One. 2011 Apr 26;6(4):e19194.

196. Massudi H, Grant R, Braidy N, Guest J, Farnsworth B, Guillemin GJ. Age-associated changes in oxidative stress and NAD+ metabolism in human tissue. PLoS One. 2012;7(7):e42357.

197. Chang HC, Guarente L. SIRT1 mediates central circadian control in the SCN by a mechanism that decays with aging. Cell. 2013 Jun 20;153(7):1448-60.

198. Yoshino J, Mills KF, Yoon MJ, Imai S. Nicotinamide mononucleotide, a key NAD(+) intermediate, treats the pathophysiology of diet- and age-induced diabetes in mice. Cell Metab. 2011 Oct 5;14(4):528-36.

199. Cavadini G, Petrzilka S, Kohler P, Jud C, Tobler I, Birchler T, et al. TNF-alpha suppresses the expression of clock genes by interfering with E-box-mediated transcription. Proc Natl Acad Sci U S A. 2007 Jul 31;104(31):12843-8.

200. Belenky PA, Moga TG, Brenner C. Saccharomyces cerevisiae YOR071C encodes the high affinity nicotinamide riboside transporter Nrt1. J Biol Chem. 2008 Mar 28;283(13):8075-9.

201. Belenky P, Stebbins R, Bogan KL, Evans CR, Brenner C. Nrt1 and Tna1-independent export of NAD+ precursor vitamins promotes NAD+ homeostasis and allows engineering of vitamin production. PLoS One. 2011 May 11;6(5):e19710.

202. Belenky P, Racette FG, Bogan KL, McClure JM, Smith JS, Brenner C. Nicotinamide riboside promotes Sir2 silencing and extends lifespan via nrk and Urh1/Pnp1/Meu1 pathways to NAD+. Cell. 2007 May 4;129(3):473-84.

203. Nikiforov A, Dolle C, Niere M, Ziegler M. Pathways and subcellular compartmentation of NAD biosynthesis in human cells: From entry of extracellular precursors to mitochondrial NAD generation. J Biol Chem. 2011 Jun 17;286(24):21767-78.

204. Bogan KL, Brenner C. Nicotinic acid, nicotinamide, and nicotinamide riboside: A molecular evaluation of NAD+ precursor vitamins in human nutrition. Annu Rev Nutr. 2008;28:115-30.

205. Rongvaux A, Shea RJ, Mulks MH, Gigot D, Urbain J, Leo O, et al. Pre-B-cell colony-enhancing factor, whose expression is up-regulated in activated lymphocytes, is a nicotinamide phosphoribosyltransferase, a cytosolic enzyme involved in NAD biosynthesis. Eur J Immunol. 2002 Nov;32(11):3225-34.

206. Samal B, Sun Y, Stearns G, Xie C, Suggs S, McNiece I. Cloning and characterization of the cDNA encoding a novel human pre-B-cell colony-enhancing factor. Mol Cell Biol. 1994 Feb;14(2):1431-7.

207. Fukuhara A, Matsuda M, Nishizawa M, Segawa K, Tanaka M, Kishimoto K, et al. Visfatin: A protein secreted by visceral fat that mimics the effects of insulin. Science. 2005 Jan 21;307(5708):426-30.

208. Prusty D, Mehra P, Srivastava S, Shivange AV, Gupta A, Roy N, et al. Nicotinamide inhibits plasmodium falciparum Sir2 activity in vitro and parasite growth. FEMS Microbiol Lett. 2008 May;282(2):266-72.

209. Li S, Sims S, Jiao Y, Chow LH, Pickering JG. Evidence from a novel human cell clone that adult vascular smooth muscle cells can convert reversibly between noncontractile and contractile phenotypes. Circ Res. 1999 Aug 20;85(4):338-48.

210. van der Veer E, Nong Z, O'Neil C, Urquhart B, Freeman D, Pickering JG. Pre-B-cell colony-enhancing factor regulates NAD+-dependent protein deacetylase activity and promotes vascular smooth muscle cell maturation. Circ Res. 2005 Jul 8;97(1):25-34.

211. van der Veer E, Ho C, O'Neil C, Barbosa N, Scott R, Cregan SP, et al. Extension of human cell lifespan by nicotinamide phosphoribosyltransferase. J Biol Chem. 2007 Apr 13;282(15):10841-5.

212. Ho C, van der Veer E, Akawi O, Pickering JG. SIRT1 markedly extends replicative lifespan if the NAD+ salvage pathway is enhanced. FEBS Lett. 2009 Sep 17;583(18):3081-5.

213. Borradaile NM, Pickering JG. Nicotinamide phosphoribosyltransferase imparts human endothelial cells with extended replicative lifespan and enhanced angiogenic capacity in a high glucose environment. Aging Cell. 2009 Apr;8(2):100-12.

214. Rongvaux A, Galli M, Denanglaire S, Van Gool F, Dreze PL, Szpirer C, et al. Nicotinamide phosphoribosyl transferase/pre-B cell colony-enhancing factor/visfatin is required for lymphocyte development and cellular resistance to genotoxic stress. J Immunol. 2008 Oct 1;181(7):4685-95.

215. Tempel W, Rabeh WM, Bogan KL, Belenky P, Wojcik M, Seidle HF, et al. Nicotinamide riboside kinase structures reveal new pathways to NAD+. PLoS Biol. 2007 Oct 2;5(10):e263.

216. Bieganowski P, Brenner C. Discoveries of nicotinamide riboside as a nutrient and conserved NRK genes establish a preiss-handler independent route to NAD+ in fungi and humans. Cell. 2004 May 14;117(4):495-502.

217. Li J, Rao H, Burkin D, Kaufman SJ, Wu C. The muscle integrin binding protein (MIBP) interacts with alpha7beta1 integrin and regulates cell adhesion and laminin matrix deposition. Dev Biol. 2003 Sep 1;261(1):209-19.

218. Creider JC, Hegele RA, Joy TR. Niacin: Another look at an underutilized lipid-lowering medication. Nat Rev Endocrinol. 2012 Sep;8(9):517-28.

219. Ginsberg HN, Reyes-Soffer G. Niacin: A long history, but a questionable future. Curr Opin Lipidol. 2013 Dec;24(6):475-9.

220. Lavigne PM, Karas RH. The current state of niacin in cardiovascular disease prevention: A systematic review and meta-regression. J Am Coll Cardiol. 2013 Jan 29;61(4):440-6.

221. Wu BJ, Yan L, Charlton F, Witting P, Barter PJ, Rye KA. Evidence that niacin inhibits acute vascular inflammation and improves endothelial dysfunction independent of changes in plasma lipids. Arterioscler Thromb Vasc Biol. 2010 May;30(5):968-75.

222. Huang PH, Lin CP, Wang CH, Chiang CH, Tsai HY, Chen JS, et al. Niacin improves ischemia-induced neovascularization in diabetic mice by enhancement of endothelial progenitor cell functions independent of changes in plasma lipids. Angiogenesis. 2012 Sep;15(3):377-89.

223. Kaplon RE, Gano LB, Seals DR. Vascular endothelial function and oxidative stress are related to dietary niacin intake among healthy middle-aged and older adults. J Appl Physiol (1985). 2014 Jan 15;116(2):156-63.

224. Chen J, Cui X, Zacharek A, Jiang H, Roberts C, Zhang C, et al. Niaspan increases angiogenesis and improves functional recovery after stroke. Ann Neurol. 2007 Jul;62(1):49-58.

225. Yamamoto T, Byun J, Zhai P, Ikeda Y, Oka S, Sadoshima J. Nicotinamide mononucleotide, an intermediate of NAD+ synthesis, protects the heart from ischemia and reperfusion. PLoS One. 2014 Jun 6;9(6):e98972.

226. Wang M, Zhang J, Jiang LQ, Spinetti G, Pintus G, Monticone R, et al. Proinflammatory profile within the grossly normal aged human aortic wall. Hypertension. 2007 Jul;50(1):219-27.

227. Csiszar A, Ungvari Z, Koller A, Edwards JG, Kaley G. Aging-induced proinflammatory shift in cytokine expression profile in coronary arteries. FASEB J. 2003 Jun;17(9):1183-5.

228. Vasto S, Candore G, Balistreri CR, Caruso M, Colonna-Romano G, Grimaldi MP, et al. Inflammatory networks in ageing, age-related diseases and longevity. Mech Ageing Dev. 2007 Jan;128(1):83-91.

229. Tunaru S, Kero J, Schaub A, Wufka C, Blaukat A, Pfeffer K, et al. PUMA-G and HM74 are receptors for nicotinic acid and mediate its anti-lipolytic effect. Nat Med. 2003 Mar;9(3):352-5.

230. Wise A, Foord SM, Fraser NJ, Barnes AA, Elshourbagy N, Eilert M, et al. Molecular identification of high and low affinity receptors for nicotinic acid. J Biol Chem. 2003 Mar 14;278(11):9869-74.

231. Bitterman KJ, Anderson RM, Cohen HY, Latorre-Esteves M, Sinclair DA. Inhibition of silencing and accelerated aging by nicotinamide, a putative negative regulator of yeast sir2 and human SIRT1. J Biol Chem. 2002 Nov 22;277(47):45099-107.

232. Yang T, Chan NY, Sauve AA. Syntheses of nicotinamide riboside and derivatives: Effective agents for increasing nicotinamide adenine dinucleotide concentrations in mammalian cells. J Med Chem. 2007 Dec 27;50(26):6458-61.

233. Canto C, Houtkooper RH, Pirinen E, Youn DY, Oosterveer MH, Cen Y, et al. The NAD(+) precursor nicotinamide riboside enhances oxidative metabolism and protects against high-fat diet-induced obesity. Cell Metab. 2012 Jun 6;15(6):838-47.

234. Brown KD, Maqsood S, Huang JY, Pan Y, Harkcom W, Li W, et al. Activation of SIRT3 by the NAD(+) precursor nicotinamide riboside protects from noise-induced hearing loss. Cell Metab. 2014 Dec 2;20(6):1059-68.

235. Khan NA, Auranen M, Paetau I, Pirinen E, Euro L, Forsstrom S, et al. Effective treatment of mitochondrial myopathy by nicotinamide riboside, a vitamin B3. EMBO Mol Med. 2014 Apr 6;6(6):721-31.

236. Cerutti R, Pirinen E, Lamperti C, Marchet S, Sauve AA, Li W, et al. NAD(+)-dependent activation of Sirt1 corrects the phenotype in a mouse model of mitochondrial disease. Cell Metab. 2014 Jun 3;19(6):1042-9.

237. Felici R, Lapucci A, Cavone L, Pratesi S, Berlinguer-Palmini R, Chiarugi A. Pharmacological NAD-boosting strategies improve mitochondrial homeostasis in human complex I-mutant fibroblasts. Mol Pharmacol. 2015 Jun;87(6):965-71.

238. Scheibye-Knudsen M, Mitchell SJ, Fang EF, Iyama T, Ward T, Wang J, et al. A high-fat diet and NAD(+) activate Sirt1 to rescue premature aging in cockayne syndrome. Cell Metab. 2014 Nov 4;20(5):840-55.

239. Tummala KS, Gomes AL, Yilmaz M, Grana O, Bakiri L, Ruppen I, et al. Inhibition of de novo NAD(+) synthesis by oncogenic URI causes liver tumorigenesis through DNA damage. Cancer Cell. 2014 Dec 8;26(6):826-39.

240. Umemura K, Kimura H. Determination of oxidized and reduced nicotinamide adenine dinucleotide in cell monolayers using a single extraction procedure and a spectrophotometric assay. Anal Biochem. 2005 Mar 1;338(1):131-5.

241. Gyori BM, Venkatachalam G, Thiagarajan PS, Hsu D, Clement MV. OpenComet: An automated tool for comet assay image analysis. Redox Biol. 2014 Jan 9;2:457-65.

242. Rawling JM, Jackson TM, Driscoll ER, Kirkland JB. Dietary niacin deficiency lowers tissue poly(ADP-ribose) and NAD+ concentrations in fischer-344 rats. J Nutr. 1994 Sep;124(9):1597-603.

243. Hayashi S, McMahon AP. Efficient recombination in diverse tissues by a tamoxifen-inducible form of cre: A tool for temporally regulated gene activation/inactivation in the mouse. Dev Biol. 2002 Apr 15;244(2):305-18.

244. Yan T, Feng Y, Zheng J, Ge X, Zhang Y, Wu D, et al. Nmnat2 delays axon degeneration in superior cervical ganglia dependent on its NAD synthesis activity. Neurochem Int. 2010 Jan;56(1):101-6.

245. Giblin W, Skinner ME, Lombard DB. Sirtuins: Guardians of mammalian healthspan. Trends Genet. 2014 Jul;30(7):271-86.

246. Yang T, Chan NY, Sauve AA. Syntheses of nicotinamide riboside and derivatives: Effective agents for increasing nicotinamide adenine dinucleotide concentrations in mammalian cells. J Med Chem. 2007 Dec 27;50(26):6458-61.

247. Ciobanasu C, Faivre B, Le Clainche C. Integrating actin dynamics, mechanotransduction and integrin activation: The multiple functions of actin binding proteins in focal adhesions. Eur J Cell Biol. 2013 Oct-Nov;92(10-11):339-48.

248. Yamin R, Morgan KG. Deciphering actin cytoskeletal function in the contractile vascular smooth muscle cell. J Physiol. 2012 Sep 1;590(Pt 17):4145-54.

249. Wehrle-Haller B. Structure and function of focal adhesions. Curr Opin Cell Biol. 2012 Feb;24(1):116-24.

250. Mandel KG, Lively MK, Lombardi D, Amos H. Reactivation of NAD(H) biosynthetic pathway by exogenous NAD+ in nil cells severely depleted of NAD(H). J Cell Physiol. 1983 Feb;114(2):235-44.

251. Jackson TM, Rawling JM, Roebuck BD, Kirkland JB. Large supplements of nicotinic acid and nicotinamide increase tissue NAD+ and poly(ADP-ribose) levels but do not affect diethylnitrosamine-induced altered hepatic foci in fischer-344 rats. J Nutr. 1995 Jun;125(6):1455-61.

252. Tas Hekimoglu A, Toprak G, Akkoc H, Evliyaoglu O, Tas T, Kelle I, et al. Protective effect of 3-aminobenzamide, an inhibitor of poly (ADP-ribose) polymerase in distant liver injury induced by renal ischemia-reperfusion in rats. Eur Rev Med Pharmacol Sci. 2014;18(1):34-8.

253. Crawford RS, Albadawi H, Atkins MD, Jones JE, Yoo HJ, Conrad MF, et al. Postischemic poly (ADP-ribose) polymerase (PARP) inhibition reduces ischemia reperfusion injury in a hind-limb ischemia model. Surgery. 2010 Jul;148(1):110-8.

254. Nakagawa T, Guarente L. Sirtuins at a glance. J Cell Sci. 2011 Mar 15;124(Pt 6):833-8.

255. Bai P, Canto C, Oudart H, Brunyanszki A, Cen Y, Thomas C, et al. PARP-1 inhibition increases mitochondrial metabolism through SIRT1 activation. Cell Metab. 2011 Apr 6;13(4):461-8.

256. Abdellatif M. Sirtuins and pyridine nucleotides. Circ Res. 2012 Aug 17;111(5):642-56.

257. Nakagawa T, Guarente L. SnapShot: Sirtuins, NAD, and aging. Cell Metab. 2014 Jul 1;20(1):192,192.e1.

258. Mei Y, Thompson MD, Cohen RA, Tong X. Autophagy and oxidative stress in cardiovascular diseases. Biochim Biophys Acta. 2015 Feb;1852(2):243-51.

259. D'Onofrio N, Vitiello M, Casale R, Servillo L, Giovane A, Balestrieri ML. Sirtuins in vascular diseases: Emerging roles and therapeutic potential. Biochim Biophys Acta. 2015 Jul;1852(7):1311-22.

260. Rosado MM, Bennici E, Novelli F, Pioli C. Beyond DNA repair, the immunological role of PARP-1 and its siblings. Immunology. 2013 Aug;139(4):428-37.

261. Janke C, Bulinski JC. Post-translational regulation of the microtubule cytoskeleton: Mechanisms and functions. Nat Rev Mol Cell Biol. 2011 Nov 16;12(12):773-86.

262. North BJ, Marshall BL, Borra MT, Denu JM, Verdin E. The human Sir2 ortholog, SIRT2, is an NAD+-dependent tubulin deacetylase. Mol Cell. 2003 Feb;11(2):437-44.

263. Skoge RH, Dolle C, Ziegler M. Regulation of SIRT2-dependent alpha-tubulin deacetylation by cellular NAD levels. DNA Repair (Amst). 2014 Nov;23:33-8.

264. Patel VP, Chu CT. Decreased SIRT2 activity leads to altered microtubule dynamics in oxidatively-stressed neuronal cells: Implications for parkinson's disease. Exp Neurol. 2014 Jul;257:170-81.

265. Poruchynsky MS, Komlodi-Pasztor E, Trostel S, Wilkerson J, Regairaz M, Pommier Y, et al. Microtubule-targeting agents augment the toxicity of DNA-damaging agents by disrupting intracellular trafficking of DNA repair proteins. Proc Natl Acad Sci U S A. 2015 Feb 3;112(5):1571-6.

APPENDICES

Appendix A – List of Primer Probes used in this Thesis

Anti-Oxidant Genes

hSOD1-F:CTCACTCTCAGGAGACCATTGC
hSOD1-R: CCACAAGCCAAACGACTTCCAG

hSOD2-F: CTGGACAAACCTCAGCCCTAAC
hSOD2-R: AACCTGAGCCTTGGACACCAAC

hPPARGC1A(PGC-1a)-F: CCAAAGGATGCGCTCTCGTTCA
hPPARGC1A(PGC-1a)-R: CGGTGTCTGTAGTGGCTTGACT

hCAT-F: GTGCGGAGATTCAACACTGCCA
hCAT-R: CGGCAATGTTCTCACACAGACG

hPRDX5-F: TGATGCCTTTGTGACTGGCGAG
hPRDX5-R: CCAAAGATGGACACCAGCGAATC

Sirtuins

hSirt1-F: TAGACACGCTGGAACAGGTTGC
hSirt1-R: CTCCTCGTACAGCTTCACAGTC

hSirt2-F: CTGCGGAACTTATTCTCCCAGAC
hSirt2-R: CCACCAAACAGATGACTCTGCG

hSirt3-F: CCCTGGAAACTACAAGCCCAAC
hSirt3-R: GCAGAGGCAAAGGTTCCATGAG

hSirt4-F: GTGGATGCTTTGCACACCAAGG
hSirt4-R: GGTTCAGGACTTGGAAACGCTC

hSirt5-F: GTCCACACGAAACCAGATTTGCC
hSirt5-R: TCCTCTGAAGGTCGGAACACCA

hSirt6-F: TGGCAGTCTTCCAGTGTGGTGT
hSirt6-R: CGCTCTCAAAGGTGGTGTCGAA

hSirt7-F: TGGAGTGTGGACACTGCTTCAG
hSirt7-R: CCGTCACAGTTCTGAGACACCA

CURRICULUM VITAE

Krista Hawrylyshyn

UNIVERSITY EDUCATION

Candidate for Master of Science- Biochemistry **Expected completion: Spring 2015**
The University of Western Ontario, London, ON

Bachelors of Medical Science, Honours Specialization in Medical Cell Biology, *with distinction* **2013**
The University of Western Ontario, London, ON

HONOURS, SCHOLARSHIPS AND AWARDS

The University of Western Ontario Gold Medal **2013**
- Awarded for obtaining the highest average of the graduating class for the Honors Specialization in Medical Cell Biology (cGPA 3.88/4.0)

Laurene Paterson Estate Scholarship **2011**
- Awarded to forty-seven students within the Faculty of Science at the University of Western Ontario based on academic merit, amount determined by financial need

Dean's Honor Roll **2010-13**
- Awarded in recognition of academic success during the 2010, 2011, 2012 and 2013 academic terms

The University of Western Ontario Entrance Award of Excellence **2009- 10**
- Received a $2,500 scholarship: Achieved an entering average above 90%

Queen Elizabeth II Aiming for the Top Award **2009-12**
- Annual need-based scholarship awarded for academic merit to the top percent of students finishing secondary education dependent on continued academic success

RESEARCH-BASED HONOURS, SCHOLARSHIPS AND AWARDS

Frederick Banting and Charles Best Canada Graduate Scholarship- Master's Award **2013**
- $17,500 scholarship awarded by the Canadian Institute of Health Research to Masters students who show outstanding future research potential

Western Graduate Research Scholarship **2013-14**
- $4,500 annual scholarship awarded to graduate students entering with and maintaining a minimum 80% average

RESEARCH EXPERIENCE HIGHLIGHTS

Masters in Biochemistry Graduate Student **May 2013 – Ongoing**
Pickering Lab, Robarts Research Institute, London, ON

- Successfully completed 4999E undergraduate course including seminar presentation to the Department of Biochemistry, prerequisite for 16-month Accelerated Masters Program
- Developed laboratory skills for Western Blots, PCR, cell culture, NAD^+ quantification assays, immunofluorescence, viability assays
- Attended & presented seminar at Department of Biochemistry weekly seminars

Fourth Year Thesis Student **Summer 2012**
Pickering Lab, Robarts Research Institute, London, ON

- Successfully completed a written thesis, oral presentation and poster titled, "Pathways for Restoring Cellular NAD^+"
- Assessed ability of Nicotinamide Riboside to alter cellular NAD^+ homeostasis in vascular cells

SickKids Summer Research Student **Summer 2011**
Wilson Lab, SickKids Hospital- McMaster Building, Toronto, ON

- Performed anterior thoracotomies on New Zealand white rabbits and excised the heart to isolate cardiomyocytes using a Langendorff preparation
- Studied the cardio-protective effects of indanyloxyacetic acid 94 and cyclosporin A using 48 hour primary culture cardiomyocytes and simulated ischemia & reperfusion
- Studied the effects of valinomycin & ionomycin on mitochondrial permeability using calcein AM fluorescence with cobalt chloride and confocal microscopy
- Participated in Leducq Foundation weekly meetings and summer student weekly seminars

Clinical Research Assistant **Fall 2011 - Spring 2012**
Norozi Lab, Children's Hospital- London Health Sciences Centre, London, ON

- Assisted with study of non-invasive measurement of cardiac output in hypertensive children with operated congenital heart defect
- Assessed muscle function of children ages 8-17 using mechanography collected through a force plate
- Collected blood pressure measurements and assisted with cardiac output measurements

Work-Study Laboratory Assistant **Fall 2010 - Spring 2011**
Chidiac Lab, The University of Western Ontario, London, ON

- Assisted in constructing plasmids using PCR, gel electrophoresis and DNA purification techniques
- Catalogued the stored plasmids within the lab and began a sequencing project to identify the inserts

Research Assistant **Winter, Spring, Fall 2010**
Neff Lab, The University of Western Ontario, London, ON

- Assisted with study of phenotypic variation in the Major Histocompatibility Complex of Guppy fish
- Performed PCR experiments on samples and followed up with gel electrophoresis and analysis of gels
- Isolated DNA from fish tissue to prepare field samples for testing

PUBLICATIONS

Peer-Reviewed Journals

1. Wilson, G., Hawrylyshyn, K., Cioci, S., Guglani, S., and Diaz, R. 2014. Remote Ischemic Preconditioning Cardio-protection via Enhanced Cell Volume Regulation Requires Activation of Swelling-Activated Chloride ($I_{Cl\text{-}swell}$) Channels. *Cardiol Parmacol.* 3:117.

2. Diaz, R., Fernandes, K., Lytvyn, Y., Hawrylyshyn, K., Harvey, K., Hossain, T., Hinek, A., and Wilson, G. 2013. Enhanced Cell Volume Regulation in Cyclosporin A Cardioprotection. *Cardiovasc Res.* 98(3):411-9.

3. Tran, K., Fraser, D., Hawrylyshyn, K., and Norozi, K. 2012. Cardiac failure following inadvertent administration of high dose epinephrine subcutaneously. *J Pediatric Intensive Care.* 1(4):221–225.

PRESENTATIONS & ABSTRACTS

London Health Research Day **March 2014**
London Convention Centre, London, ON

- Prepared an abstract and presented a poster titled, "Managing Oxidative Damage with NAD^+ Precursors"
- Poster was also presented at an internal poster fair, *Robarts Research Retreat* (June 2014)

SickKids Summer Research Program Symposium **August 2011**
SickKids Hospital, Toronto, ON

- Prepared an abstract and presented a poster titled, "Role of chloride channel activity in cyclosporine A induced protection against ischemia/reperfusion injury in rabbit cultured cardiomyocytes"

TEACHING EXPERIENCE

Leadership Education Program Facilitator **Fall 2013**
The University of Western Ontario, London, ON

- Facilitated *What is Leadership?* and *Team Building and Motivation* workshops for undergraduate students, class sizes ranged from 40-60 students
- Organized module content and facilitated a total of eight two-hour workshops

LEADERSHIP EXPERIENCE HIGHLIGHTS

Board Member **Fall 2011-ongoing**
London Intercommunity Health Centre, London, Ontario

- Official voting board member on the Quality & Finance and Planning & Development committees
- Participated as a non-voting board intern during the 2011-2012 academic term
    - Attended workshops on not-for-profit governing covering topics such as roles & responsibilities of board members, structure of a board meeting, strategic planning and financial statements